DEPARTMENT OF TRANSPORTATION

# Solutions to Mitigate Dowel/ Tie-Bar Propagated Cracking - Phase 1

**Shreenath Rao, Principal Investigator**
Applied Research Associates, Inc.

**April 2024**

Final Report NRRA202402

NRRA National Road Research Alliance

To request this document in an alternative format, such as braille or large print, call 651-366-4718 or 1-800-657-3774 (Greater Minnesota) or email your request to ADArequest.dot@state.mn.us. Please request at least one week in advance.

## Technical Report Documentation Page

| 1. Report No. | 2. | 3. Recipients Accession No. | |
|---|---|---|---|
| NRRA202402 | | | |
| 4. Title and Subtitle<br>Solutions to Mitigate Dowel/Tie-Bar Propagated Cracking - Phase 1 | | 5. Report Date<br>April 2024<br>6. | |
| 7. Author(s)<br>Shreenath Rao, Ph.D., P.E., Hesham Abdualla, Ph.D., Abu Sufian, Ph.D. | | 8. Performing Organization Report No. | |
| 9. Performing Organization Name and Address<br>Applied Research Associates, Inc.<br>100 Trade Centre Dr.<br>Champaign, IL 61820 | | 10. Project/Task/Work Unit No.<br>11. Contract (C) or Grant (G) No.<br>(c) 1034445 | |
| 12. Sponsoring Organization Name and Address<br>Minnesota Department of Transportation<br>Office of Research & Innovation<br>395 John Ireland Boulevard, MS 330<br>St. Paul, Minnesota 55155-1899 | | 13. Type of Report and Period Covered<br>Final Report<br>14. Sponsoring Agency Code | |
| 15. Supplementary Notes<br>http://mdl.mndot.gov/ | | | |


16. Abstract (Limit: 250 words)

This Phase 1 study was undertaken to evaluate cracking related to dowel bars and tie bars in concrete pavement. The results of the literature review and field studies suggest that under some conditions, restraint caused by dowel bars and tie bars in the concrete result in high early age stresses that contribute to cracking. Field evaluation of six sites conducted as part of this research suggests that this type of cracking is not an isolated phenomenon. While a notional description of the potential mechanism is described in this report, details regarding the extent to which various factors impact this type of cracking and appropriate reasonable steps to take to mitigate this type of cracking is not fully understood. To gain a more detailed understanding, a combination of finite element (FE) analysis with laboratory experiment is proposed for Phase 2. The analysis proposed includes an evaluation of key parameters and their influence on dowel bar cracking followed by validation through laboratory experimentation and model refinement.


| 17. Document Analysis/Descriptors | 18. Availability Statement | | |
|---|---|---|---|
| Dowels, Tie bars, Concrete pavements, Pavement cracking, Delamination | No restrictions. Document available from: National Technical Information Services, Alexandria, Virginia 22312 | | |
| 19. Security Class (this report)<br>Unclassified | 20. Security Class (this page)<br>Unclassified | 21. No. of Pages<br>142 | 22. Price |

# Solutions to Mitigate Dowel/Tie-Bar Propagated Cracking – Phase 1

# Final Report

*Prepared by:*

Shreenath Rao, Ph.D., P.E.
Applied Research Associates, Inc.

Hesham Abdualla, Ph.D.
Applied Research Associates, Inc.

Abu Sufian, Ph.D.
Applied Research Associates, Inc.

## April 2024

*Published by:*

Minnesota Department of Transportation
Office of Research & Innovation
395 John Ireland Boulevard, MS 330
St. Paul, Minnesota 55155-1899

This report represents the results of research conducted by the authors and does not necessarily represent the views or policies of the Minnesota Department of Transportation or Applied Research Associates, Inc. This report does not contain a standard or specified technique.

The authors, the Minnesota Department of Transportation, and Applied Research Associates, Inc. do not endorse products or manufacturers. Trade or manufacturers' names appear herein solely because they are considered essential to this report.

# Acknowledgements

Thank you to the members of this project's Technical Advisory Panel: Peter Kemp (chair and technical liaison, Wisconsin Department of Transportation), Thomas Burnham (Minnesota Department of Transportation), Maria Masten (Minnesota Department of Transportation), Leo Mahserelli (California Department of Transportation), Brett Trautman (Missouri Department of Transportation), James Parry (Wisconsin Department of Transportation), Larry Scofield (American Concrete Pavement Association), Kevin McMullen (Wisconsin Concrete Pavement Association), and Ashish Gandhi (Owens Corning).

Thank you to the Wisconsin Department of Transportation, the Minnesota Department of Transportation, and the Illinois Tollway for providing information, data, coordination, and access to their roadways for field testing and evaluation. Thank you to the Federal Highway Administration for lending the ultrasonic tomography device (MIRA) to the research team.

# Table of Contents

# List of Figures

# List of Tables

# Executive Summary

Cracking and spalling of concrete pavements reduce the service life of the roadway and result in added costs to an agency and disruptions to the traveling public when the damage is repaired. Cracks and spalls in concrete occur due to a wide range of reasons. This Phase 1 study focuses on cracking and spalling associated with dowel bars and tie bars in jointed plain concrete pavements.

Dowel bars and tie bars are needed for most jointed plain concrete pavements. Dowel bars perform the important role of providing load transfer across necessary transverse joints and tie bars prevent longitudinal joints from opening. Without transverse joints spaced at regular intervals, the concrete pavement would crack at irregular locations and in an irregular pattern. Without dowel bars at transverse joints, there would be poor load transfer across these joints, resulting in increased faulting and roughness over the life of the pavement. Without tie bars at longitudinal joints, these joints would open, and the lanes would potentially slide relative to one another. By helping transfer load across a joint, dowel bars and tie bars also reduce deflections and stresses at slab edges and corners, which extends the fatigue life of the pavement.

Dowel bars and tie bars are typically made of steel, which is stiffer than hardened concrete by about a factor of five to ten. During the early age of the concrete hydration and strength gain, this factor can be much higher as the concrete elastic modulus is significantly lower, while the steel elastic modulus is unchanged. Concrete is continuously moving by shrinking, expanding, curling, and warping as it hydrates and responds to the environment. The significant difference in modulus between steel and the early age concrete causes the steel to act as a restraint to the movement of the concrete. This restraint to concrete movement results in stresses in the concrete around the steel. If the concrete has not gained sufficient strength, and the restraint stresses from the dowel bars and tie bars in the concrete are high, these stresses can potentially result in microcracking in the concrete. These microcracks could potentially heal or stay localized as the concrete continues to hydrate and gain strength. However, if they don't, these microcracks could coalesce and continue to grow, particularly if the restraint stresses remain high for extended periods. Over the life of the pavement, with continuous traffic loading, these cracks extend into the concrete, turn up to the surface, and spall or crack the concrete at some distance from the dowel bars or tie bars.

Phase 1 of this study, focuses on this phenomenon by performing a thorough literature review. Several studies that discussed the issue of dowel bar and tie bar cracking are summarized in this report. While several researchers have contributed significantly to the state of the knowledge, the findings of the literature review indicate that a thorough understanding of the factors and mechanisms responsible for dowel bar and tie bar cracking is still deficient.

The literature review was followed by a field evaluation that consisted of six sites in Wisconsin, Illinois, and Minnesota. Field evaluation testing included ultrasonic tomography device (MIRA), pulse induction scans, ground penetrating radar (GPR), coring, and visual inspection. The field evaluation showed that the cracks within the concrete typically start around the depth of the dowel bar near the joint as delamination cracks and then migrate upward toward the surface, eventually breaking up and spalling

the concrete. These spalls are related to the presence of dowel bars and tie bars embedded in the concrete and can be distinguished from typical durability-related spalling by their extent and size, their depth, and lack of any significant amount of hairline cracking associated with or around the spalled concrete. These spalls are just as likely to occur on the leave side of the joint as they are on the approach side of the joint.

MIRA scans and coring showed that these cracks were observed on several joints that did not exhibit any signs of visible distresses at the surface of the concrete. These cracks extended through multiple dowel bars, and in some cases almost the full transverse length of the joint. The delamination cracks extended for several feet away from the transverse joints in the longitudinal direction. Cores taken closer to the joints have the cracks at the mid-depth of the core at the level of the dowel bar, whereas cores taken two or more feet away from the joints show the delamination crack at mid-depth or higher or lower than mid-depth. Cores typically showed cracks progress through the aggregate rather than around the aggregate, suggesting the crack tip approached the aggregate when the concrete had gained sufficient strength. In some cases, cores closer to the joint had cracks go around the aggregates, suggesting these cracks near the joints, and consequently near the dowel bars, happened during the early age of the concrete when the concrete was not very strong. The results of the trenching operations suggested that the delamination action was caused by the combined action of multiple dowel bars (acting in sync) rather than that of one or two dowel bars. At the very least, it likely indicated a horizontal zone of weakness for the crack tip to propagate.

Even with the notional knowledge of the above mechanism, the extent of the impacts of various potential parameters driving this mechanism is not fully understood. Of specific interest are understanding the extent to which concrete properties and dowel bar properties impact initiation, propagation, and deterioration of delamination cracks; the level of stresses under different ambient conditions that can be expected during the early ages in the concrete around and between dowel bars; and how these stresses compare with the concrete tensile and flexural strengths. Also of interest is the role of environmental stresses and the impact of temperature and moisture gradients on this type of cracking and the criteria that should be established to ensure that localized stresses that develop in the concrete around and between dowel bars during early ages is low.

To gain a more comprehensive understanding, a combination of detailed finite element (FE) analysis with a laboratory experiment is proposed for Phase 2. The FE analysis proposed includes an evaluation of key parameters and their influence on dowel bar cracking. The FE analysis will be validated through laboratory experimentation and analysis. The results of the laboratory testing will be used to refine the FE models and quantify the impact of various parameters that influence dowel bar cracking. Once the impact of various parameters is quantified, the potential factors and solutions can be updated to take into account the model predictions.

# Chapter 1: Introduction

Most early age cracking—cracking that manifests in the first 10 years of a pavement's life—occurs because, at some point during the very early life (first few days) of the pavement, during hydration and strength gain of the concrete, local stresses exceed the tensile or flexural strength, causing local damage in the form of microcracking. During this very early life, in effect, there is a race between concrete strength development and build-up of stresses from various sources of restraints and from early loads.

Examples of such restraint and loads include temperature curling plus moisture warping resulting in separation between the concrete slab and the base and associated unsupported concrete weight (which can be exacerbated by early application of construction traffic), dowel bars and tie bars restricting vertical and horizontal movements, friction between base and concrete restricting horizontal movement, mechanical interlock or bonding between the top of the base and the bottom of the concrete slab restricting vertical movement, volume change in concrete due to rising bleed water being restricted by dowel bars and tie bars, and shrinkage-related restraints, etc. Although this type of microcracking begins within the concrete during the very early age of strength gain and often when the concrete is transitioning or has just transitioned from a plastic state to a hardened state, it may not manifest itself until later in the life of the pavement. This delay happens because the concrete may not have fully cracked during the early life but may have only deteriorated to a sufficient extent to where application of additional repeated thermal-, moisture-, and load-related stresses increase the deterioration, culminating in the observed cracking. With sufficient cumulation of traffic and environmental loadings, damage increases, microcracks connect, grow, and eventually propagate into a crack that is visible at the surface of the concrete pavement.

By contrast, most late-age cracking occurs even when the stresses in the concrete are less than the strength. Local stresses from each load application cause microcracking or fatigue within the hardened concrete resulting in local damage. Thousands and millions of such load repetitions result in a continuous increase in damage, which varies from one location in the slab to another. With additional load and environmental stresses, damage exceeds a critical value resulting in local cracking, which over time, propagates into a visible crack.

Cracking propagating from and around dowel bars and tie bars generally falls under the early age category and these cracks are typically restraint cracks that may be exacerbated or manifested following repeated or even early age traffic and environmental loading. These cracks typically manifest themselves in the form of short longitudinal cracks originating from the transverse or longitudinal joint (Figure 1.1 and Figure 1.2). In some cases, these cracks continue to fully form into a longitudinal crack, transverse crack, corner break (Figure 1.3), or delamination (Figure 1.4).

**Figure 1.1 Photo. Cracking propagating from both tie bars and dowel bars on I-70 in Colorado.**

**Figure 1.2 Photo. Cracking propagating from tie bars on US 2 in Wisconsin.**

**Figure 1.3 Photo. Fully formed longitudinal crack and corner break that initiated as a dowel bar crack on I-70 in Colorado.**

**Figure 1.4 Photo. Delamination cracking on US 2 in Wisconsin.**

# Chapter 2: Mechanism and Classification of Cracking

Several researchers have classified concrete cracks based on their understanding of the mechanism of cracking. Figure 2.1 and Table 2.1 show the type of cracks classified into two categories: before hardening and after hardening (TRB 2006). Some of these cracks are grouped according to the cause of cracking, such as drying shrinkage cracking, plastic cracking, and settlement cracks (Safiuddin et al. 2018). Cracks in the plastic stage are divided into three main categories: construction movement, plastic cracks, and frost damage.

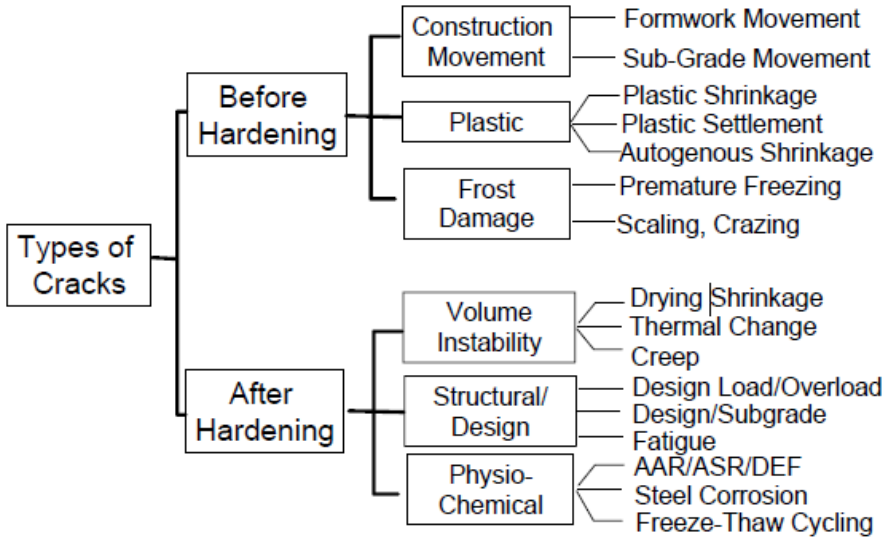


**Figure 2.1 Flowchart. Common causes of cracking in concrete (TRB 2006).**

**Table 2.1 Classification of cracks (TRB 2006).**

| Type of cracking | Form of Crack | Primary Cause | Time of Appearance |
|---|---|---|---|
| Plastic settlement | Over and aligned with reinforcement, subsidence under reinforcing bars | Poor mixture design leading to excessive bleeding, excessive vibrations | 10 min to 3 h |
| Plastic shrinkage | Diagonal or random | Excessive early evaporation | 30 min to 6 h |
| Thermal expansion and contraction | Transverse | Excessive heat generation, excessive temperature gradients | 1 day to 2–3 weeks |
| Drying shrinkage | Transverse, pattern or map cracking | Excessive mixture water, inefficient joints, large joint spacings | Weeks to months |
| Freezing and Thawing | Parallel to the surface of concrete | Lack of proper air-void system, non-durable coarse aggregate | After one or more winters |
| Corrosion of Reinforcement | Over reinforcement | Inadequate cover, ingress of sufficient chloride | More than 2 years |
| Alkali–aggregate Reaction | Pattern and longitudinal cracks parallel to the least restrained side | Reactive aggregate plus alkali hydroxides plus moisture | Typically, more than 5 years, but weeks with a highly reactive material |
| Sulfate attack | Pattern | Internal or external sulfates promoting the formation of ettringite | 1 to 5 years |

# Chapter 3: Literature Dowel and Tie Bar Propagated Cracking

Fine hairline to moderately wide cracks may sometimes develop over tie bars and dowel bars. In most cases, these cracks are a surface crack with 1.0- to 1.5-inch depth from the surface. However, these cracks may also propagate up to the surface from the dowel bars (Kumar and Mathur 2009). These cracks may not reduce the load transfer capacity of dowel bar, but over time traffic and environmental loads may lead to cracking of slab surface over the dowel bars. The evaluation of risk of cracking due to these factors requires assessment of complex interactions of various factors that are difficult to predict or quantify. For example, the stresses involved in the development of the cracking, as well as the portland cement concrete (PCC) strength development, are highly sensitive to the temperature and moisture conditions during concrete placement and during the early ages of concrete. For accurate modeling of restraint stress and PCC strength development at early ages, the ability to accurately model heat flow through the pavement structure for the precise exposure conditions is needed (Tyson and Tayabji 2008).

Various mechanisms of dowel and tie bar propagated early age cracking have been identified in the literature and are summarized below.

## 3.1 Early Age Dowel and Tie Bar Cracking Due to Restraint

Cracking initiates when the level of stress in concrete pavement slab exceeds the strength of the concrete as schematically shown in Figure 3.1 (Lim and Tayabji 2005). Therefore, the potential of early age cracking can be determined by investigating both the state of stress and strength development in the concrete during early age. The level of restraint stress at any time is dependent upon many factors and their interactions. These factors may be categorized into weather condition, construction practices, structural constraints, and properties of concrete. There are also other factors or construction conditions that may affect the degrees of restraint stress. For example, time of paving during the day may greatly affect the rate and magnitude of temperature drop in the concrete slab. High curling stress can occur when concrete is placed during the early part of the day in warm days. Therefore, any possible conditions or factors should be carefully examined for their impacts on the level of stress development in the concrete slab.

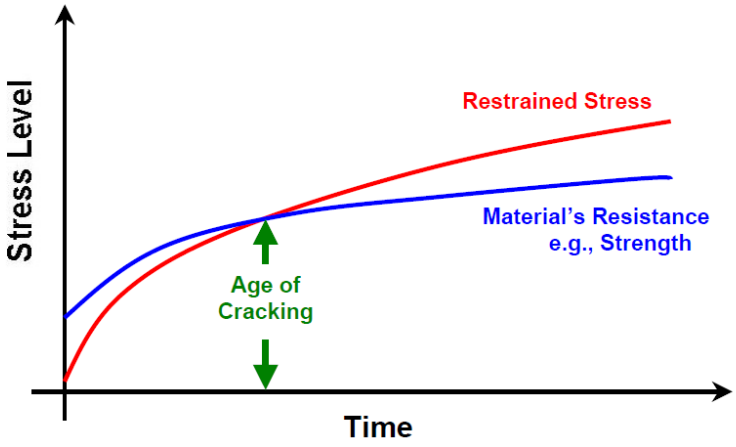


**Figure 3.1 Chart. Developments of concrete strength, restrained stress, and early age cracking (Lim and Tayabji 2005).**

As described in the American Concrete Pavement Association (ACPA) document JP010P "Stabilized and Drainable Base for Rigid Pavement—A Design and Construction Guide," for early age restraint crack to occur, two sets of factors need to be present simultaneously on a given project: (1) driving forces that induce movements in the early age concrete, and (2) factors that aggravate the impact of these movements on the tensile or flexural stresses developed in the pavement (ACPA 2005). The former set are referred to as trigger factors, or simply *triggers*. Triggers are the forcing functions that cause deformations in the PCC slabs. The latter set of factors is termed as variant factors, or *variants*. Triggers leading to early age restraint cracking include:

- Large Ambient Temperature Drops: A drop in ambient temperature of 25°F or greater, shortly after initial set of the concrete, is sufficient to elevate the risk of early restraint cracking significantly. This is particularly true when the temperature falls to a level where the strength gain of the PCC is affected significantly. For example, a temperature drop from 70 to 45°F causes a greater risk of early restraint cracking than a drop from 100 to 75°F. A large ambient temperature drop imposes a negative thermal gradient though the slab (top cooler than bottom). If the slab is sufficiently hardened, this can lead to tensile stresses at the top of the slab.
- Hot-Weather Paving: When ambient temperatures are in excess of 90°F, the risk of early restraint cracking is significantly elevated. Hot-weather concreting practices must be followed when paving under these conditions. Further, if the concrete is being placed on a dark-colored base, such as an asphalt-treated base, care needs to be taken to cool the surface of the base prior to PCC placement. If hot-weather paving precautions are ignored, excessive drying shrinkage can lead to warping and axial deformations. The effect of warping is similar to that of a negative thermal gradient. Axial deformations lead to stress build-up at locations of restraint such as slab/base interface, tie bars, etc. Restraint cracking can be of any orientation depending on the variants present.
- High Surface Evaporation Rate: Surface evaporation rates exceeding 0.1 lb/ft$^2$ elevate the risk of early age restraint cracking in PCC slabs. High evaporation rates can occur due to a critical

combination of high ambient and concrete temperatures, high wind speeds, and low ambient relative humidity values. High surface evaporation rates generally result in plastic shrinkage cracking. However, they can also lead to early age restraint cracking, particularly due to their ability to cause differential volumetric shrinkage through the slab (slab warping).

Although not included in JP010P, to this list of triggers must be added solar radiation, which during midday heats up the top of the concrete. This heat combined with the heat of hydration causes the top 4 inches or so of the slab to be much hotter than the bottom of the slab, which dissipates heat into the colder base course. The concrete in the upper part of the slab sets (becomes a solid) at a much higher temperature than the concrete in the lower portion of the slab. During the first night, the top of the slab cools while the bottom remains at about the same temperature resulting in a negative built-in temperature gradient through the slab and an upward curling of the slab. If this gradient is high enough, it will lead to top-down initiated cracking near the restraints (such as dowel bars and tie bars), in both the transverse and longitudinal directions. This can develop within a day or two or it can develop in combination with traffic loadings over the design period.

Variants influencing early age restraint cracking include both base properties as well as PCC layer related factors. The most important variants and their disposition leading to early age restraint cracking include:

- Design Variants
    - Excess base thickness (for stabilized bases that bond to the PCC).
    - PCC panels with large aspect ratios.
    - Excessive restraint within the slab.
    - Dowel bar and tie bar spacing.
- Materials Variants
    - High PCC/base interface friction or absence of bond breaker.
    - Excess base strength/stiffness.
    - High PCC cement factor.
    - Shrinkage susceptible PCC mixture.
    - High water content.
    - Dowel bar and tie bar size and stiffness.
- Construction Variants
    - Surface condition of base prior to paving.
    - Shrinkage cracking in base.
    - Late sawing or inadequate sawcut depth.
    - Absence of bond-breaker.
    - Inadequate PCC curing.
    - Poor vibration or consolidation.

Table 3.1 from JP010P presents an overview of the relationship between two key trigger conditions, the variants that combine with them to cause early age cracking, and the modes of cracking resulting from this combination. This table helps illustrate the “cause and effect” relationship that exists between triggers and variants.

**Table 3.1 Effect of triggers and variants on pavement responses and early age cracking (ACPA 2005).**

| Trigger Factor | Effect on Pavement Response & Potential Distress Modes | Aggravating Variants and Interactions |
|---|---|---|
| Large temperature drop-induced thermal shock caused by an approaching cold front or a significant rain/snow event. | • Imposes a negative thermal gradient though the slab (top cooler than bottom).<br><br>If the slab is sufficiently hardened, this can lead to tensile stresses at the top of the slab and a potential for top-down cracking. | • Late sawing or inadequate sawcut depth.<br>• Long PCC slab panels or high slab aspect ratios.<br>• Very thick or stiff base.<br>• Improper timing of PCC placement with respect to the timing of thermal shock (e.g., placing it when the heat of hydration is maximum at the time of steepest temp. drop).<br>• Excessive restraint at the slab/base interface.<br><br>Inadequate planning or execution of cold weather paving plans. |
| Hot weather paving conditions caused by high ambient temperatures, high solar radiation, low relative humidity, and high wind speeds. | • Causes excessive drying shrinkage through the slab leading to warping and axial deformations.<br><br>The effect of drying shrinkage is similar to that of a negative thermal gradient. Axial deformations cause stress build-up at locations of restraint (e.g., slab/base interface, tie bars). Cracking can be of any orientation depending on variants present. | • Hot concrete temperatures (> 85°F [29°C]).<br>• Inadequate or late curing.<br>• Late sawing or inadequate sawcut depth.<br>• Excessive restraint at the slab/base interface.<br>• High cement factor concretes without supplementary admixtures.<br>• Shrinkage susceptible PCC mixture.<br>• Certain types of chemical admixtures (e.g., high-range water reducers).<br>• Placing PCC in a way that the maximum heat from hydration occurs during the hottest part of the day.<br>• Placing PCC on a hot base layer.<br><br>Inadequate planning/execution of hot weather paving plans. |

Figure 3.2 from JP010P summarizes the various triggers and their threshold values and quantifies the risk of early restraint cracking as combination of these factors. Based on this figure, the risk of early restraint cracking for any given project can be qualitatively assessed.

Note that the presence of one trigger factor is adequate to cause cracking. However, the greater the number the triggers that are unfavorably aligned, the higher the risk of early restraint cracking. Also, as the number of trigger factors increases, fewer variants need to be unfavorably aligned for the risk of early restraint cracking to increase. Figure 3.2 suggests that with two or more triggers and three or more variants, the risk of early age restraint cracking is “definite.”

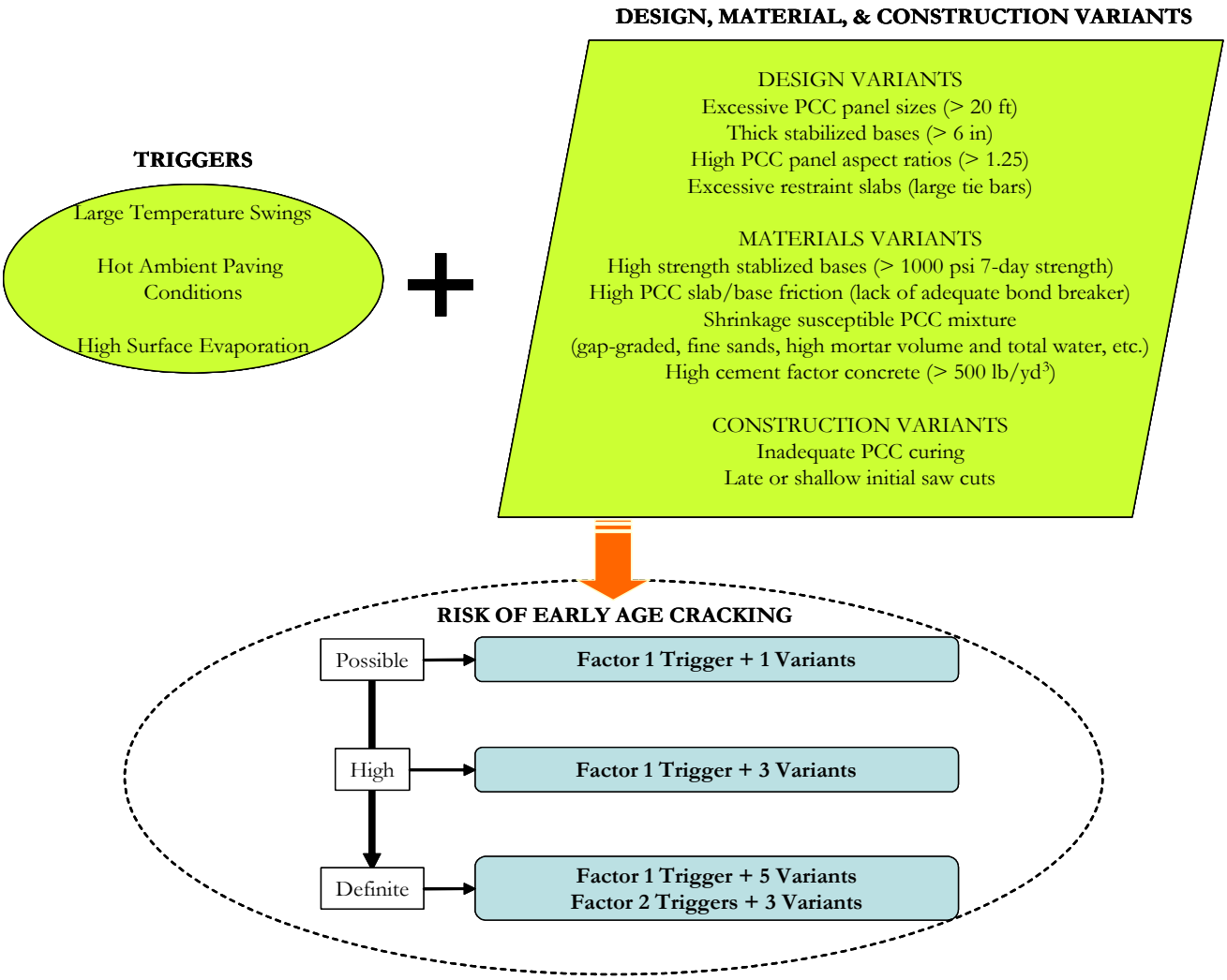


**Figure 3.2 Chart. Quantification of risk of early restraint cracking in rigid pavements (ACPA 2005). Note: To this list must be added additional triggers such as solar radiation.**

## 3.2 Early Age Dowel and Tie Bar Cracking Due to Concrete Subsidence or Settlement

Another trigger not directly included in JP010P is the differential settlement of the concrete, particularly in high slump mixtures. Immediately following consolidation and finishing of the concrete, bleed water rises to the top as the higher density constituents such as aggregate and cement tends to settle. Rigid inclusions such as tie bars and dowel bars can hinder this settlement above the bars resulting in subsidence or settlement cracks. Voigt (2002) indicated that these partial-depth cracks run parallel to and directly over embedded dowel or reinforcing bars (Figure 3.3). At the time of initial set, the high-slump concrete over the embedded bars causes surface tears if the near-surface concrete has dried (or "crusted") in relation to greener interior concrete. The rigid bars prevent uniform subsidence. If detected early enough, these cracks can be removed by reconsolidating the concrete with a spud vibrator. Subsidence cracks do not generally occur with low-slump concrete.

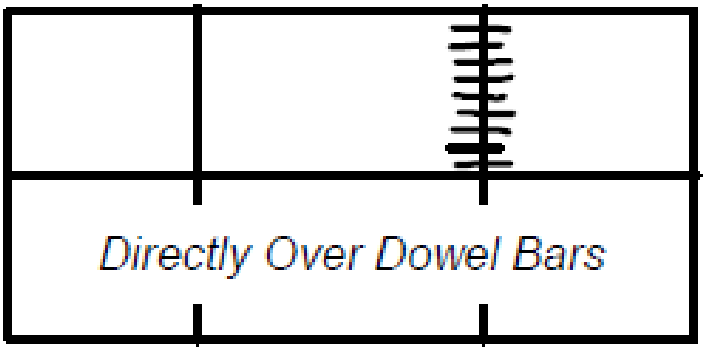


**Figure 3.3 Illustration. Subsidence cracking (Voigt 2002).**

The basic mechanism of settlement cracking is that concrete has the tendency to settle after placement and finishing while steel rebar is held steady. If this settlement is restrained by steel rebar or any obstacles, cracks will form at the concrete surface (Figure 3.4) (CCAA 2005). The magnitude of tensile stress generated by concrete settlement combined with the impact of plastic shrinkage and autogenous shrinkage may be sufficient to initiate cracks (CCAA 2005). Settlement cracks typically occur once the concrete has been placed up to the initial setting time of the concrete and their time of appearance ranged from 10 minutes to 3 hours after placement (TRB 2006, Combrinck and Boshoff 2014). These cracks may become visible while concrete is still in a plastic stage, thus remedial measures can be taken.

Settlement cracks are typically distinguished from other cracks by their unique pattern, which follow the pattern of restraining elements (e.g., reinforcing, dowel bars, tie bars, or a large aggregate). Cracks typically initiate at the surface and continue to propagate down to the restraining elements over time, which could allow the penetration of deicing chemicals to cause severe damage (e.g., spalling or cracking) and corrosion to reinforcing steel, dowel or tie bars. These cracks are sometimes accompanied by a small void below the restraining elements. This void could result in reduced load transfer efficiency by allowing differential slab deflections under traffic loads.

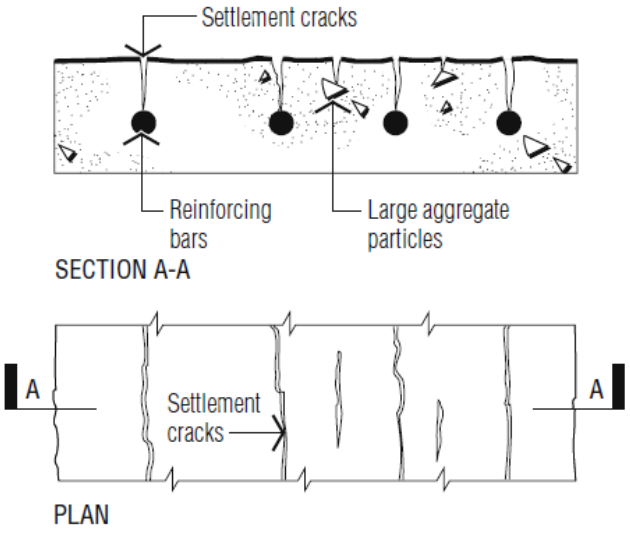


**Figure 3.4 Illustration. Settlement cracking mechanism (CCAA 2005).**

The primary cause of plastic settlement cracks is poor mixture design that leads to excessive bleeding and excessive vibrations and some restraint to the settlement (TRB 2006, Mehta and Monteiro 2006). In the last several decades, many studies of settlement cracks show that there are many factors that can increase or decrease the risk of settlement cracks. A summary of these risk factors for settlement cracks is listed below (Kyle 2001, Antommattei 2018, ACI 224R-01 2001, Dakhil et al. 1975):

- Low concrete cover increases the likelihood of settlement cracks occurrence. According to the ACI 22R-01, settlement cracks in bridge decks can be mitigated by increasing the concrete cover along with mixture proportioning that reduces bleeding and settlement. Since the mechanism of settlement cracks is the same for both bridge and pavement, the ACI's recommendations should apply to pavements as well.
- Concrete consistency/slump that is significantly high increases the risk of settlement cracks. ACI 22R-01 noted that a low-slump concrete is recommended to help prevent settlement cracks.
- Reinforcement bar size and spacing have an impact on the occurrence of settlement cracks. The larger the bar size and spacing between bars, the higher the risk for settlement cracks.
- When formwork is used, movement of the concrete formwork allows plastic concrete to move after concrete placement, which may be sufficient to cause cracks.
- Insufficient consolidation of concrete showed an increase in settlement cracking.
- Poor design, material selections, and construction practices are all causes of settlement cracks.

Dakhil et al. (1975) conducted a study to quantify the effect of cover depth, concrete slump, and reinforcement bar size on the tendency to produce settlement cracks. Although the study investigated the effect of these factors for bridge decks, the findings of this study apply to concrete pavements as well. They found that smaller cover depth, larger reinforcement size, and higher slump result in settlement cracks, as shown in Figure 3.5. However, other studies found no correlation between concrete slump and settlement cracking (Saadeghvaziri and Hadidi 2002, Antommattei 2018).

Dakhil et al. (1975) also calculated the tensile stress over reinforcement bars induced by restraints to plastic settlement by using the photoelastic phenomenon. Photoelastic material (i.e., gelatin) was used to mimic the behavior of fresh concrete settlement due to its weight and its restraint due to obstacles like reinforcement or dowel bars. A photoelastic model was employed to compute the tensile stress due to the uneven settlement of fresh concrete for various bar size, spacing, and cover depths. They found that the effect of restraint on the settlement was noticeable at the surface of the concrete samples. The tensile stress occurred above the reinforcement that ranged from 0.30 to 1.20 psi as the depth of cover decreased from 2.0 to 0.75 inches.

Kyle (2001) cast concrete specimens with #5 reinforcement bars and various cover depths, bar spacing and two concrete mixture types to determine the influence of epoxy coated reinforcement, cement type and bar spacing on the probability of subsidence cracking. No significant difference in the probability of cracking of concrete between concrete cast with epoxy coated reinforcing steel and bare reinforcing steel was observed. Concrete subsidence cracking was however found to be dependent on the clear cover depth and cement type.

The amount of settlement of mortar occurring between the time of placement to setting was determined (TRB 2006, Kayir and Weiss 2002). The results showed that the amount of settlement was significantly impacted by the mixing and placement time, and a drop of 50 percent of settlement was observed when mixture placed immediately as opposed to a mixture placed after 40 minutes. Qi et al. (2005) quantified the settlement of fresh concrete using a non-contact laser system on the surface area of the concrete. This system can measure the settlement over time from placement to set. Concrete specimens with various cover depths and fiber reinforcement were tested to understand the impact of these factors on differential settlement. They found that concrete cover thickness had a significant impact on differential settlement and that samples with fiber reinforced concrete exhibited less differential settlement and less plastic cracking over reinforcement bars.

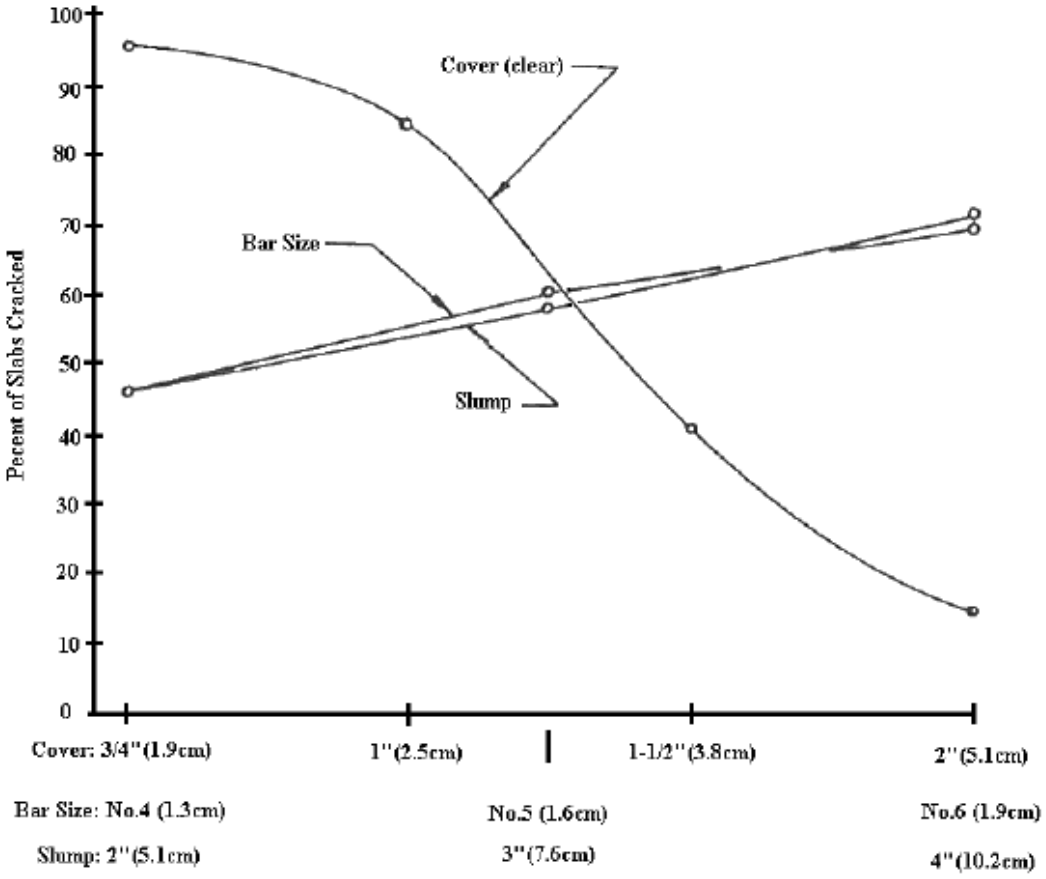


**Figure 3.5 Chart. Cracking as a function of bar size, slump, and concrete cover (Dakhil et al. 1975).**

A more recent study evaluated the impact of slump and the inclusion of fibers on settlement cracking (Brettmann et al. 2015). A laboratory test procedure was developed to examine the concrete specimens prepared with additives (e.g., synthetic fiber or rheology modifier), different slump values ranged from ½ to 9 inches, and various methods of finishing and curing. The study concluded that the addition of fiber or rheology modifier to normal concrete decreases settlement cracking, and settlement cracks

increases as slump increases. Concrete specimens cured with hard plastic and enclosed in plastic sheeting for 24 hours after placement eliminated the effect of plastic shrinkage cracking compared to other curing techniques.

Combrink and Boshoff (2014) conducted laboratory tests to investigate the formation of plastic settlement cracks, the influence of cover depth, and the spacing of the reinforcement bars on the cracks' behavior. They found that vertical cracks started from the surface of the concrete and then propagate downward above the bar, as shown in Figure 3.6. Shear stress caused the crack to initiate at an angle of about 42 degrees on both edges of the rebar. These shear cracks formed from the bottom upward and were not visible from the surface. They concluded that vertical and angle cracks resulted because of the difference in settlement between the solid particles and reinforcement bar and that the vertical cracks appeared before angled cracks. Settlement cracks increased as the cover depth and bar spacing decreased.

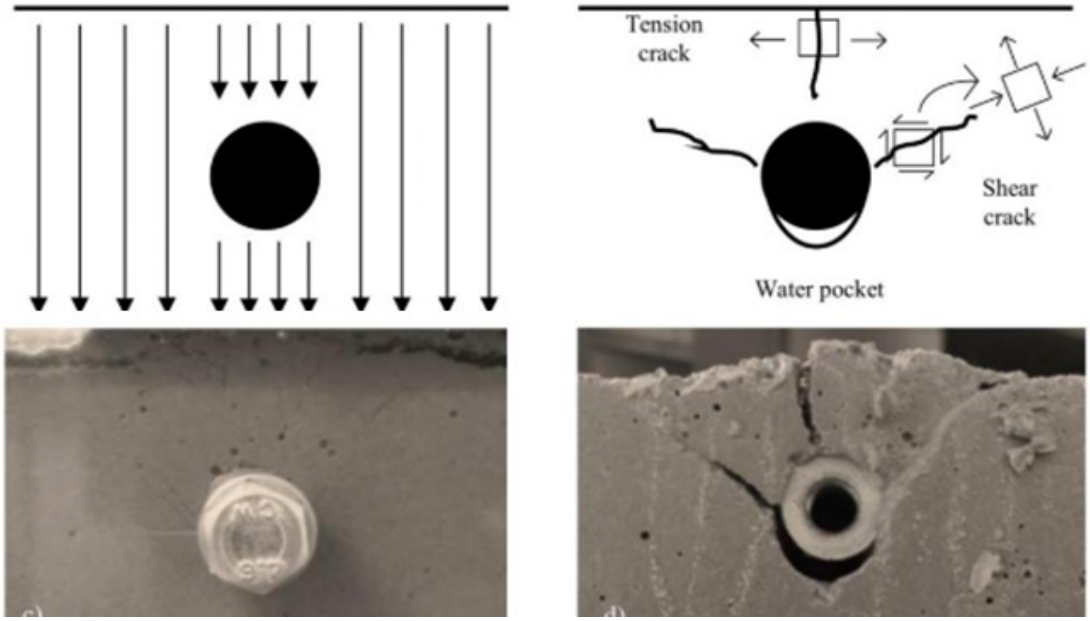


**Figure 3.6 Illustrations and Photos. Settlement cracks caused by a reinforcement steel bar (Combrink and Boshoff 2014).**

There are several methods to prevent settlement cracks, which include reduction of bleeding, reduction of tendency for settlement by providing adequate impediments to settlement, and revibrating of concrete (Mehta and Monteiro 2006). Bleeding results from the lack of ability to maintain all mixing water in a dispersed state as the solid particles settle (Mehta and Monteiro 2006). Bleeding is a form of segregation since solid particles tend to settle down due to gravity. It is important to reduce the tendency for bleeding in a concrete mixture to avoid settlement cracking and plastic shrinkage cracking. The bleeding rate of concrete can be reduced by using various methods including low water-to-cementitious (w/cm) ratio, use of fine cement particles, silica fume, air-entraining admixtures, and superplasticizers (Soroka and Ravina 1998, Khajehdehi 2018). The use of fine cement particles improves the hydration process and minimize the settlement of the paste while silica fume, air-entraining

admixtures, and superplasticizers reduce water-to-cementitious ratio along with other mixture improvements.

Since reinforcement bars are inherent in the design of structures, tensile stresses that occur over reinforcement bars cannot completely be eliminated. Several studies identified practical solutions to mitigate the risk of settlement cracks related to concrete mixtures and construction (Saadeghvaziri and Hadidi 2002, TRB 2006, Safiuddin et al. 2018, Antommattei 2018). These solutions include:

- Develop good quality concrete mixtures with lower bleeding characteristics, lower slump, and more consistent mixture. The addition of fibers to concrete has shown promising results in reducing settlement cracks.
- Avoid a longer setting time, for example by using retarding admixtures, when concrete is exposed to low temperature environment.
- Pre-wet the subgrade prior to placing concrete to prevent excessive water loss through foundation support of the concrete.
- Properly compact, vibrate, and cure the concrete.
- Stabilize formwork (if used) to avoid cracks that may appear if formwork starts moving during placement.

Settlement cracks have a significant impact on the durability of concrete since it has the potential to accelerate the rate of corrosion from the penetration of chemical agents and then, spalling or other deteriorations of concrete can occur. Over time, these cracks will continue to propagate due to volume changes caused by shrinkage (Combrinck and Boshoff 2014, Safiuddin et al. 2018). Revibration and refinishing of concrete can be used to eliminate these cracks while concrete is still in a plastic stage. However, this method could be time-consuming and labor-intensive when used for large areas (Combrink and Boshoff 2014). If cracks are observed after the concrete has hardened, these cracks may be filled with proper materials.

## 3.3 Early Age Dowel and Tie Bar Cracking due to Plastic Shrinkage

Plastic shrinkage cracking results from several factors including evaporation, autogenous shrinkage, and plastic settlement (Qi et al. 2005). Plastic shrinkage cracks appear on the surface soon after concrete placement when the concrete surface dries because the rate of evaporation exceeds the rate of bleeding. Plastic cracks typically appear as hairline cracks and then propagate in size as restraints (such as from dowel bars and tie bars) increase over time (Balakumaran et al. 2018). These cracks can be mitigated or eliminated by reducing the loss of evaporation from the surface and using proper concrete mixtures and curing techniques. Table 2.1 provides the primary cause and time of appearance for the most common concrete cracks (TRB 2006).

Concrete undergoes volumetric changes due to environmental loads and will exhibit no cracks if it is free to move. Shrinkage in hardened concrete is caused by the loss of moisture from concrete surfaces. The development of concrete strength (cracking resistance) versus residual stress generated from restraints

is shown in Figure 3.7a. Cracks will initiate if the strength of concrete is lower than the residual stress. The residual stress is a function of free shrinkage, creep, and relaxation effects and cannot be computed by multiplying free shrinkage by the elastic modulus since stress relaxation occurs. Stress relaxation is defined as a reduction in stress under constant deformation, and creep is defined as a time-dependent deformation due to constant load. When a specimen is restrained and cannot deform, residual stress induced by restraining drying shrinkage will decrease due to creep or stress relaxation, as illustrated in Figure 3.7b (ACI 224R-01 2001). The creep relaxation reduces with age so that cracks will tend to become greater with increased time (ACI 224R-01 2001). The correlation between free shrinkage, restraints, and reduction in stress can be explained in six steps (Figure 3.7b):

1. Initial specimen length: the specimen length is decreased as it loses moisture.
2. Shrinkage effect: if the specimen is unrestrained, there will be a decrease in length (ΔL+) due to drying shrinkage; thus, cracks will not occur.
3. Restraint effect: It is assumed that the change in specimen length is fixed, and a force is applied to prevent shrinkage movements.
4. Creep effect: if the specimen is assumed to increase freely in length due to creep effect and the length of specimen would increase by (ΔL-).
5. Stress relaxation: It is assumed that the change in specimen length is fixed, and an opposite force/stress is applied.
6. Final stress state: the final stress is reduced by the effect of street relaxation. The reduction of the magnitude of the final (net) stress ranges from 30 to 70 percent due to the effect of creep.

In general, concrete experiences shrinkage over its lifetime, and creep typically occurs at the same time, especially during concrete placement (Kovler 1999). Tensile stress due to shrinkage is developed, and these stresses induce additional creep that counters the effect of shrinkage (Jeong and Zollinger 2005). Tensile stress due to shrinkage can be calculated by considering three terms: free shrinkage, effective modulus of elasticity, and degree of restraint, which is used to evaluate the tendency of concrete to either crack (e.g., tensile stress exceeds tensile strength) or to shrink without potential cracking (Nadelman et al. 2017). The creep effect is included as a part of the effective modulus of elasticity.

The cracking mechanism due to drying shrinkage is illustrated in Figure 3.8. The figure shows that if concrete pavement is free to shrink, concrete exhibits no cracks. The friction between pavement and subbase is always present and its magnitude largely depends on subbase types (e.g., unbound or stabilized). Dowel bars and tie bars also act as restraints to shrinkage. In addition to drying shrinkage, tensile stress driven by thermal movements should be considered. These movements can be caused by changes in temperature due to air temperature, heat of hydration, sunshine, cooling rate, and solar radiation. Most early age cracking of concrete occur before the concrete hardens and immediately after hardening due to many factors. These factors include shrinkage in fresh and hardened concrete, thermal movement, poor design, and construction practices (Krauss et al. 2017).

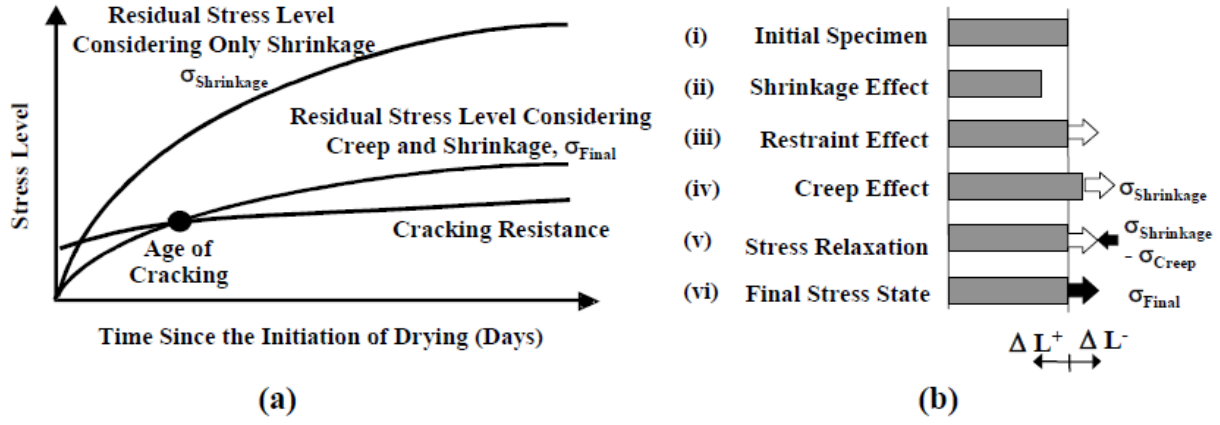


**Figure 3.7 Chart and Illustration. (a) Stress development and (b) conceptual description of relaxation (TRB 2006).**

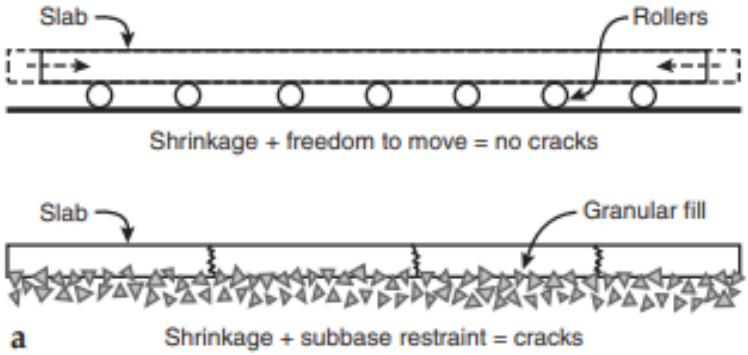


**Figure 3.8 Illustration. Shrinkage and cracking (Kosmatka and Panarese 2011).**

## 3.4 Early Age Dowel and Tie Bar Cracking Due to Misalignment

The development of initial cracking (cracks form when the concrete is hardening) will not be affected by the presence or misalignment of dowel bars (Kumar and Mathur 2009). However, after the transverse joints are formed, dowels that are significantly out of alignment can result in lock up of portions of transverse joints, which then become a factor of restraint. These restraints may create a non-uniform transverse joint face increasing the risk of cracking due to locked joints.

Rao and Premkumar (2020) conducted magnetic imaging tomography (MIT) scanning on 121 Specific Pavement Studies-2 and 3 General Pavement Studies-3 Long-Term Pavement Performance (LTPP) test sections. Dowel alignment parameters such as joint score, and equivalent dowel diameter were calculated as part of the analysis. Statistical analysis was performed to determine any relationship between the joint score and cracking and between the joint score and spalling. The analysis did not indicate any definitive relationship between the joint score and cracking or the joint score and spalling

within the analysis range for most States, although some effect was observed for three States. They concluded that this lack of relationship does not mean severely misaligned dowels have no effect on pavement performance, particularly localized distresses. While dowel misalignment may be a contributing factor, its effects were found to be secondary, as there are many other factors that affect pavement performance. However, they acknowledged that restraints caused by severe misalignments may contribute to added dowel-concrete bearing stresses. These added stresses may result in higher risk of cracking and spalling.

## 3.5 Delamination Cracks Over Dowel Bars and Tie Bars Due to Chloride Penetration

The main cause of corrosion of dowel bars and tie bars in concrete is deicing chemical agents such as sodium, calcium, and magnesium chlorides (Harrington et al. 2018). Chloride ions will penetrate the protective oxide film easier than other ions, leaving the dowel bars and tie bars vulnerable to corrosion. The penetration rate of chloride ions into concrete depends on many factors including the permeability of the concrete and the amount of applied chlorides on concrete surface. If steel reinforcement in the concrete has no corrosion coating or has defective coatings, in the presence of moisture and oxygen, eventually the concentration of chlorides on the reinforcing steel will cause corrosion, which can result in delamination/spalling (Figure 3.9).

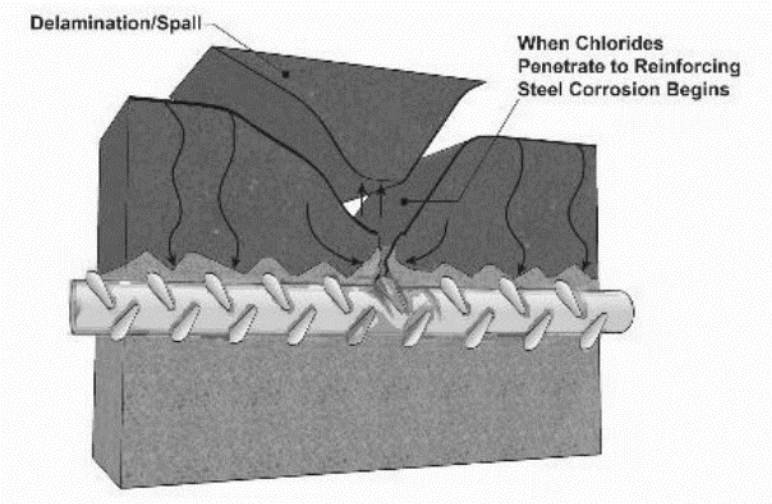


**Figure 3.9 Illustration. Delamination/spalling of deformed tie bar due to applications of chlorides from deicing salt (Harrington et al. 2018).**

## 3.6 Tie Bar Cracking Due to Over-Reinforcing of Tied Longitudinal Joints

The inclusion of too many or too large tie bars can over reinforce the joint and offset the effects of joint sawing to create a weakened plane for joint formation (Harrington et al. 2018). In such cases, a crack often forms 18 to 24 inches from the joint, just beyond the ends of the tie bars (Figure 3.10). This type of

condition sometimes results from the use of a standard one-size-fits-all tie bar design, without regard for panel thickness, friction, bond between the slab and base, or the distance the nearest free edge. This type of cracking can usually be avoided by performing a proper tie bar design, i.e., one that considers the primary factors that influence tie bar design at any given longitudinal joint.

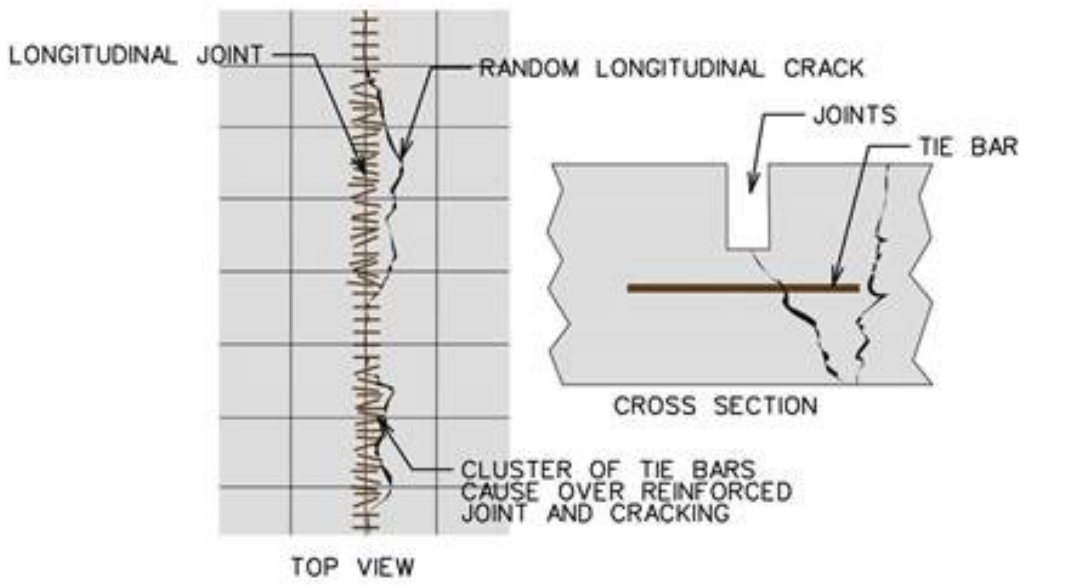


**Figure 3.10 Illustration. Longitudinal cracking along the ends of tie bars on a 7-inch concrete containing tie bars that were clustered together resulting in reinforcing the joint (Harrington et al. 2018).**

## 3.7 Tie Bar Cracking Due to Tying New Lanes to Existing Lanes with Activated Transverse Joints

Longitudinal cracking has been associated with construction of tied concrete shoulders or added tied concrete lanes arising from longitudinal temperature-related expansion in the existing concrete pavement lanes. This cracking potentially happens when the new lanes or shoulders are constructed during cooler weather and well after the construction of the existing lanes (Harrington et al. 2018).

When concrete pavement is constructed during the summer months, it can experience both drying shrinkage and thermal contraction. In many cases, only some of the pavement transverse joints will have activated a short time after placement, creating what are sometimes called “dominant transverse joints” at regular intervals. These dominant joints open much wider than they would have if all the joints were active joints. During warm weather, thermal expansion drives all the transverse joints in the hardened concrete towards a fully closed condition. Dominant mainline pavement joints cannot close all the way because the adjacent transverse joints in the newer tied concrete lanes or tied shoulder close completely, thereby restraining the dominant joints from closing completely and causing very large shear stresses to build along the tied longitudinal joint interface (Figure 3.11).

If the newer concrete (lane or shoulder) is of similar strength to that of the older concrete lane, a shear fracture initiates at the transverse joint of the older concrete, often directly over the dowel bar. Dowel bars reduce the effective thickness at that location, creating a plane of weakness as seen in Figure 3.12. This type of cracking may be mitigated by (Harrington et al. 2018):

- Paving adjacent lanes when all existing lane joints are uniformly activated and of similar narrow width (e.g., paving in warmer weather).
- Plunge-cutting new pavement transverse joints to provide a width that is similar to that of the existing pavement joints (to eliminate restraint of existing pavement joint closure in warmer weather).
- Using no more tie bars than necessary and providing as much distance between the joint and the first tie bar on either side as possible. The use of isolation or bond-breaking material along the joint between the tie bars may also be effective in reducing stress concentrations along the joint.

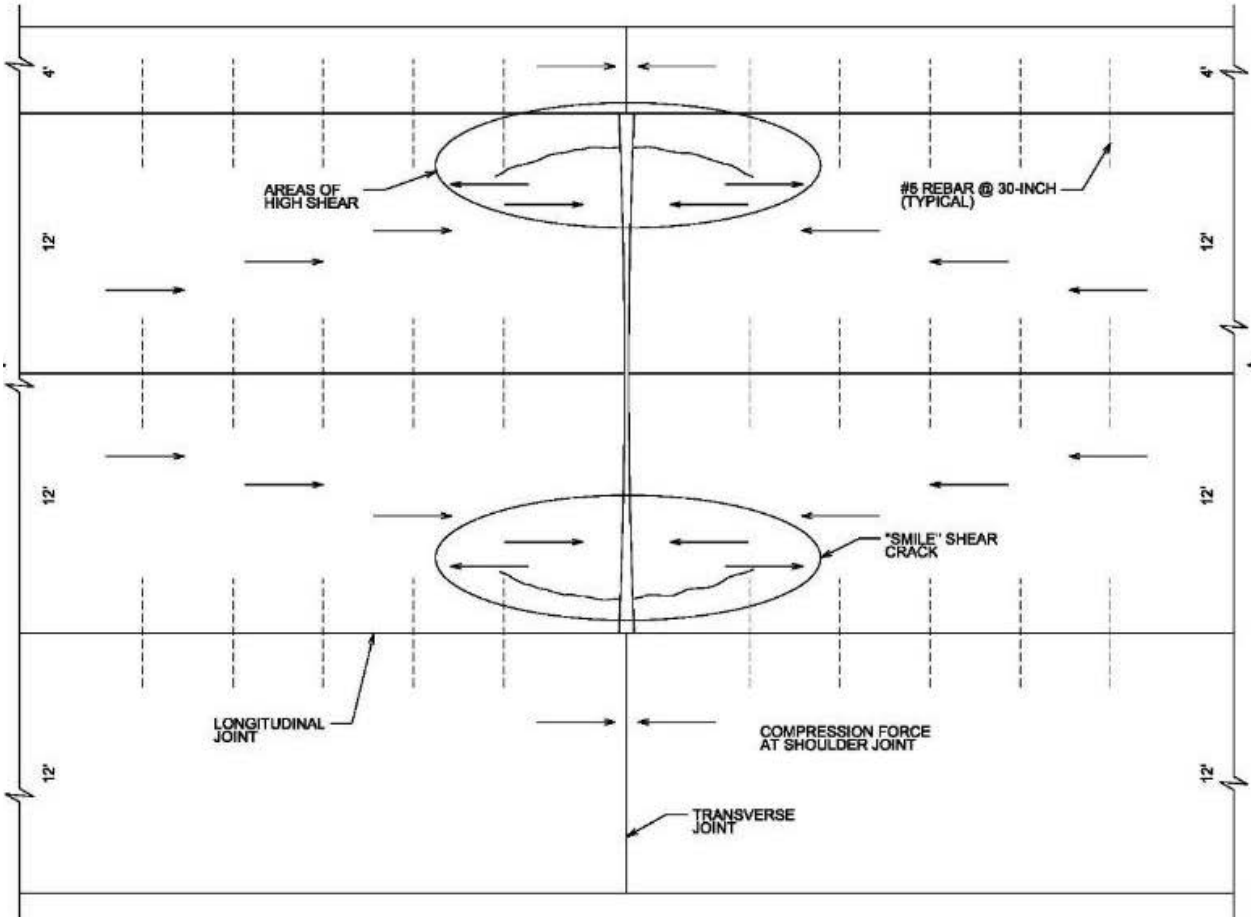


**Figure 3.11 Illustration. Longitudinal cracking in a pavement lane with activated joints when joint movement is restrained by tying on a new adjacent lane (Harrington et al. 2018). Figure depicts existing 12-foot lanes (middle of figure) with the addition of new 12-foot outside shoulder (bottom of figure) and new 4-foot inside shoulder (top of figure).**

**Figure 3.12 Photo. Longitudinal shear restraint crack of dowel initiating over dowels at two locations on opposite sides of the joint (Harrington et al. 2018).**

# Chapter 4: Literature Case Studies of Dowel and Tie Bar Propagated Cracking

## 4.1 Wisconsin

Premature distresses of doweled jointed plain concrete pavement (JPCP) were observed at I-90/94 in Juneau and Sauk Counties in Wisconsin, approximately 5-years after pavement opened to traffic (Rasmussen et al. 2007). The primary distresses include corner cracks, delamination/horizontal cracks, and mid-panel cracks. The JPCP was built in 1992 by two different paving contractors who used dowel inserters for some portions of the roadway and dowel baskets for other portions of the roadway. The JPCP structure consists of a 12-inch PCC over a 4-inch cement-stabilized open-graded base course over an existing 4- to 9-inch dense-graded aggregate subbase. Joints were doweled using 1.5-inch diameter dowel bars and skewed with random joint spacing that varied from 12 to 20 feet. The passing lane consists of 12-foot-wide concrete slabs and the traffic lane consists of 14-foot-wide slabs (with 12-foot lanes) along with an asphalt concrete shoulder.

Field investigations were conducted on a 15-mile section to identify the causes of these distresses. These investigations include visual surveys, coring, deflection and profile data, and other test results. A 3-dimensional (3D) finite element (FE) analysis was also performed to assess the impact of several factors that correlate with the observed distresses. A field visit was conducted in 2006 during the replacement of the distressed pavement to inspect the damaged slabs. Figure 4.1 and Figure 4.2 show the removed damaged slabs with horizontal delamination at the dowel bar level and the condition of dowel bars. The key findings of the field visit include:

- Horizontal delamination was observed at the dowel bar level on both damaged and undamaged slabs. The majority of delamination occurred on the acute angle of the slab and extended up to 5 feet from the slab corner before appearing as a surface crack.
- The condition of dowel bars on the damaged slab showing ineffectiveness of epoxy coating that may have contributed to corrosion of the dowel bars. This could be a factor that initiated the delamination cracks which were then worsened by the impact of repeated heavy traffic loads.
- Corner cracks were widely observed to occur on the acute angle. Skewed joints are no longer used in Wisconsin since they have an increased potential to exhibit corner cracking.
- In some locations, delamination had occurred prior to the development of corner cracks, which may eventually manifest in the form of corner cracks.
- The majority of distresses occurred in the outer lane. Heavy traffic loads in the outer lane may have exacerbated the microcracks that generated at the weakened plane at the dowel bar level and further propagated to the surface as corner cracks or spalls.
- The source of weakened plane may be attributed to many factors including curling and warping and other restraint variables such as dowel bars and weight of the concrete slab.
- Laboratory testing of concrete cores didn't show poor consolidation below mid-depth of the slab.

The effect of curling and warping restrained due to dowel bars were also assessed since they have a significant impact on the occurrence of delamination, corner cracks, and mid-panel cracks. Stresses caused by environmental loads due to temperature and/or moisture changes can detrimentally impact the occurrence of delamination cracks from the restrained movement of slab edges and corners as shown in Figure 4.3. The upward curling or warping and the weight of the slab along with various restraint factors such as dowel bars result in high concentration stresses around dowel bars and high tensile stresses at the top of the slabs. The higher the upward curling, the higher the stresses around the dowel bars and at the top of the slab. The combination of heavy traffic along with curling/warping effects can accelerate the propagation of horizontal crack that initiated at the weakened plane in the slab (Rasmussen et al. 2007).

**Figure 4.1 Photo. Corner crack showing delamination at dowel depth level and the difference conditions of dowel bars (Rasmussen et al. 2007).**

**Figure 4.2 Photo. Dowel bar conditions showing ineffectiveness of epoxy coating and abrasion (Rasmussen et al. 2007).**

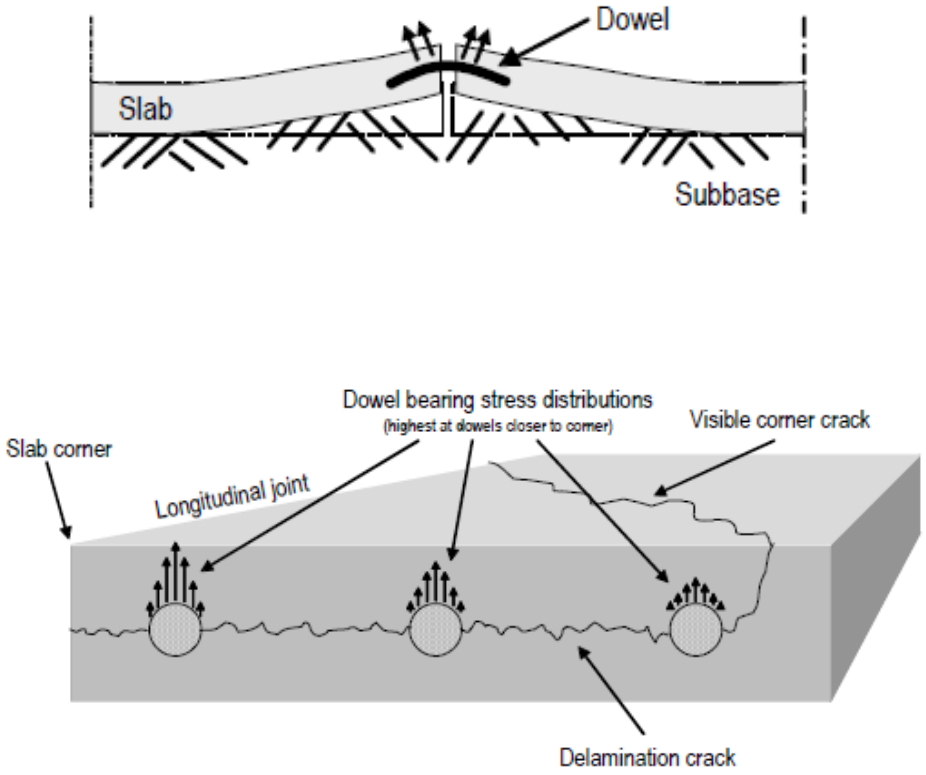


**Figure 4.3 Illustration. Corner cracking mechanism due to dowel bearing stresses (Rasmussen et al. 2007).**

A 3D FE analysis was conducted to assess the impact of joint spacing and the presence of dowel bars on the magnitude of the stresses generated due to restraints. The 3D FE results indicated that the longitudinal edge mid-panel stresses at the top of the slab increased by 25 percent compared to slab without dowel bars due to negative temperature gradients of 1 °F/inch. Longer joint spacing also exhibited up to 10 percent higher longitudinal edge mid-panel stresses when the joint spacing increased from 18 to 20 feet.

Sensitivity analysis using the 3D FE models showed that stress concentrations along the plane of weakness occur near slab edges and especially at slab corners. The stress decreases in magnitude with greater distance from the discontinuity (such as a dowel bar). Rasmussen et al. state that higher than normal deflections resulted from a combination of curling, acute angles (from the joint skew), and an unstable base, which led to a weakness at the slab corners. These, in turn, led to high stress concentrations at the dowels themselves, resulting from a combination of traffic and environmental loading. These loads caused a “prying” effect of one slab upon another (Figure 4.3), which manifested itself in the form of delamination and eventual corner breaks.

Several recommendations were developed to reduce the occurrence of delamination, corner cracks, and mid-panel cracks based on the field visits and results of the numerical analysis as summarized below:

- Smaller diameter dowel bars with alternate dowel bar spacing configurations were recommended to reduce the stresses concentration at the dowel-concrete interface, thus reducing occurrences of delamination crack. The authors acknowledged that several agencies use large diameter dowels (i.e., 1.5 inches) and they may not experience delamination cracking.
- Longer transverse joint spacing of 18 feet or above was not recommended since it increases longitudinal edge mid-panel stresses at the top of the slab. Joints may open wider than normal, which may reduce load transfer efficiency, and increased occurrences of corner breaks.
- It was noticed that the stability of open graded base was reduced due to the use of a uniform gradation resulting in non-uniform and unstable support for the concrete slab. Rasmussen et al. recommended the use of more stable based course with denser gradation.
- Temperature during concrete placement and particularly the time when the concrete starts to solidify is critical as it has a direct impact on the amount of built-in curling and curling and warping effects. Caution should be taken when paving in hot temperatures to keep the concrete temperature from getting too high and by using proper curing methods and timing of curing compound application.

## 4.2 South Korea

Longitudinal cracking at transverse joints caused by dowel bars in jointed concrete pavements in Korea was investigated by Seo and Kim (2012). Field observation and numerical analyses were conducted to ascertain the causes of the longitudinal crack. They observed that longitudinal cracks developed before the pavement was open to traffic. Longitudinal cracks occurred at transverse joints at one side or both sides of the slab as shown in Figure 4.4. Several longitudinal cracks were observed at the joint and the distances between adjacent cracks were consistent. Some longitudinal cracks at the joint were combined with severe spalling. In general, longitudinal cracks were observed near the central area of the slab at the transverse joint.

Concrete cores were taken at the longitudinal crack and MIT scanning was performed to better understand the development of such cracking. A longitudinal crack was exhibited over the dowel bar and the dowel bar was observed to be above the mid-depth as shown in Figure 4.5. A few cores showed horizontal delamination at the dowel bar depth. Concrete cores indicated that the longitudinal cracks did not propagate through aggregates particles, which implied that the cracks occurred during the early age of concrete. The primary factor that caused the occurrence of the longitudinal cracks was attributed to environmental load resulting from temperature and moisture variations across the pavement depth.

**Figure 4.4 Photo. Longitudinal cracks at joint (Seo and Kim 2012).**

**Figure 4.5 Photo. Core taken from longitudinal crack location (Seo and Kim 2012).**

FE models were used to evaluate transverse stresses along the joint when dowel bars were vertically translated, and the slabs curled up under environmental loading. An analysis was performed on a concrete slab having two of the dowel bars located near the slab surface while the remaining of the other dowel bars were located at the mid-depth of the slab. Figure 23 shows the effect of vertical translation of the dowel bar on the transverse stress distribution. The results indicated that dowel bars located above the mid-depth of slab tend to increase the surface transverse stresses. Sensitivity analysis of various factors also were conducted to determine the effects on occurrence of the longitudinal cracks. These factors include concrete elastic modulus, concrete thermal expansion coefficient, foundation stiffness, vertical temperature gradient, bond characteristic between concrete and dowel bar, and depth of the vertical translation of dowel bar.

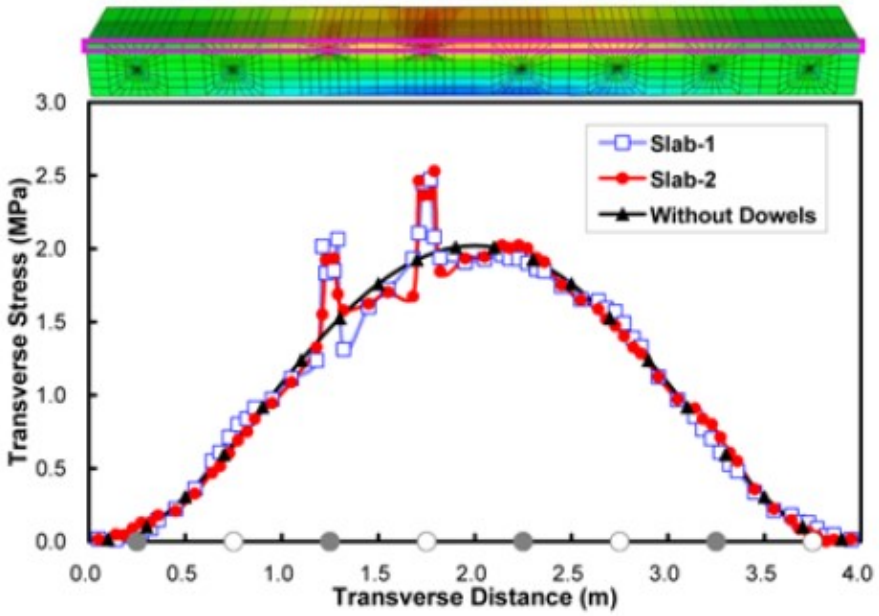


**Figure 4.6 Chart. Effect of vertically translated dowel location on surface transverse stress distribution (Seo and Kim 2012).**

The key findings of the field forensic investigation and FE models are summarized below:

- The results of the field investigation showed that primary causes of longitudinal cracks at joints were found to be related to the vertical translation of dowel bar and the curling of the jointed concrete pavement slab due to environmental loading.
- If a dowel bar is translated above the mid-depth of the slab, transverse stresses at the joint around that dowel location increase, and the stress increment becomes larger when the vertically translated dowel bar location is closer towards the slab transverse center. Accordingly, there is a higher risk of longitudinal cracking when a dowel bar is vertically translated near the slab transverse center.
- When a dowel bar is vertically translated, transverse stresses and the possibility of longitudinal cracking at the transverse joint become larger as the concrete elastic modulus, concrete thermal expansion coefficient, foundation stiffness, vertical temperature gradient, and amount of the vertical translation of dowel bar increases.
- To mitigate longitudinal cracking at the joint, dowel bars should be installed at the mid-depth of the slab and care must be taken when installing dowel bars to prevent vertical translation and provide adequate cover.

## 4.3 Colorado

A mechanistic-empirical tie bar design approach for concrete pavements was developed based on FE modeling. Mallela et al. (2009) conducted a comprehensive literature review on the current method of design tie bar along with its limitations. The current method of tie bar design is based on the concepts of subgrade drag theory. The theory determines the quantity of steel required to drag a concrete slab over

an underlying layer without yielding or pulling out the steel bars. The dragging force is calculated based on the slab thickness, its unit weight, the friction between the slab and the underlying layer, and the distance to the closest free edge of the pavement. Based on this concept, the American Association of State Highway and Transportation Officials (AASHTO) 1993 Guide for Design of Pavement Structures provides charts for estimating tie bar sizes and spacings. However, this method does not take into account the effects of temperature drop, drying shrinkage, and loading conditions on tie bar design when determining the required steel content. The study addresses the following aspects of tie bar and concrete pavement design:

- To maintain the structural benefit of concrete shoulders for given site conditions, what is the required spacing of deformed tie bars, and what is their optimum diameter and embedment length for various longitudinal joints?
- How many traffic lanes and shoulders can be tied together over a wide range of climates and base courses to avoid significant risk of longitudinal cracking?

Researchers collected two types of in-service pavement information related to tie bars. The first type involved gathering anecdotal evidence to (1) identify typical longitudinal joint performance issues that might be predominately attributable to improper tie bar design or construction and (2) determine if tying greater-than-recommended pavement widths increases the likelihood of longitudinal cracking. In addition, field testing was performed on the long-term pavement performance (LTPP) Specific Pavement Studies 2 (SPS-2) national and supplemental experimental sections in some states. These states include Arizona, Missouri, and Colorado. The information gathered revealed that typical joint failures include excessive joint openings, longitudinal joint faulting, and slab slippage. The data supported the notion that well designed and constructed tied joints maintain tight joint openings and high load transfer efficiencies over the life of the pavement. Both design and construction causes for failures of tied joints were identified during the data collection process.

The field investigations were not conclusive regarding the role of tying too many lanes together on pavement distress. Longitudinal cracking was observed on pavements with varying tied widths starting from as low as 24 feet, establishing it as a form of distress that needs to be addressed in design. Figure 4.7 shows an example of a low severity crack above a tie bar, typical of a majority of joints at a Colorado site. Also shown is Test Joint B with a 1.25-inch joint opening and detached sealant. The cause of the crack above a tie bar was not investigated. The pavement section consisted of a 9.5-inch JPCP, a 7- to 10-inch asphalt treated base, and a 10-inch silty sand subbase. The pavement lane width was 12 feet, and the slab length was 15 feet. MIT scanning was performed to determine the tie bar alignment. Tests showed that the mean depth to the tie bars was 3.1 inches in the control joints, shallower than the mid-thickness depth of 4.75 inches. The load transfer efficiency and joint movement data as a function of temperature from this site were evaluated.

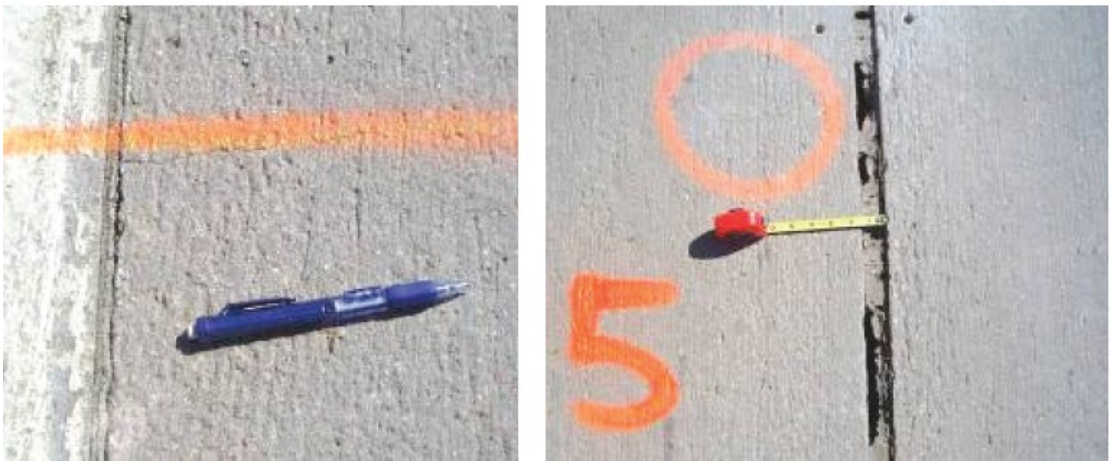

**Figure 4.7 Photo. Control Joint A (left) with low-severity crack above a tie bar and Test Joint B (right) open 1.25 in, showing the detached sealant at the Colorado testing site.**

The impact of multiple tied lanes and shoulder on slab stresses was evaluated by using ISLAB2005 FE model. The model was used to compute tensile stress in the slab that might lead to longitudinal cracking when more than two lanes are tied together due to the applied total equivalent free strains. Cases with different tie bar configurations and base types were selected for evaluation. Figure 4.8 and Figure 4.9 illustrate the tensile stresses that develop in a concrete slab constructed on a cement-treated base due to an applied total equivalent axial free strain of 800 microstrain applied perpendicular to the direction of traffic. The results indicated that the concrete tensile stresses did not increase significantly when three or more lanes were tied. However, a significant increase in stresses was observed when the number of tied lanes increased from two to three (Figure 4.10). In comparing the selected base types, the tensile stresses in the slabs were lowest on unbound bases and highest on lean concrete bases. As the base modulus and friction between the slab and base increased, the tensile stresses in the concrete slabs also increased.

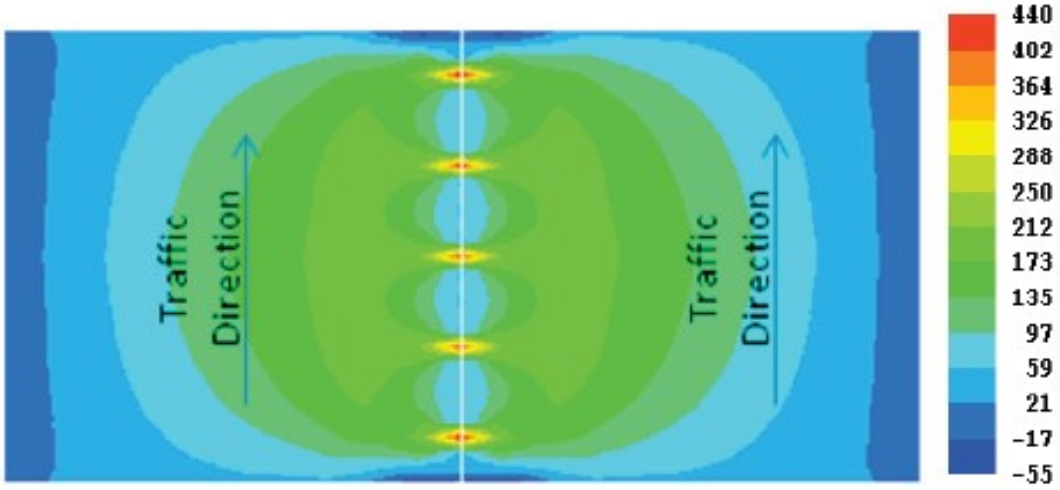


**Figure 4.8 Contour Plot. Tensile concrete stresses; two tied concrete pavement lanes on 6-inch cement-treated base, 800 microstrain equivalent axial free strain in the direction perpendicular to traffic.**

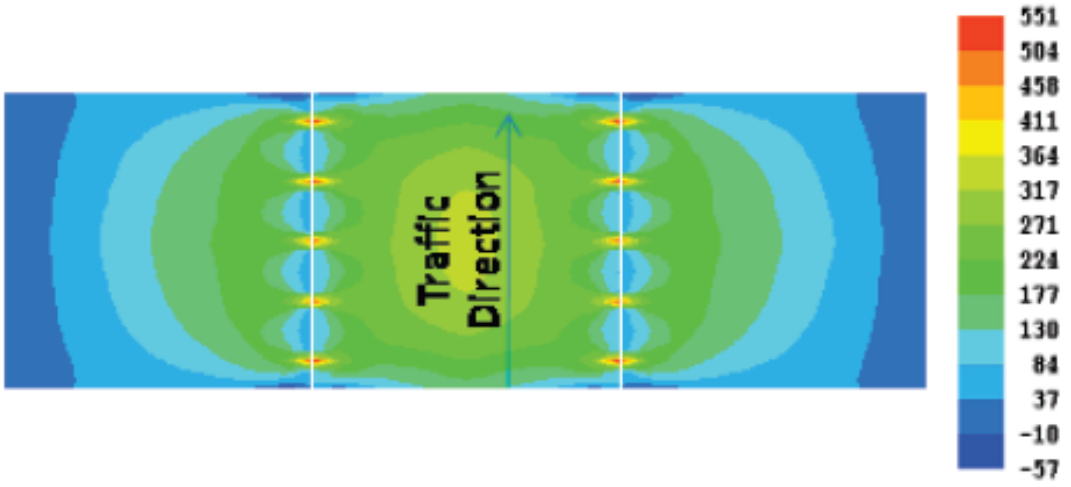


**Figure 4.9 Contour Plot. Tensile concrete stresses; three tied concrete pavement lanes on 6-inch cement treated base, 800 microstrain equivalent axial free strain in the direction perpendicular to traffic.**

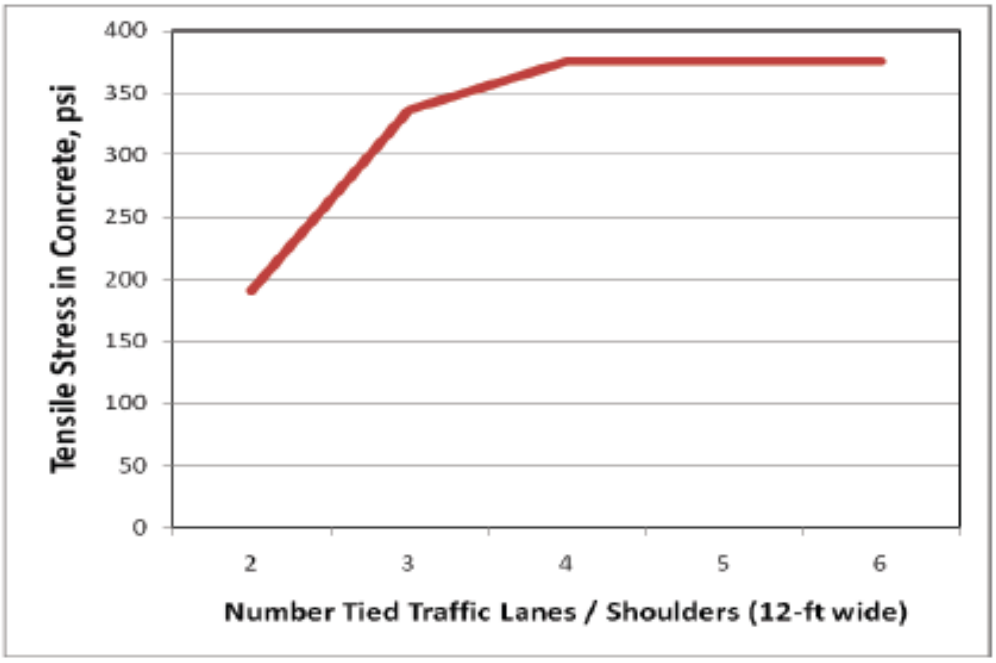


**Figure 4.10 Chart. Tensile stress in the concrete slab built over a cement-treated base vs. the number of tied lanes/shoulders.**

## 4.4 North Dakota and Oklahoma

Tyson et al. (2008) presented issues and solutions related to two types of early age cracking in JPCP: (1) those related to base restraint and curling/warping stresses, and (2) those caused by edge restraint. They state that various factors can affect the risk of early age cracking, including paved width, joint spacing, slab thickness, interface friction, modulus of subgrade reaction, temperature and moisture

conditions during construction, and concrete modulus of elasticity, as well as strength. The potential for this type of cracking diminishes once the saw cuts are made to relieve the restraint stresses. However, if several adverse factors are at work in concrete, it may not be possible to saw early enough to prevent cracking. Figure 4.11 shows the pattern of edge-restraint cracking. Tyson et al. stated that this type of cracking can occur if the tied concrete shoulders are paved at a significantly lower temperature than the temperature at the time of mainline paving. Therefore, the temperature difference at the time of paving shoulders and mainline should be minimized to mitigate the edge-restrain cracking.

A project in North Dakota and another in Oklahoma developed cracking during construction. In both cases, the cracking was attributed to restrained movement. The North Dakota I-94 case study demonstrated the risk of base-restraint cracking. The PCC experienced early age cracking during the reconstruction of a section of I-94 in 2015. The cracking was predominantly longitudinal (Figure 4.12), but transverse cracking and corner breaks also occurred. The pavement is a 9-inch JPCP constructed on a 4-inch cement-treated permeable base and a 4-inch aggregate subbase. The project was 10 miles, but the cracking occurred only on one day's paving in two areas totaling less than 0.5 miles. The cause of cracking was not conclusively determined; however, both the weather conditions at the time of paving and penetration of fresh concrete into the highly permeable, cement-stabilized base were identified as significant factors. Tyson et al. concluded that the cracking experienced on I-94 is characteristic of the base-restraint cracking. Given the limited extent of the cracking problem, it is very likely that the weather conditions during paving played a significant role.

**Figure 4.11 Photo. Characteristic pattern of edge-restraint cracking.**

The North Dakota project demonstrated the potential risk of base-restrain cracking due to the use of a highly permeable stabilized base. The penetration of fresh concrete into the base not only has the effect of bonding the PCC surface to the base to restrain the movement of the PCC surface, the incidence also effectively increases the slab thickness, leaving the possibility of the saw-cut depth being inadequate.

Tyson et al. recommended using either an asphalt layer or geotextile as a separator layer to prevent bonding between concrete slab and cement treated permeable base.

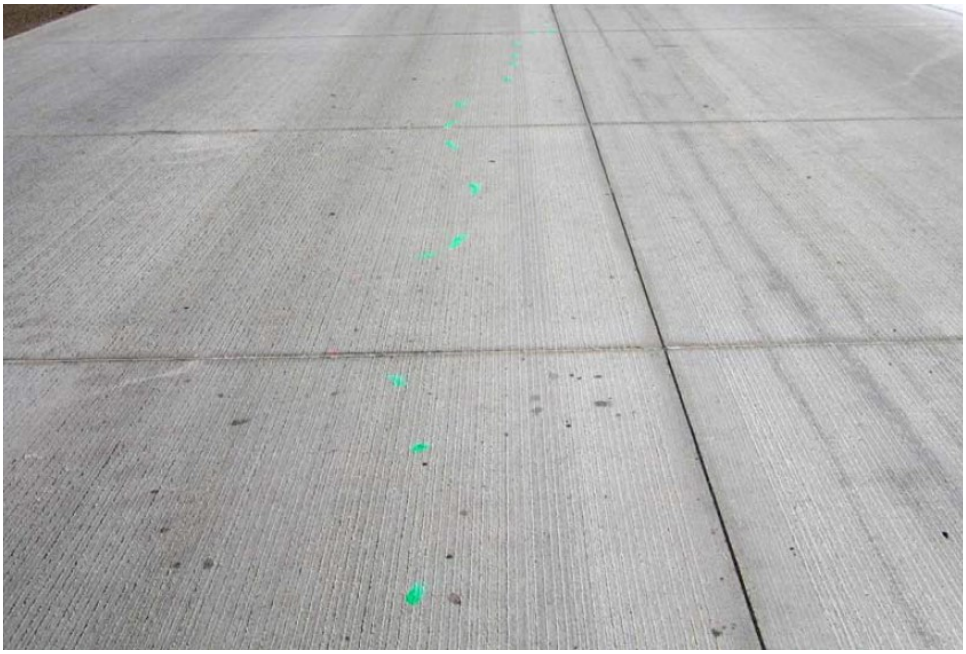

**Figure 4.12 Photo. Early age longitudinal cracking on I-94 in North Dakota.**

The cracking that occurred on I-35 in Oklahoma in 2005 is an example of edge-restraint cracking. The pavement was constructed as an overlay over the existing asphalt concrete pavement. The overlay is 10.5-inch thick, and the transverse joints were sawed at 15-foot spacing. The mainline pavement consisting of two 12-foot lanes tied at the center was placed first. Later, 10-foot outside and 4-foot inside tied concrete shoulders were added. The cracking initiated at the transverse joints and propagated diagonally inward at approximately 30-degree angle, as shown in Figure 4.13.

The Oklahoma DOT investigations into the cause of cracking identified the edge-restraint as the most probable cause of the cracking. The analysis results showed that a temperature difference of 20 to 30 °F between the temperatures at the time of paving of the mainline and tied concrete shoulders would have been sufficient to initiate cracking in the mainline, if the shoulders were placed at the lower temperature. As a result, Oklahoma DOT placed the following restrictions on the paving temperatures:

- Tied concrete shoulders may be placed at equal or greater ambient air temperature than that at the time of mainline paving.
- The ambient air temperature at the time of tied concrete shoulder placement may be no less than 20 °F below that at the time of mainline paving.

Tyson et al. concluded that best way to avoid early age cracking is to avoid high-risk designs and paving conditions; and following the recommended construction practices. The high-risk conditions include the following:

- High friction base.

- Excessive joint spacing.
- High ambient temperature.
- Low ambient temperature.

Proper curing was also stated to be extremely important to prevent excessive warping and plastic shrinkage cracking, especially in hot, dry areas. The awareness of the risks is important to avoid early age cracking, even if the risk is low. If the high-risk conditions cannot be avoided, identify the risks involved and monitor the critical items, which may include ambient temperature, concrete temperature, and concrete strength. Tyson et al. stated that the risk of early age, restraint cracking can be assessed using HIPERPAVE.

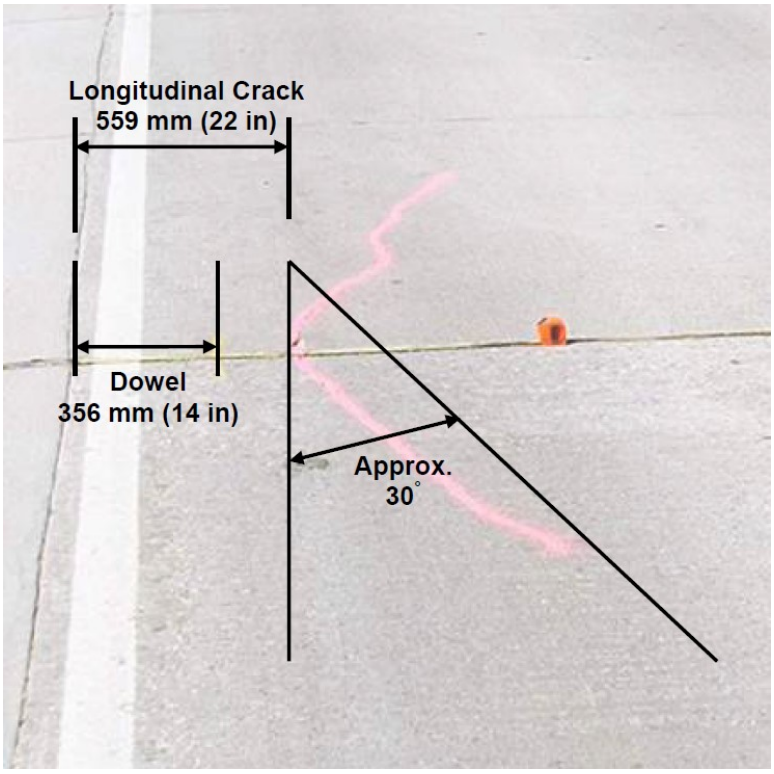


**Figure 4.13 Photo. Longitudinal cracking on I-35 in Oklahoma.**

## 4.5 Bolivia

Darter and Rufino (2007) conducted a forensic study of Tarija-Potosi Highway in Bolivia to determine the cases of premature cracking along with solution for areas that have been cracked. The construction of the concrete pavement of the highway started in September 2005. The pavement structure is 7.5-inch JPCP, 6.0-inch aggregate base course, asphalt surface treatment shoulder, 13.0-feet transverse joint spacing with 1.0-inch diameter dowel bars spaced at 12 inches, and 12.0-feet-wide traffic lane with tie bars across the longitudinal center joint. Longitudinal cracking was observed in some slabs shortly after the initial placement of the concrete and continued to increase over time. Transverse cracking also developed after opening to traffic and increased over time. Longitudinal cracking occurred

approximately in the middle of each lane in each direction as shown in Figure 4.14. Premature longitudinal cracks were mostly top-down as shown in Figure 4.15 and do not cross the longitudinal joint. It was noted that the longitudinal cracks occurred above the dowel bars. The longitudinal joints were observed to have formed properly.


**Figure 4.14 Photo. Cracking pattern when both lanes where placed together.**


**Figure 4.15 Photo. Typical cracking mode: top down.**

Darter and Rufino determined the cause of premature longitudinal cracking by performing three key tests: coefficient of thermal expansion of the concrete, temperature control during setting time, and corner-to-center deflection analysis. The results of the field forensic investigation and analysis performed on causation of the cracking are summarized as follows:

- Cracking was observed in the center of the traffic lanes regardless of whether were placed together or separately. When two lanes were placed together the longitudinal joint was sawed at least 1/3 of the thickness as soon as possible to avoid spalling of the joint. The depth was verified by coring.
- Coring showed that these longitudinal cracks initiated at the top of the slab and propagated downward through the slab.
- Measurement of upward curling of the slabs throughout the project indicated a very large curling (e.g., 0.2 to 0.6 inches).
- Shrinkage (from drying) of the concrete was not measured but could have been a factor in the upward warping of the slabs. An ultimate shrinkage of strain of 683 microstrain was estimated based on mix properties.
- The major possible causes of the upward curling were identified as follows:
    - High built-in negative temperature gradient.
    - High drying shrinkage of the top 1 to 2 inches of the slab.
    - High hourly temperature gradients particularly during the night when the top of the slab is cool, and the bottom is warm (the high elevation creates a very high negative temperature gradient through the night).

## 4.6 SPS-2

Senn K. (2018) conducted a field survey to evaluate the performance of the SPS-2 of the LTPP test sections in Arizona, Colorado, Washington, Iowa, Kansas, and North Dakota. During the site visit, recommendations of pavement preservation treatments were provided for some sections. Cracks over dowel bars were observed in Kansas and North Dakota. It was noted that several sections in Kansas exhibited small longitudinal cracks along transverse joints. These cracks were mostly observed on the 8-inch-thick 900-psi flexural strength sections and aligned over the dowel bars. Also, longitudinal cracks over dowel bars were observed on many test sections in North Dakota that occurred shortly after construction as shown in Figure 4.16. Senn states that “map cracking was commonly present on the 900 psi test sections…” suggesting that the higher flexural strength of the concrete may have had a role in the observed cracking. However, Senn also states that detailed investigations into the reasons for the noted observations have not yet been completed.

**Figure 4.16 Photo. Crack over dowel bars in SPS-2 in North Dakota.**

# Chapter 5: Literature Numerical Analyses and Laboratory Studies

## 5.1 Li et al. (2012)

Li et al. (2012) conducted a nonlinear 3D FE analysis and laboratory study to investigate the interaction between dowel bars embedded in JPCP and surrounding concrete under traffic impact loads in China. According to Li et al., one of the benefits of using a 3D solid element over a 2D element is that it can accurately capture deformation gradients in concrete slab under multiple traffic loads. In the 3D FE analysis, three single axle loads with dual tires, 20kip (10t), 40kip (20t), and 60kip (30t), were applied on a virtual concrete slab to determine the stresses distribution at the dowel-concrete interface. The FE analysis results indicated that the maximum principal stresses are mainly distributed near the upper half-circle contact surface of dowel bars along with vertical and shear stresses distribution, as shown in Figure 5.1.

The 3D model was compared and validated with measured data. Sensitivity analysis of various parameters (e.g., dowel bar diameter, dowel spacing, slab thickness, concrete grades, and base types) was conducted using the validated 3D model to evaluate their effect on the stress distribution between the dowel-concrete interface. The results of the sensitivity analysis showed that the increase in dowel bar diameter, slab thickness, high-grade concrete, and subgrade support capacity has the potential to reduce the stresses at the dowel-concrete interface. Representative dowel-concrete samples were prepared for laboratory testing, and in-house loading equipment was developed to simulate the effect of traffic loads, as shown in Figure 5.2. Strain gages were placed on the concrete samples to measure the strain responses and to compare them with those obtained from the 3D model. The strain results obtained from both the 3D model and laboratory were comparable. Li et al. concluded that the high stresses at the dowel-concrete interface have the potential to cause microcracks that could propagate to the surface.

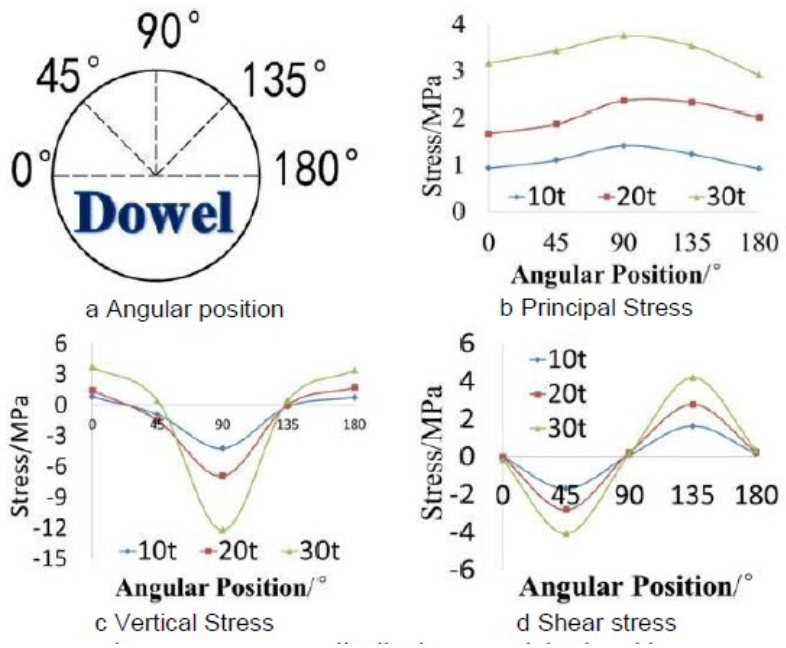


**Figure 5.1 Graphs. The maximum principal, vertical, and shear stresses distribution around the dowel bar (Li et al. 2012).**

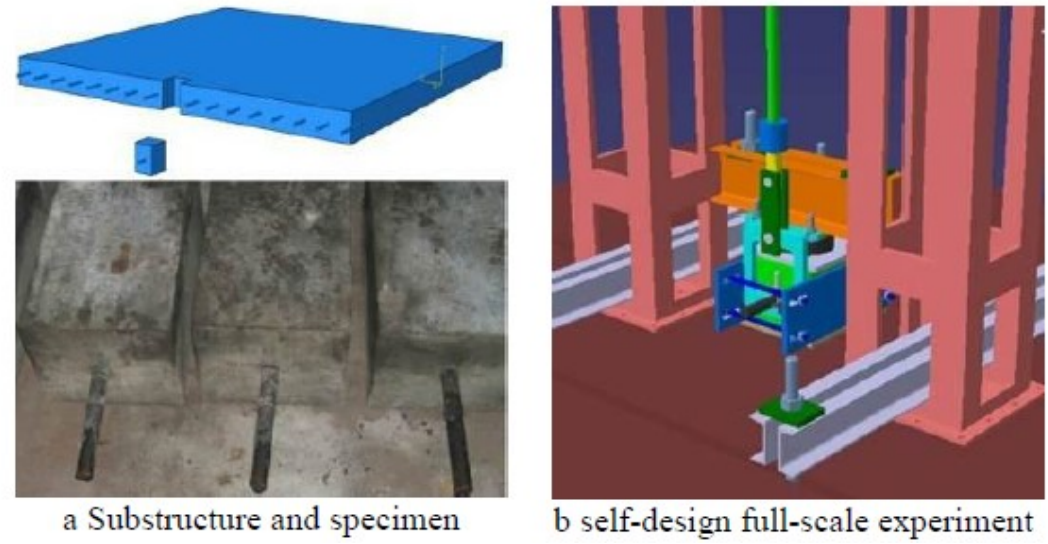


**Figure 5.2 Photo and 3D Graphic. Laboratory dowel bars specimen and loading equipment (Li et al. 2012).**

## 5.2 Shoukry et al. (2004)

Shoukry et al. (2004) also developed a 3D FE analysis and laboratory study to evaluate the stress concentration at the dowel-concrete interface that has the potential to cause microcracks in concrete. The 3D FEM was developed for doweled JPCP over a base and subgrade. The magnitude of stresses at the dowel-concrete interface, under an applied standard axle load at the transverse joint, was calculated

using the 3D FE analysis. High compressive stresses on top of dowel-concrete interface were observed along with high tensile stresses concentration on both sides of the dowel-concrete interface. The magnitude of the compressive stresses was observed to be lower than the compressive strength of the concrete, which will not cause the initiation of concrete to crack. Laboratory testing was conducted to compare and validate the 3D FE analysis results. Figure 36 illustrates the experimental setup. The concrete sample was instrumented with strain gages in the vicinity of dowel bars to measure strain. The strains obtained from the 3D model were compared with those obtained from the strain gages. Shoukry et al. noted that microcracks at the dowel-concrete interface were initiated if the maximum principal stress at the edges of the dowel-concrete interface reaches the value of concrete modulus of rupture. Based on this study, an alternative method was developed by Shoukry et al. to design a dowel bar that reduces the stress concentration in concrete.

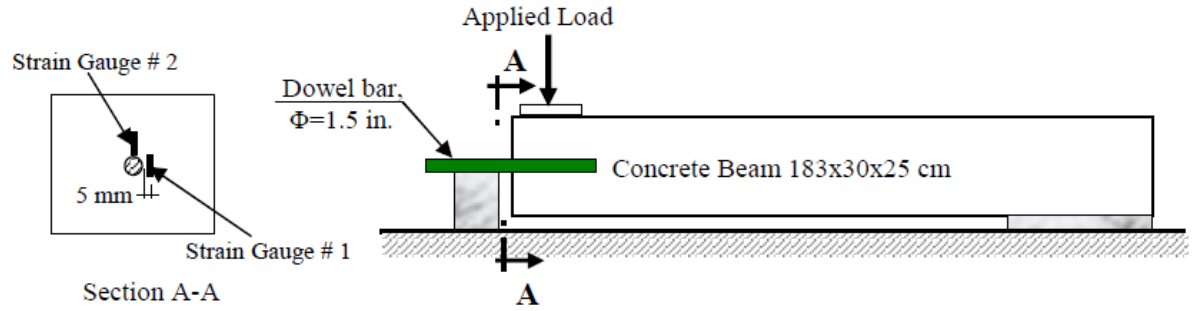


**Figure 5.3 Illustration. Laboratory experimental setup (Shoukry et al. 2004).**

## 5.3 Zuzulova et al. (2020)

Zuzulova et al. (2020) conducted laboratory tests in the Czech and Slovak Republics for doweled JPCP to determine tensile stresses and potential to microcracks at the dowel-concrete interface. Static and cyclic loads were applied on concrete samples with the embedded dowel, as shown in Figure 37. Strain gages were mounted on the transverse joint face of the samples. The locations of the strain gages (SG1, SG2, and SG3) are shown in Figure 38. Concrete samples were also prepared with different embedded dowel sizes and configurations; (1) embedded at the middle of the sample, (2) at vertical translation (downwards 0.8 inches), and (3) at vertical tilt (toward the applied force 0.8 inches) to investigate the impact of different dowel positions on tensile stresses and the risk of concrete cracking in the vicinity of the dowel. Strain measurements were recorded during the test and were converted to stresses through Hooke's law.

Zuzulova et al. indicated that the tensile stresses of a concrete sample with a vertical tilt dowel increased up to 100 percent compared to a sample having dowel embedded in the middle. A concrete sample with a vertical translation of dowel had no effect on tensile stress increase. Figure 39 shows the tensile stress distribution at the face of concrete samples with different dowel sizes obtained from the strain gages under the applied load of 2.25 kips, which is the maximum force that traffic loading may be applied to a dowel. They found that the beam with a dowel bar diameter of 0.8 inches was damaged at a

force of 2.3 kips while the beam with a dowel bar diameter of 1.5 inches was damaged (horizontal crack as shown in Figure 38) when the applied force reached 11.25 kips. As the dowel bar diameter increased, tensile stresses in the vicinity of the dowel bar decreased.

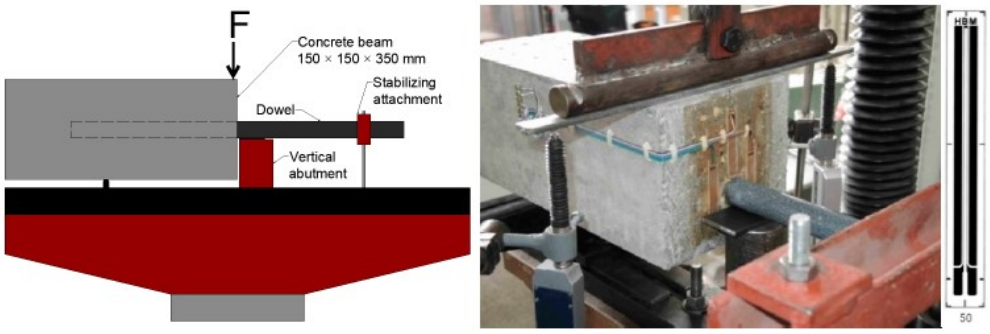


**Figure 5.4 Illustration and Photo. Laboratory experimental setup (Zuzulova et al. 2020).**

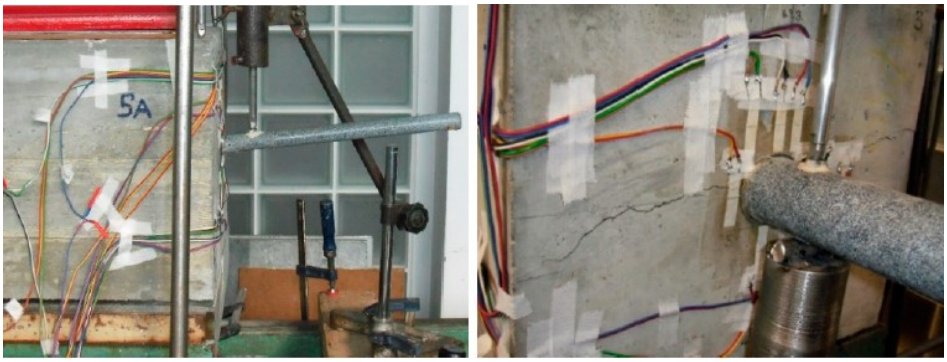


**Figure 5.5 Photo. Normal stresses obtained from strain gauges; (left) beam under loading, (right) horizontal crack through the concrete beam around dowel (Zuzulova et al. 2020).**

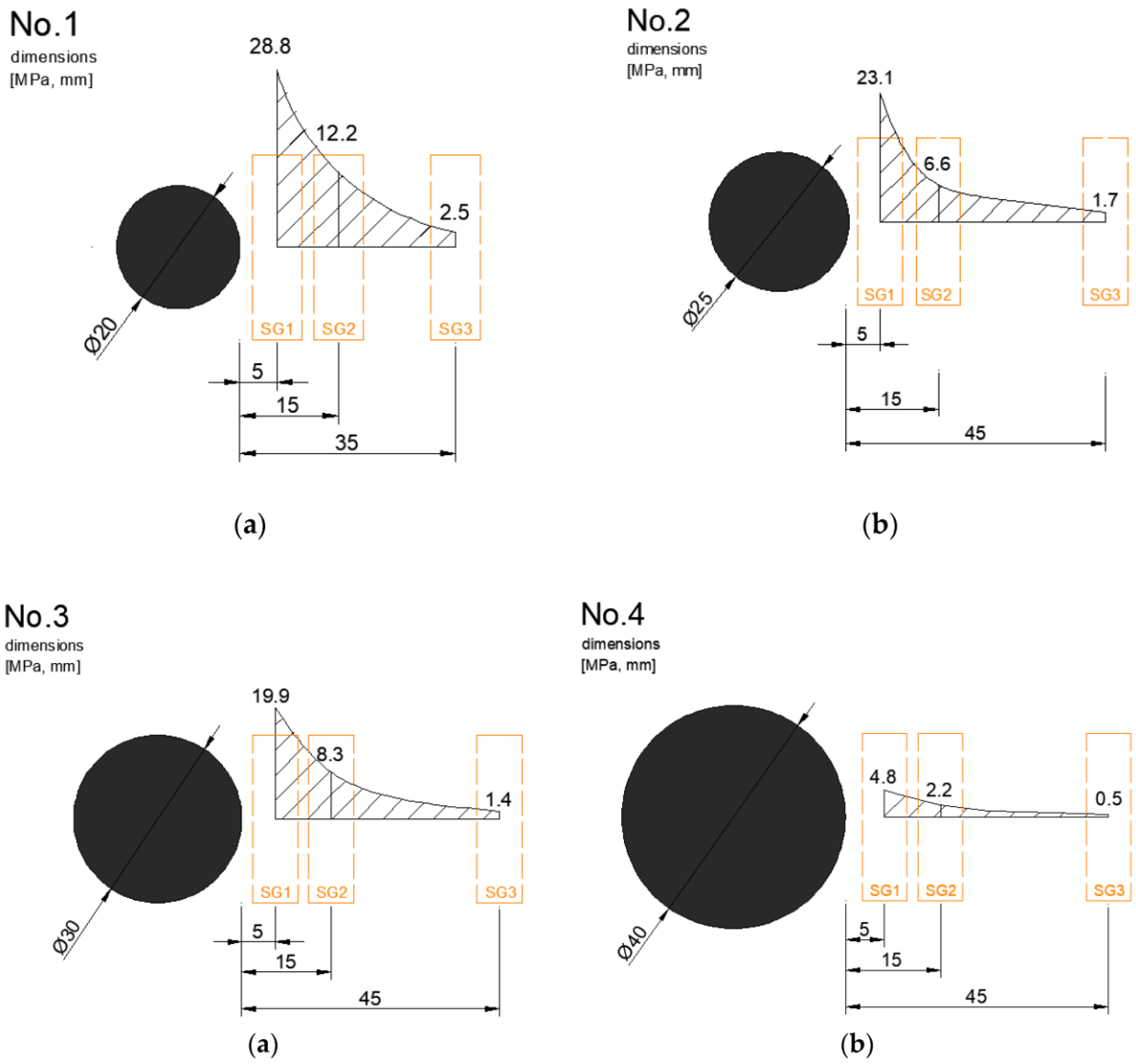


**Figure 5.6 Illustration. Normal stresses obtained from stain gages during laboratory test (applied force 2.25 kips); top left dowel diameter 0.8 inches, top right dowel diameter 1.0 inches, bottom left dowel diameter 1.2 inches, bottom right dowel diameter 1.5 inches (Zuzulova et al. 2020).**

# Chapter 6: Field Sections and Field Experiment Methods

The purpose of the field investigation is to identify and capture potential factors that contribute to dowel or tie bar propagated cracking by inspecting pavements that exhibited such cracking. Under this task, the research team worked with the Technical Advisory Panel (TAP) to identify and select projects for further evaluation.

## 6.1 Candidate Projects for Field Investigation

Based on input from the TAP, six sites were selected for field investigation and further evaluation of dowel/tie-bar propagated cracking. These are listed in Table 6.1.

**Table 6.1 Candidate sites for field evaluation.**

| Site No. | Location | Route | Built | Joint spacing | Thickness | Slab Width | Shoulder |
|---|---|---|---|---|---|---|---|
| 1 | Dane Co., WI | I-39/90 NB | 2006 | 15 ft. | 12 in. | 12 ft. | PCC, 10 ft. |
| 2 | Columbia Co., WI | I-39/90 NB | 2009 | 15 ft. | 12 in. | 12 ft. | PCC, 10 ft. |
| 3 | Columbia Co., WI | I-39 SB | 2004 | 18 ft. | 10 in. | 14 ft. | HMA, 9 ft. |
| 4 | IL Tollway | I-94 WB | 2009 | 15 ft. | 12 in. | 12 ft. | HMA, 9 ft. |
| 5 | Hennepin Co., MN | TH610 | 1999 | 15 ft. | 10 in. | 13 ft. | HMA, 8 ft. |
| 6 | Eau Claire Co., WI | US 53 NB | 2006 | 15 ft. | 9.5 in. | 14 ft. | HMA, 6 ft. |

## 6.2 Field Investigation Techniques

Field investigations were conducted on four pavement sites in Wisconsin, one in Illinois, and one in Minnesota to identify potential causes of delamination and corner cracking propagated from tie/dowel bars. The investigation method included visual distress surveys, coring, and ultrasonic evaluation using the MIRA portable ultrasonic equipment.

### 6.2.1 Visual Distress Survey

Visual distress survey of the selected field sections consisted of measuring the field sections geometry (length and width of the slab panels); documenting type, location and extent of the distresses; and recording additional observations/factors that may have influenced the distress (joint spacing, location of the dowel bar, number of lanes, paving lane construction sequence, types of dowel bars, types of longitudinal joints etc.).

### 6.2.2 Coring

Cores were taken from various locations (at the location of crack, away from the crack, through the dowel bar) to determine the location and extent of cracking.

### 6.2.3 MIRA Ultrasonic Testing

The Ultrasonic Shear-wave Tomography technique (MIRA) consists of an ultrasonic device that can diagnose subsurface concrete condition using an array of dry point contact (DPC) touch-and-go transducers (Figure 6.1). The transducers do not require any kind of surface operation and each transducer can both transmit and receive low frequency (55 khz) shear waves. The DPC transducers provide the necessary aid for impact and wavefront penetration that can go up to 3 feet deep for the typical concrete surface texture and diagnose the condition (FHWA 2017). The equipment has ten channels and each channel comprised of four transducers in a multi-static array that allows for 45 transmitting and receiving pair measurements per second scan which ensure high productivity. An example of the visual output from MIRA is shown in Figure 6.2.

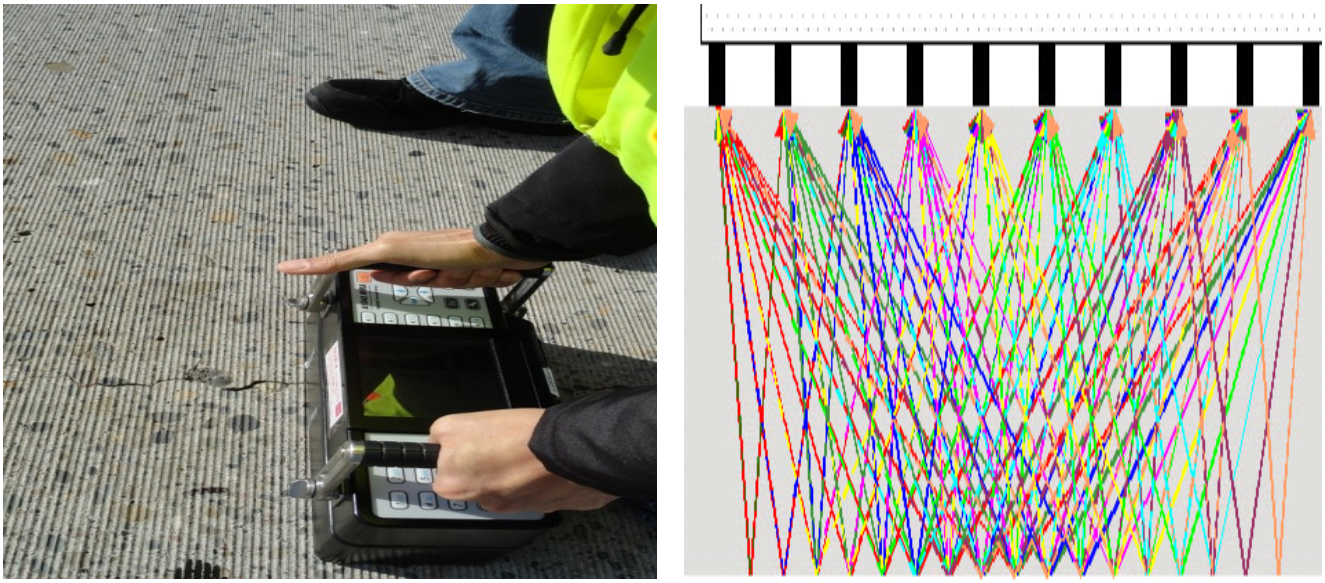

**Figure 6.1 Photo and Illustration. MIRA ultrasonic equipment (FHWA 2017).**

MIRA can be used to estimate depth of concrete layer(s) up to three feet, depth and location of reinforcement bars, consolidation/compaction level of concrete, and material properties. MIRA can also be used to detect flaws, delamination or debonding cracks, and other discontinuities, and locate joint deteroration. In this study, both 2D and 3D MIRA scans were obtained to identify delamination/horizontal cracks and dowel and tie bars' location at the selected field sites.

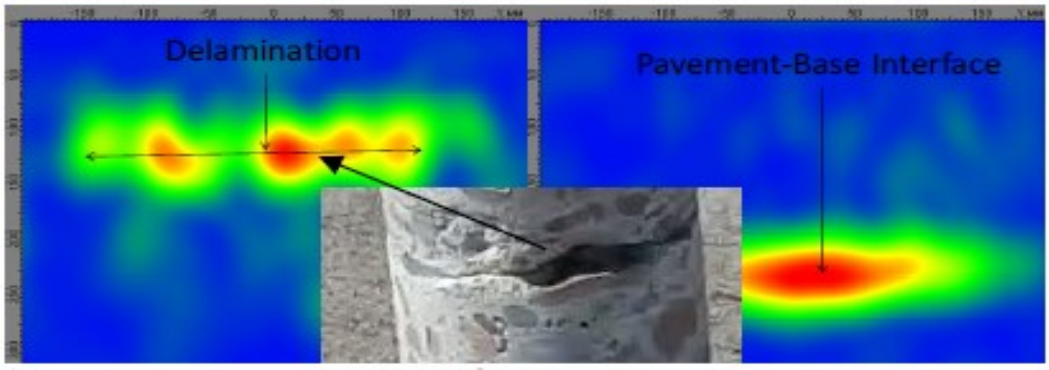


**Figure 6.2 Contour Plot. MIRA visual output example (FHWA 2017).**

# Chapter 7: Field Investigations – Surface Distresses

## 7.1 Dane County, Wisconsin

I-39 NB in Dane County, Wisconsin was constructed about 14 years ago at the time of the field survey. For a relatively new concrete pavement, this roadway exhibits significant number of large spalls. Examples of these large spalls, some that have been partially or fully repaired with hot mix asphalt (HMA) patches are shown in Figure 7.1 through Figure 7.3. The pavement also exhibited transverse cracking roughly two to three feet from the transverse joint as shown in Figure 7.4.

**Figure 7.1 Photo. Corner break observed on I-39 NB in Dane County, Wisconsin.**

**Figure 7.2 Photo. Small corner break fully patched with asphalt observed on I-39 NB in Dane County, Wisconsin.**

**Figure 7.3 Photo. Large corner break partially patched with asphalt observed on I-39 NB in Dane County, Wisconsin.**

**Figure 7.4 Photo. Full length transverse crack about two to three feet from transverse joint observed on I-39 NB in Dane County, Wisconsin.**

## 7.2 Columbia County, Wisconsin

I-39 NB in Columbia County, WI, is a relatively new pavement constructed in 2009 (11 years in service at the time of field data collection). Despite this short service life, this roadway exhibits high levels of pavement distress similar to that observed in Dane County (Figure 7.5 through Figure 7.9).

**Figure 7.5 Photo. A large spall partially filled with asphalt observed on I-39 NB in Columbia County, Wisconsin.**

**Figure 7.6 Photo. A meandering transverse crack with a partial length longitudinal crack observed on I-39 NB in Columbia County, Wisconsin.**

**Figure 7.7 Photo. Full length transverse crack with a partial length longitudinal crack observed on I-39 NB in Columbia County, Wisconsin.**

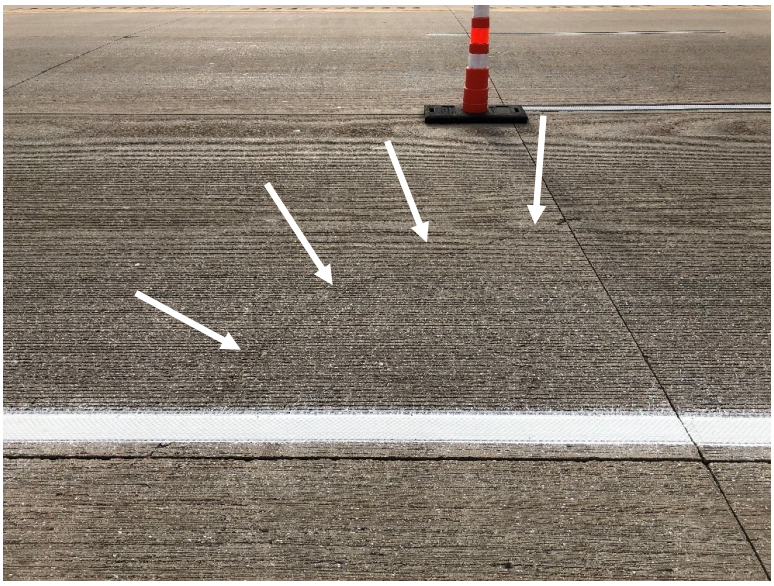

**Figure 7.8 Photo. Corner break observed on I-39 NB in Columbia County, Wisconsin.**

**Figure 7.9 Photo. Full length transverse crack with a partial length longitudinal crack and compound spalls observed on I-39 NB in Columbia County, Wisconsin.**

## 7.3 Columbia County, Wisconsin

The third pavement site investigated was also in Columbia County, Wisconsin but this time the section was on south bound of I-39. As with the previous two construction projects, this site was affected by distresses like longitudinal and transverse cracking, corner cracking, and spalling (Figure 7.10 through Figure 7.13).

**Figure 7.10 Photo. Large spall partially filled with asphalt along with meandering longitudinal crack observed on I-39 SB in Columbia County, Wisconsin.**

**Figure 7.11 Photo. Large unrepaired spall observed on I-39 SB in Columbia County, Wisconsin.**

**Figure 7.12 Photo. Large spall partially filled with asphalt along with meandering transverse crack observed on I-39 SB in Columbia County, Wisconsin.**

**Figure 7.13 Photo. Transverse crack near joint along with associated multiple partial longitudinal cracks and spalling (some filled with asphalt) observed on I-39 SB in Columbia County, Wisconsin.**

## 7.4 Illinois Tollway

These large spalls and cracks near transverse joints are not limited to a few project sites in Wisconsin. In addition to multiple projects constructed under different construction contracts in Wisconsin, these were also observed on I-94 at the Illinois Tollway as shown in Figure 7.14 and Figure 7.15. This section of the roadway was constructed in 2009, about 11 years prior to the field survey.

**Figure 7.14 Photo. Early stage joint deterioration on I-94 at the Illinois Tollway.**

**Figure 7.15 Photo. Advanced joint deterioration with patching material on I-94 at the Illinois Tollway.**

## 7.5 Hennepin County, Minnesota

Eastbound section of Minnesota state highway 610 (TH 610) was investigated for similar cracking and faulting. This section of the roadway was constructed in 1999 and the joint distresses including large spalls started appearing about 10 to 15 years following construction. Some of these spalls were repaired with HMA patches (Figure 7.16 through Figure 7.18).

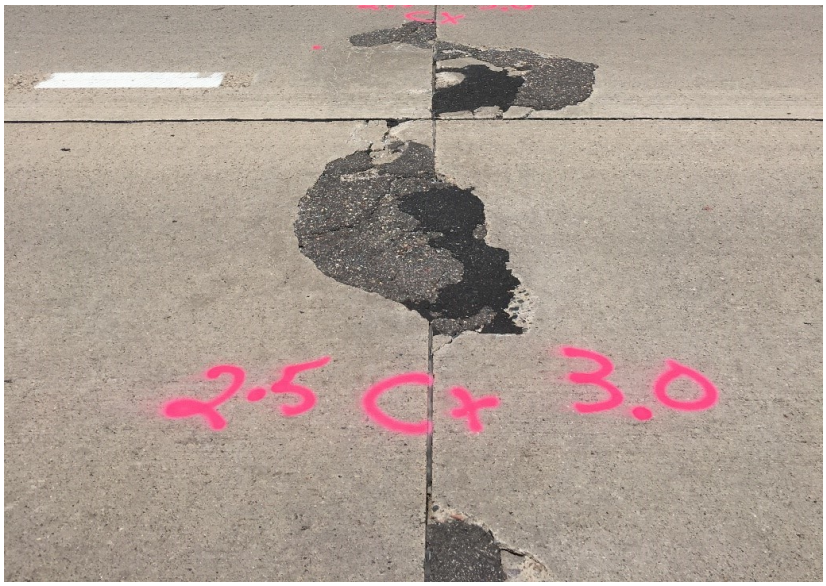


**Figure 7.16 Photo. Advanced large joint spalls with asphalt patches on TH 610 in Hennepin County, MN.**

**Figure 7.17 Photo. Joint deterioration with asphalt patch on TH 610 in Hennepin County, MN.**

**Figure 7.18 Photo. Joint spalling with asphalt patch and evidence of new cracks that could potentially lead to additional spalling on TH 610 in Hennepin County, MN.**

## 7.6 Eau Claire County, Wisconsin

The cracking and spalling observed in sites 1 through 3 are not limited to the Madison area (Dane County and Columbia County). This type of cracking was observed in other counties including US 53 in Eau Claire County as shown in Figure 7.19 through Figure 7.21. This pavement was constructed in 2006 and was only 14 years old at the time of the field survey.

**Figure 7.19 Photo. Large spall with asphalt patch and on US 53 in Eau Claire County, WI.**

**Figure 7.20 Photo. Joint spalling with asphalt patch along with longitudinal crack on US 53 in Eau Claire County, WI.**

**Figure 7.21 Photo. Several consecutive joints with spalling filled with asphalt patches on US 53 in Eau Claire County, WI.**

## 7.7 Key Findings from Surface Distress Surveys

Several JPCP projects in Wisconsin and one in Minnesota and Illinois exhibit large spalls at transverse joints. The occurrence of these spalls is relatively common within a project, observed on approximately one in ten to twenty joints after only ten to fifteen years of pavement service life following construction.

These spalls are typically one foot or more in length in both the transverse and longitudinal directions. These spalls can be distinguished from typical durability-related spalling by their extent and size, their depth, and lack of any significant amount of hairline cracking associated with or around the spalled concrete. The visual observation of the typical depths of these cracks near and away from the transverse joints suggest that they may be related to the presence of steel (dowel bars and tie bars) embedded in the concrete. The cracks within the concrete likely start around the depth of the dowel bar near the joint as delamination cracks and migrate upwards towards the surface, eventually breaking up and spalling the concrete.

# Chapter 8: Field Investigations – Time History

The research team obtained time history of spalling progression for a number of joints on I-94 at the Illinois Tollway. These are shown in Figure 8.1 through Figure 8.6.

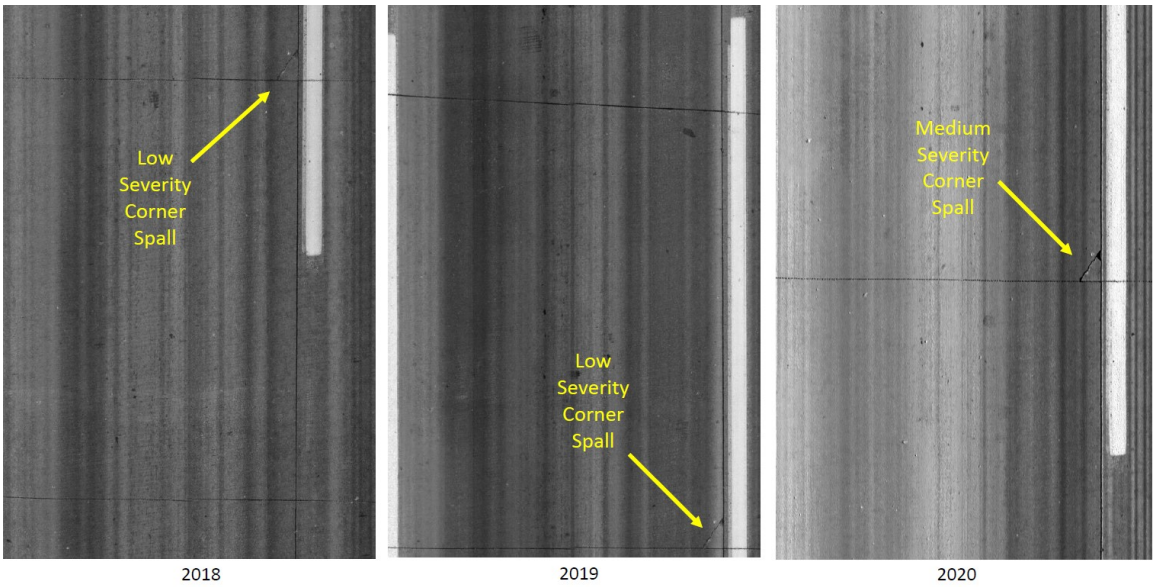


**Figure 8.1 Photo. Spall progression from 2018 through 2020 taken using a downward facing camera on I-94 EB, Lane 3, MP 18.25 at the Illinois Tollway.**

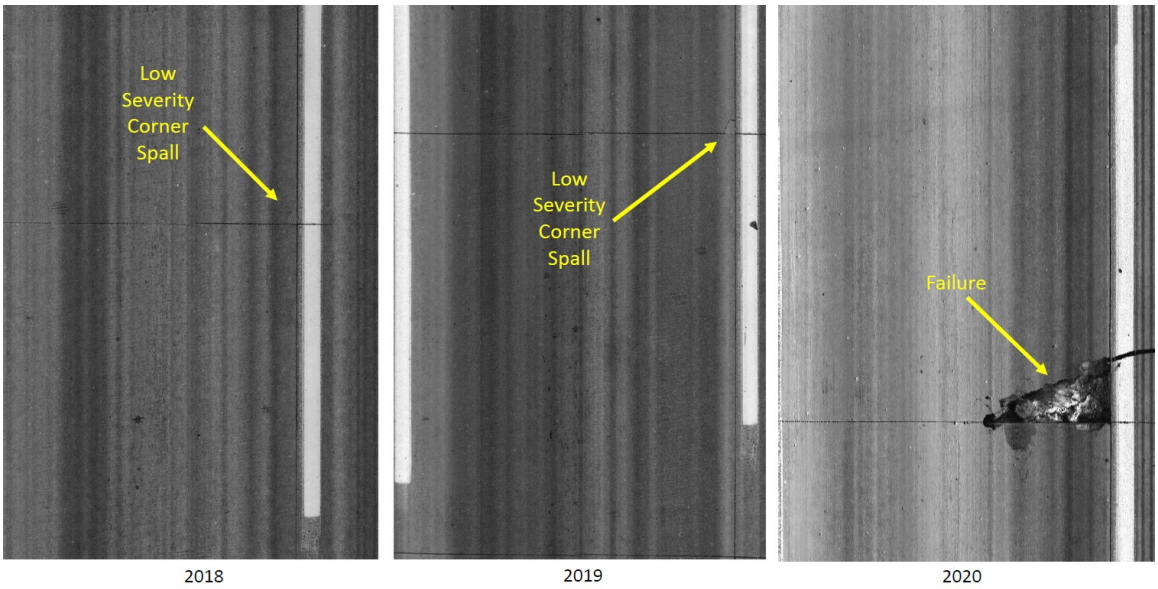


**Figure 8.2 Photo. Spall progression from 2018 through 2020 taken using a downward facing camera on I-94 EB, Lane 3, MP 18.24 at the Illinois Tollway.**

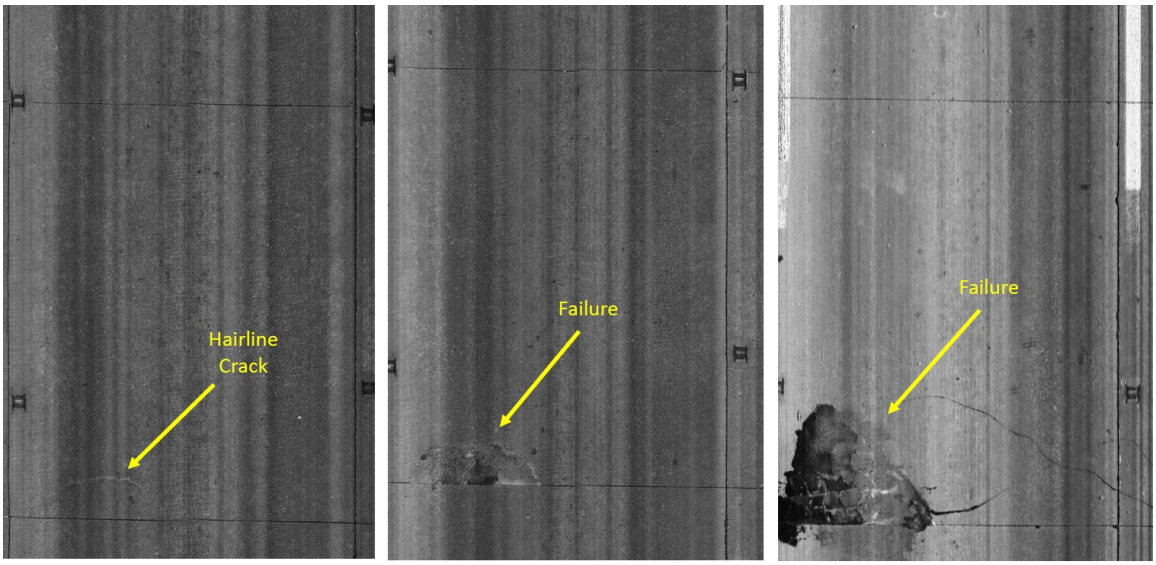


**Figure 8.3 Photo. Spall progression from 2018 through 2020 taken using a downward facing camera on I-94 EB, Lane 3, MP 18.60 at the Illinois Tollway.**

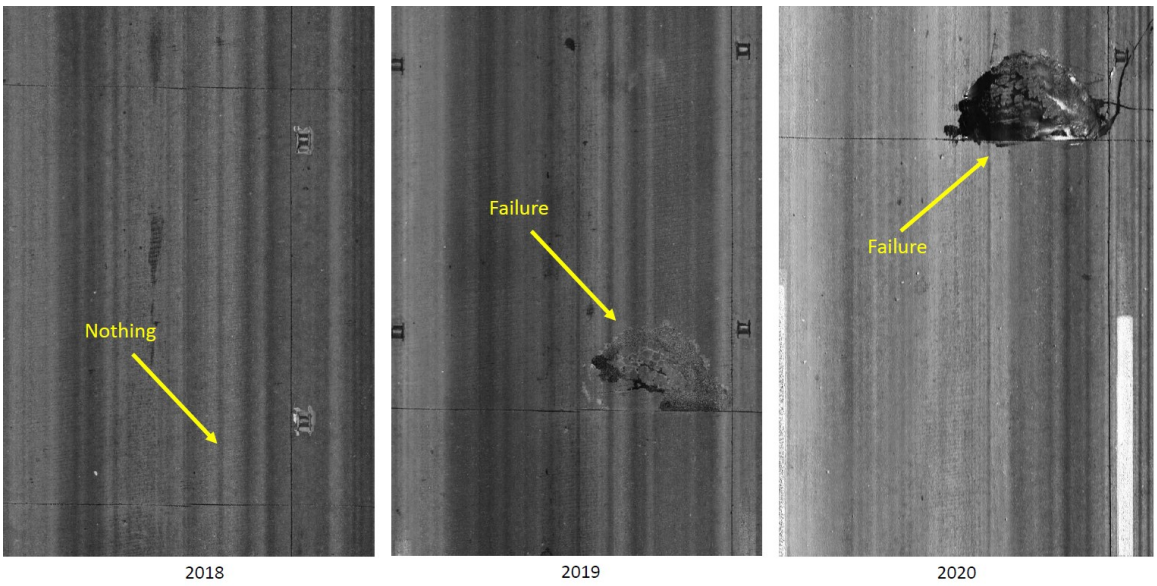


**Figure 8.4 Photo. Spall progression from 2018 through 2020 taken using a downward facing camera on I-94 EB, Lane 3, MP 18.23 at the Illinois Tollway.**


**Figure 8.5 Photo. Spall progression from 2016 through 2018 taken using a front facing camera on I-94 EB, Lane 3, MP 18.55 at the Illinois Tollway.**

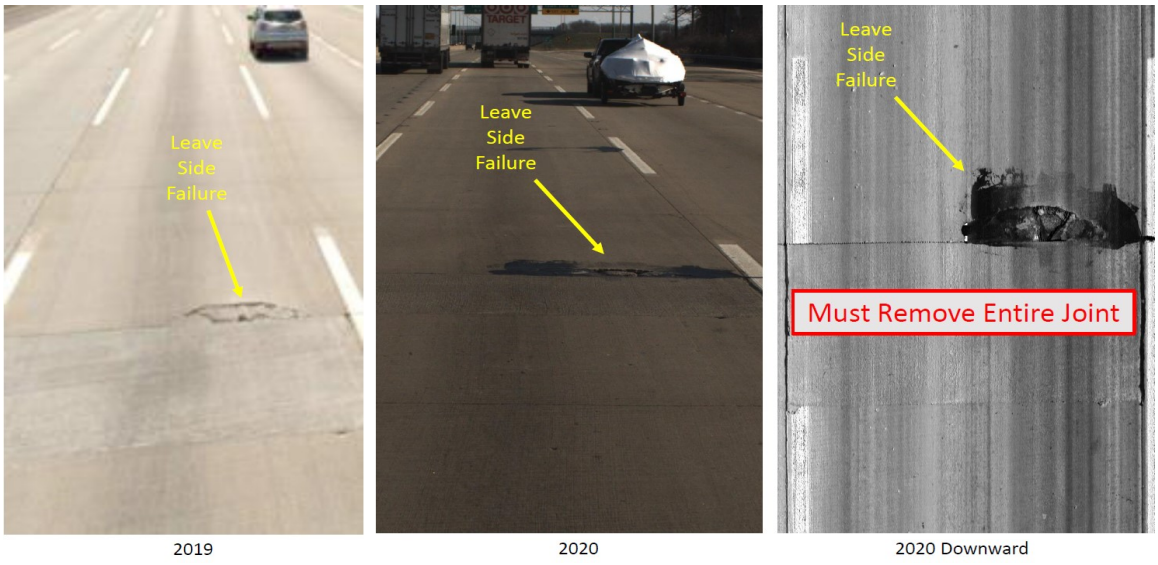


**Figure 8.6 Photo. Spall progression from 2019 through 2020 taken using a front facing and downward facing camera on I-94 EB, Lane 3, MP 18.55 at the Illinois Tollway (continuation from Figure 8.5).**

## 8.1 Key Findings from Time History Review

The time history images obtained from the Illinois Tollway suggests that the spalls progress rapidly (within 2 years) from small to large and are not limited to approach or leave side of the joint. i.e., the spalls are just as likely to occur on the leave side of the joint as they are on the approach side of the joint.

# Chapter 9: Field Investigations - MIRA

Fourteen joint locations of the I-94 WB section at Illinois tollway were inspected for cracking and delamination. Among them six were observed as good joints, whereas the remaining eight were observed and noted as distressed joints. MIRA scanning was performed on each of them.

Figure 9.1 depicts a joint (Joint #3) with longitudinal crack / corner break starting from the joint, but with no other visible distresses along the transverse length of the joint. MIRA scan however shows a delamination crack initiating between two dowel bars at roughly the center of the transverse joint. While this crack does not yet show up as a distress at the surface of the slab, with traffic and environmental loading, this crack can be expected to propagate in various horizontal directions until it turns up and results in spalling of the concrete at around the middle of the transverse joint.

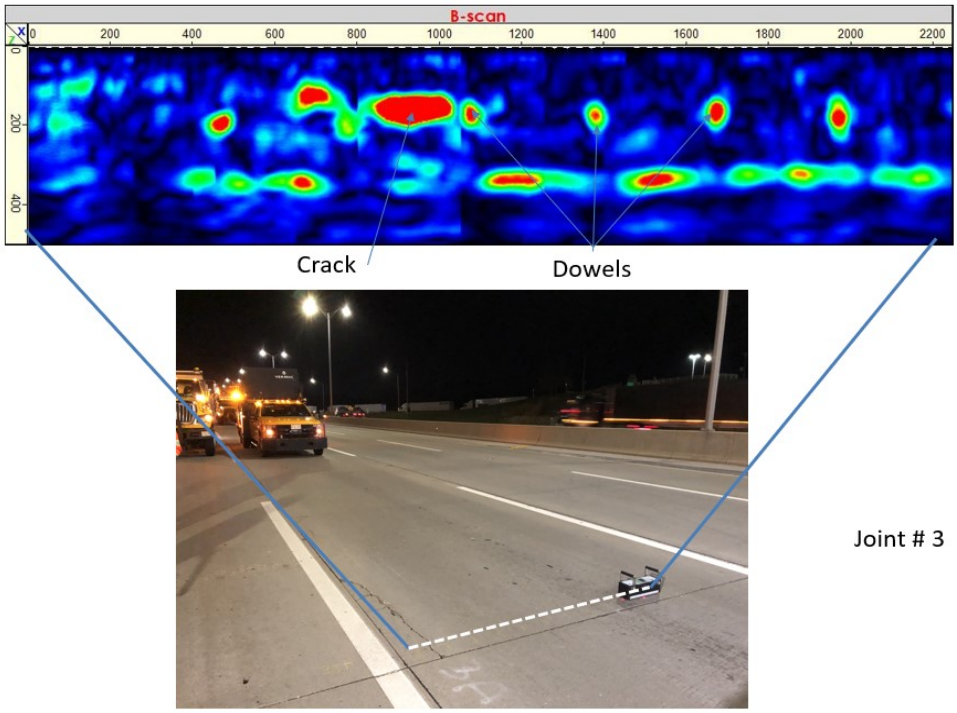


**Figure 9.1 Photo and Contour Plot. 2D MIRA scan showing crack initiating at dowel bar level for Joint #3 on I-94 at the Illinois Tollway.**

Another joint (Joint #14) shows no visible distresses at the surface of the concrete. However, the MIRA scan shows significant horizontal delamination cracks at the depth of the dowel bars. The cracking in Joint #14 is more advanced transversely than the cracking in Joint #3. As in the case of Joint #3, these cracks can be expected to progress over time until they turn up and result in one or more spalls of the concrete at the approach side of the transverse joint. The 2D and 3D MIRA scans for Joint #14 are shown in Figure 9.2 and Figure 9.3.

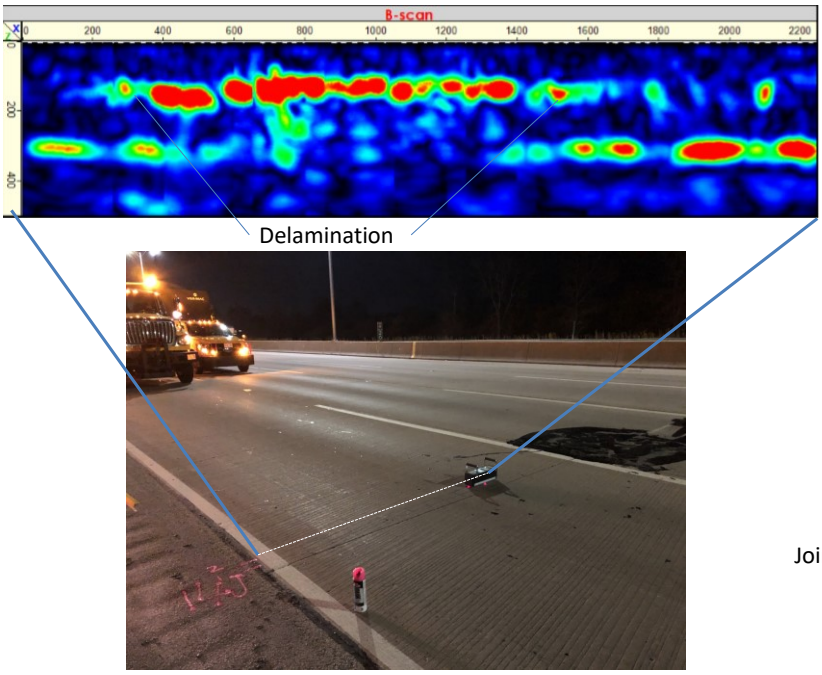


**Figure 9.2 Photo and Contour Plot. 2D MIRA scan showing delamination crack initiating at dowel bar level for Joint #14 on I-94 at the Illinois Tollway.**

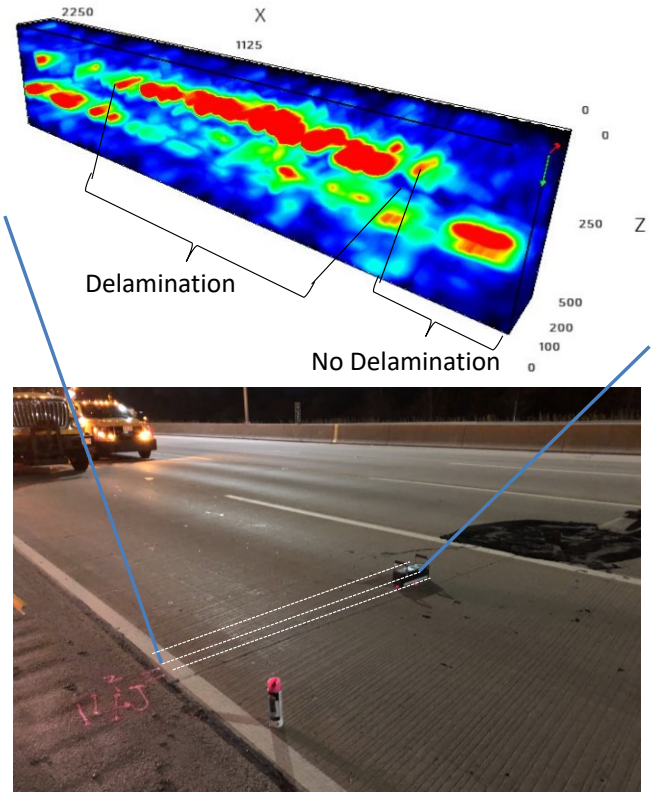


**Figure 9.3 Photo and Contour Plot. 3D MIRA scan showing delamination crack initiating at dowel bar level for Joint #14 on I-94 at the Illinois Tollway.**

Figure 9.4 through Figure 9.12 show MIRA scans from additional joints scanned on I-94 at the Illinois Tollway. Specifically, Figure 9.4 shows the scans for Joint #10 on both the approach side and leave side of the joint. The scans show subsurface delamination cracking present on both sides of the joint although no cracking is visible at the surface. The approach slab shows roughly 50% of the transverse length is cracked, while roughly 50% of the transverse length is still intact. The leave slab has greater extent of cracking and roughly 75% of the transverse length has delamination cracking in the concrete.

Figure 9.5 through Figure 9.12 show several other joints with delamination cracking at the depth of the dowel bar. Some of these extend the full length of the transverse joint, whereas others only extend partially through the length of the transverse joint. Some of these joints have large spalls while others have no visible distresses at the surface. There does not seem to be increased propensity of these delamination cracks (and associated spalling) towards the approach end or the leave end of the joint. Figure 9.9 is an example where roughly 1/3$^{rd}$ of the slab at the approach side of the joint has a delamination crack which is clearly propagating to the surface. In the future, this delamination crack may be expected to surface, eventually spalling the concrete.

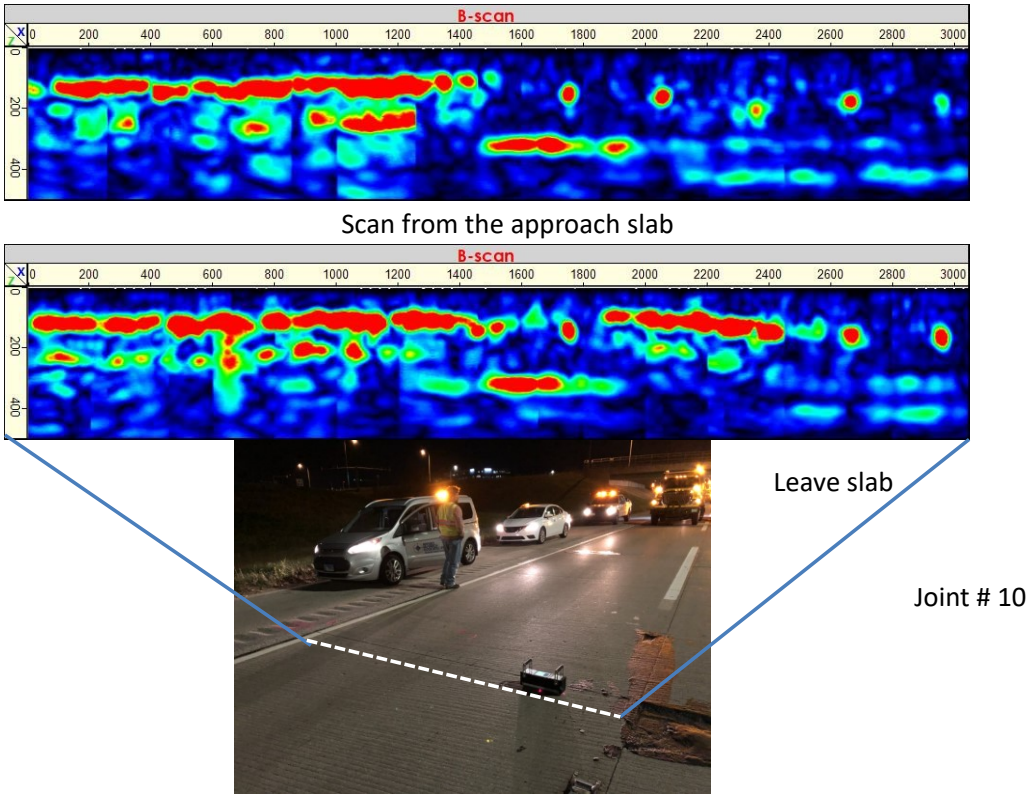


**Figure 9.4 Photo and Contour Plot. 2D MIRA scan showing delamination cracks at dowel bar level at both the approach end and leave end for Joint #10 on I-94 at the Illinois Tollway.**

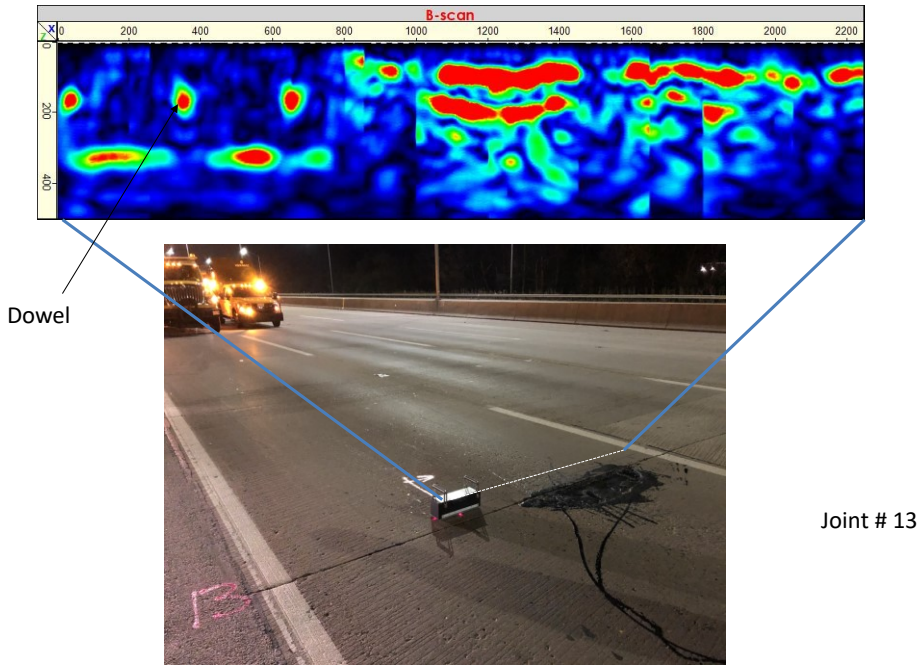


**Figure 9.5 Photo and Contour Plot. 2D MIRA scan showing delamination crack initiating at dowel bar level for Joint #13 on I-94 at the Illinois Tollway.**

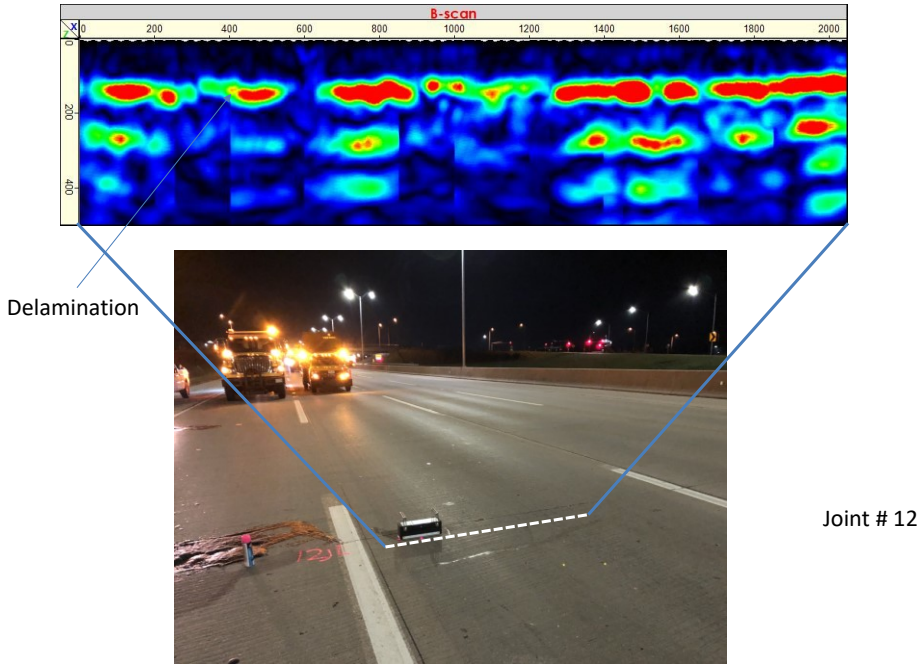


**Figure 9.6 Photo and Contour Plot. 2D MIRA scan showing delamination crack initiating at dowel bar level for Joint #12 on I-94 at the Illinois Tollway.**

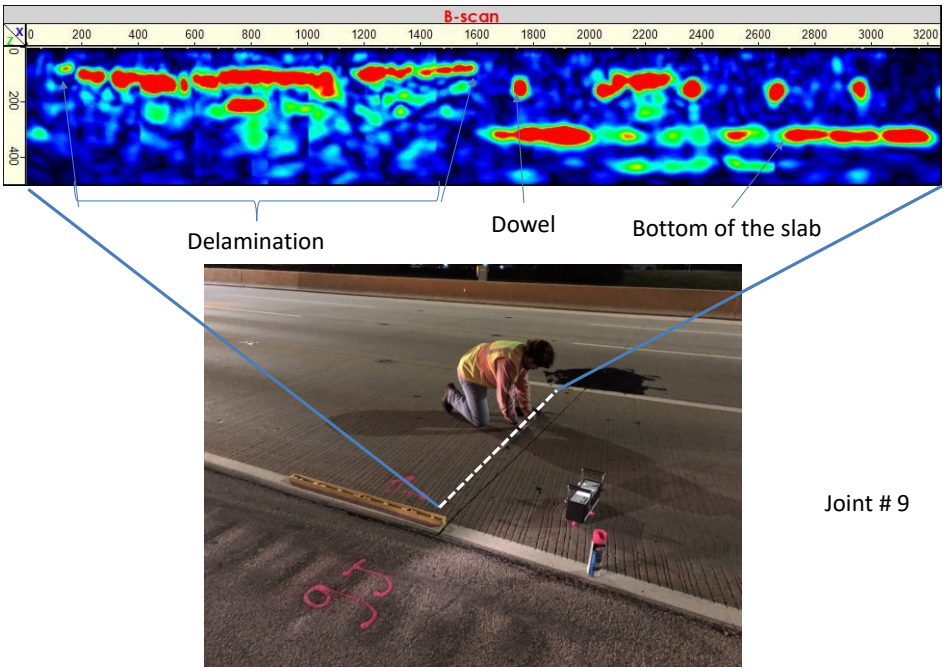


**Figure 9.7 Photo and Contour Plot. 2D MIRA scan showing delamination crack initiating at dowel bar level for Joint #9 on I-94 at the Illinois Tollway.**

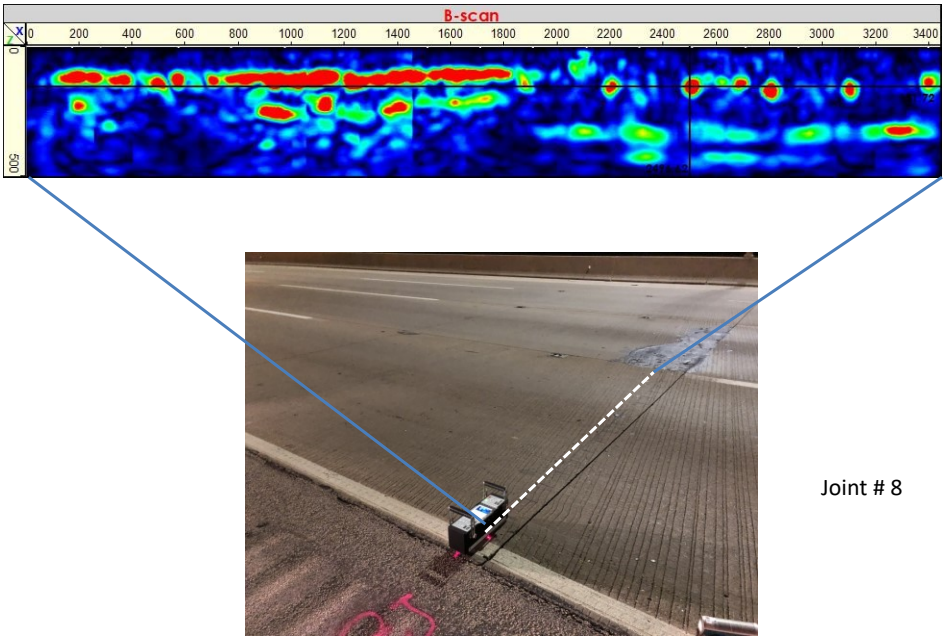


**Figure 9.8 Photo and Contour Plot. 2D MIRA scan showing delamination crack initiating at dowel bar level for Joint #8 on I-94 at the Illinois Tollway.**

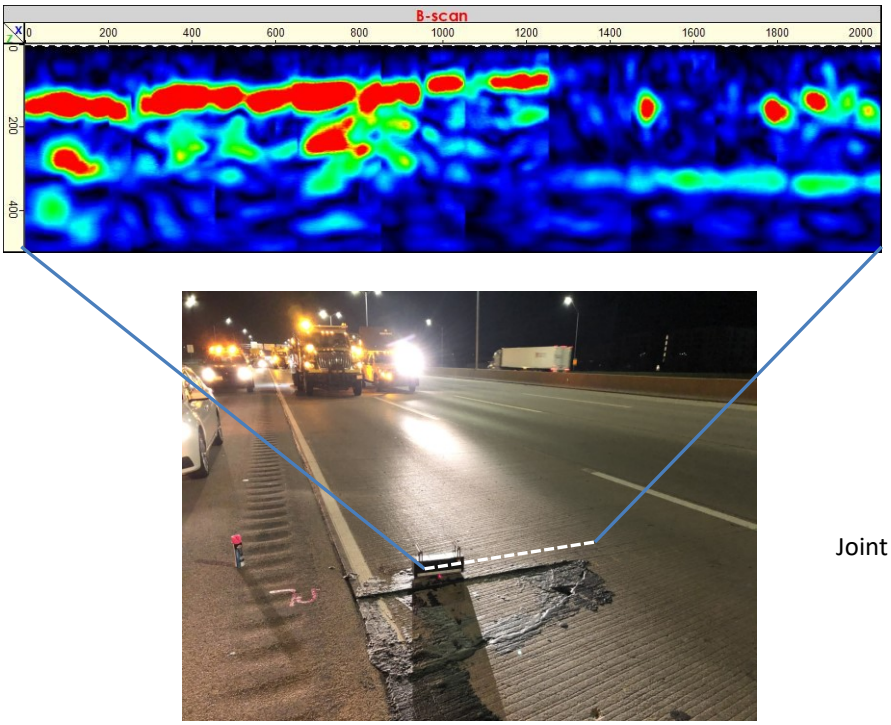


**Figure 9.9 Photo and Contour Plot. 2D MIRA scan showing delamination crack initiating at dowel bar level for approach side of Joint #7 on I-94 at the Illinois Tollway.**

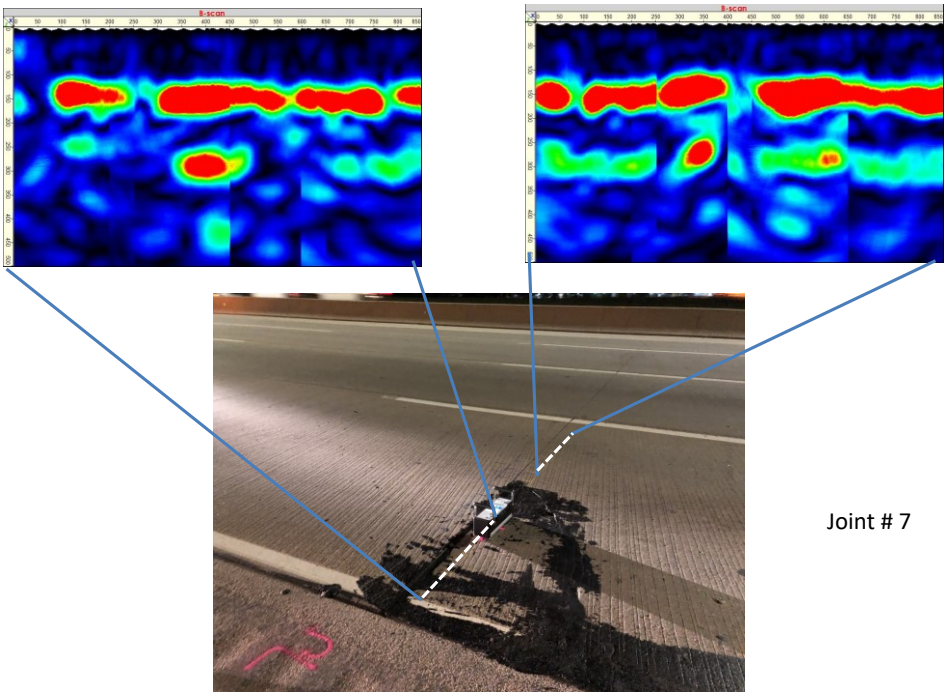


**Figure 9.10 Photo and Contour Plot. 2D MIRA scan showing delamination crack initiating at dowel bar level for leave side of Joint #7 on I-94 at the Illinois Tollway.**

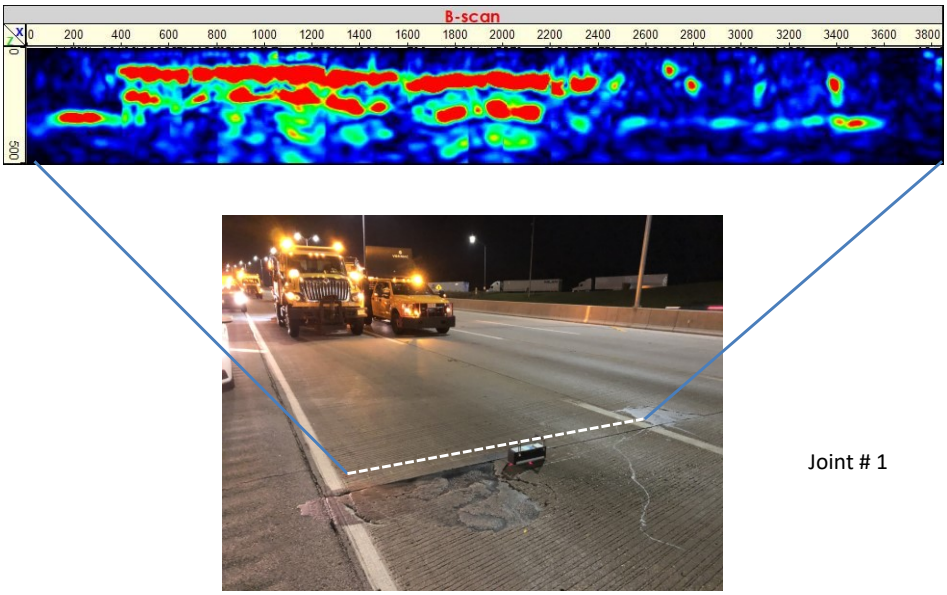


**Figure 9.11 Photo and Contour Plot. 2D MIRA scan showing delamination crack initiating at dowel bar level for approach side of Joint #1 on I-94 at the Illinois Tollway.**

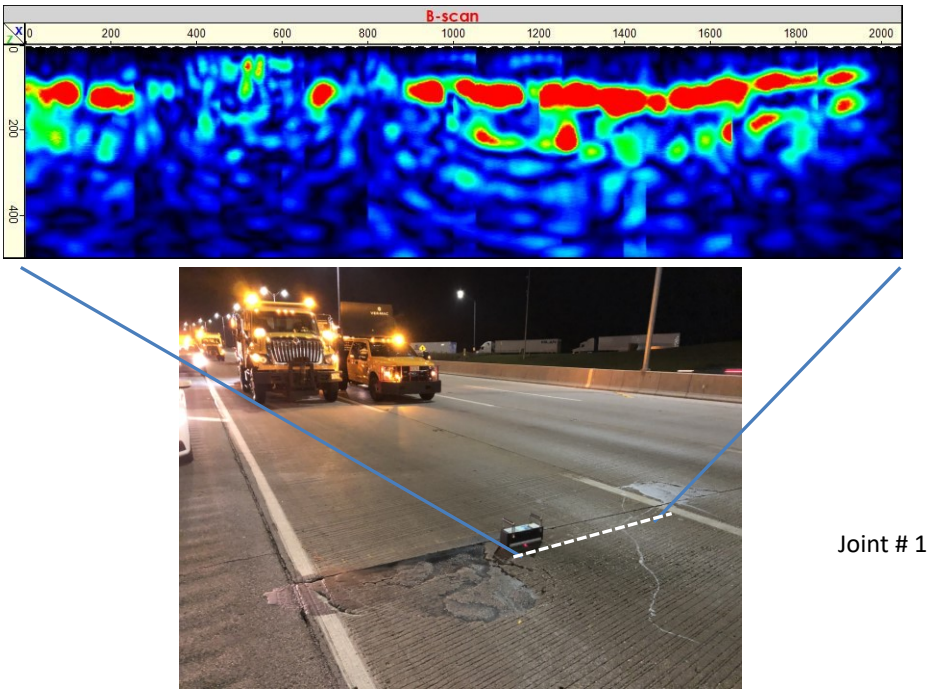


**Figure 9.12 Photo and Contour Plot. 2D MIRA scan showing delamination crack initiating at dowel bar level for leave side of Joint #1 on I-94 at the Illinois Tollway.**

The delamination observed in the MIRA scans in Wisconsin and Minnesota (Figure 9.13 through Figure 9.17) beneath the pavement surface, even when there were no visible distresses, was consistent with those observed at the Illinois Tollway.

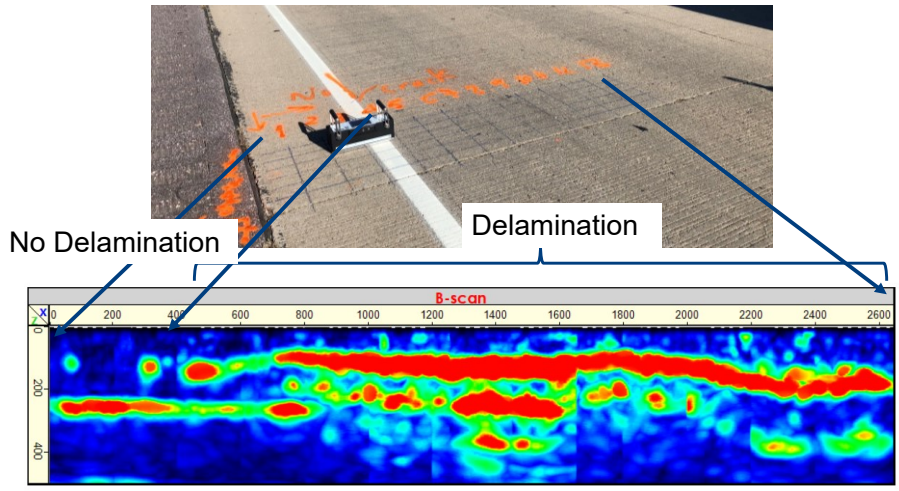


**Figure 9.13 Photo and Contour Plot. 2D MIRA scan showing delamination crack initiating at dowel bar level on I-39 SB in Columbia County, Wisconsin.**

All twelve joint locations scanned on TH 610 in Minnesota except one showed some form of damage in the concrete slab, as MIRA scans indicated there may be either a single crack or a series of smaller cracks on various location of the slab panels. For some joint locations, cracking was so severe that the signal from the crack overpowered the signal from the slab-base interface because of which MIRA scanning could not identify the slab-base interface and only displayed a wide red band which represents one or more horizontal cracks at around the depth of the dowel bars (Figure 9.16). For comparison purposes, the signal from the only area scanned that did not show any signs of delamination is shown in Figure **9.17 Photo and Contour** Plot. MIRA scan showing no delamination cracking signal further away from the joint spall on TH 610 in Hennepin County, MN.

Note that this scan was taken further away from the joint and the delamination cracking near this joint had already progressed upward into a spall closer to the joint.

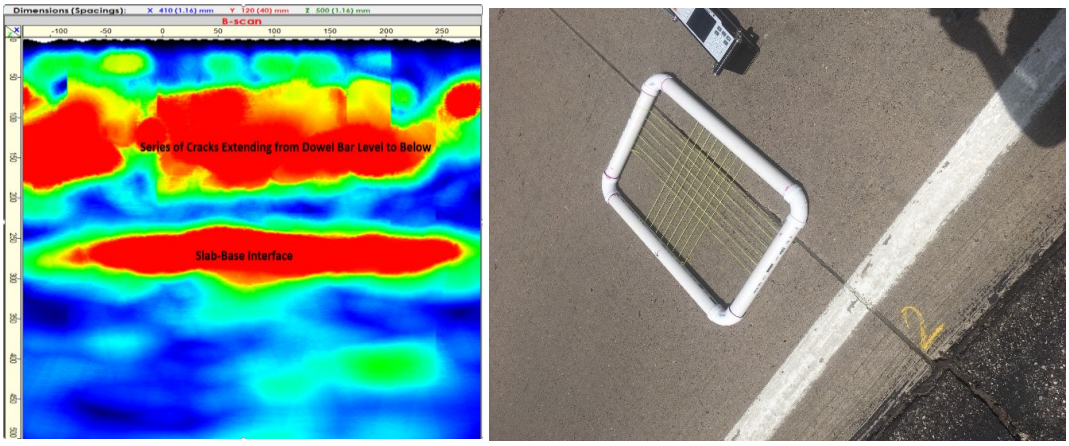


**Figure 9.14 Photo and Contour Plot. MIRA scan near intact joint showing delamination cracking beneath the surface on TH 610 in Hennepin County, MN.**

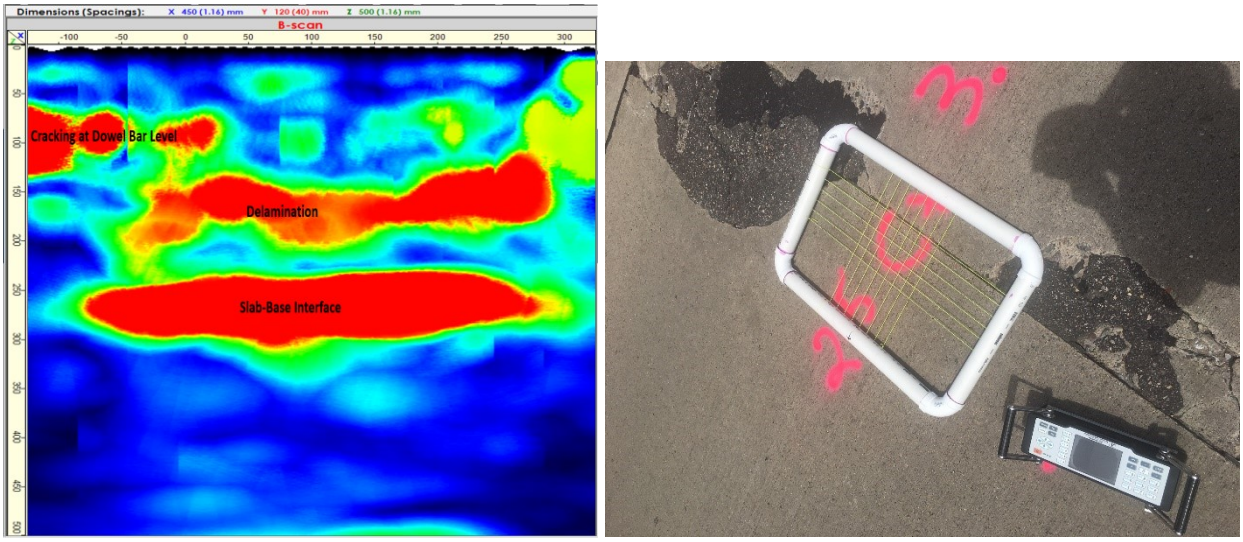


**Figure 9.15 Photo and Contour Plot. MIRA scan near spalled joint showing delamination cracking beneath the surface on TH 610 in Hennepin County, MN.**

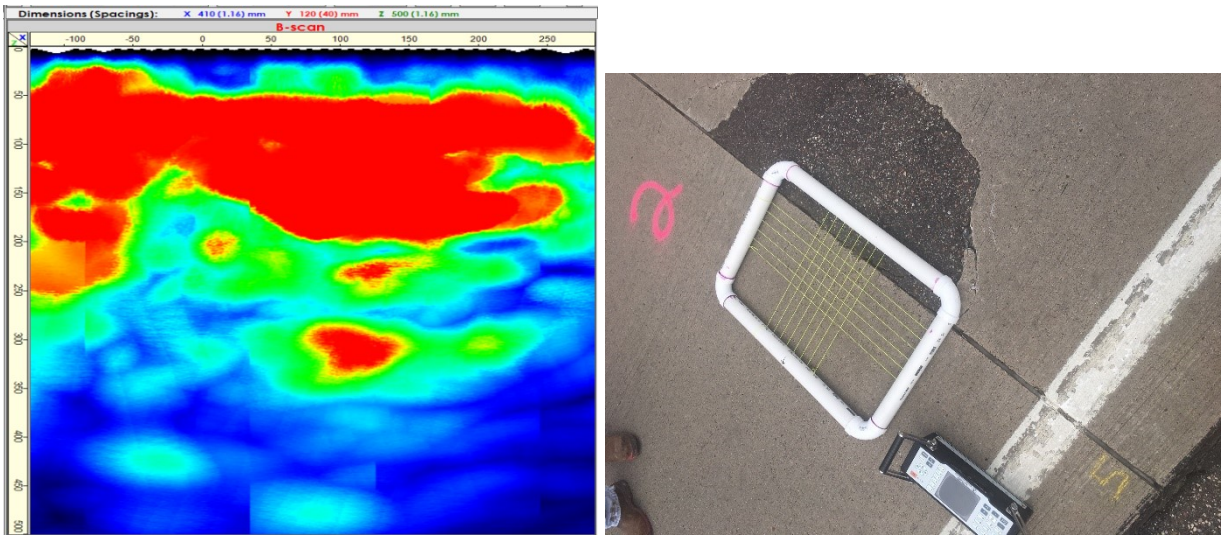


**Figure 9.16 Photo and Contour Plot. MIRA scan near spalled joint showing strong delamination cracking signal on TH 610 in Hennepin County, MN.**

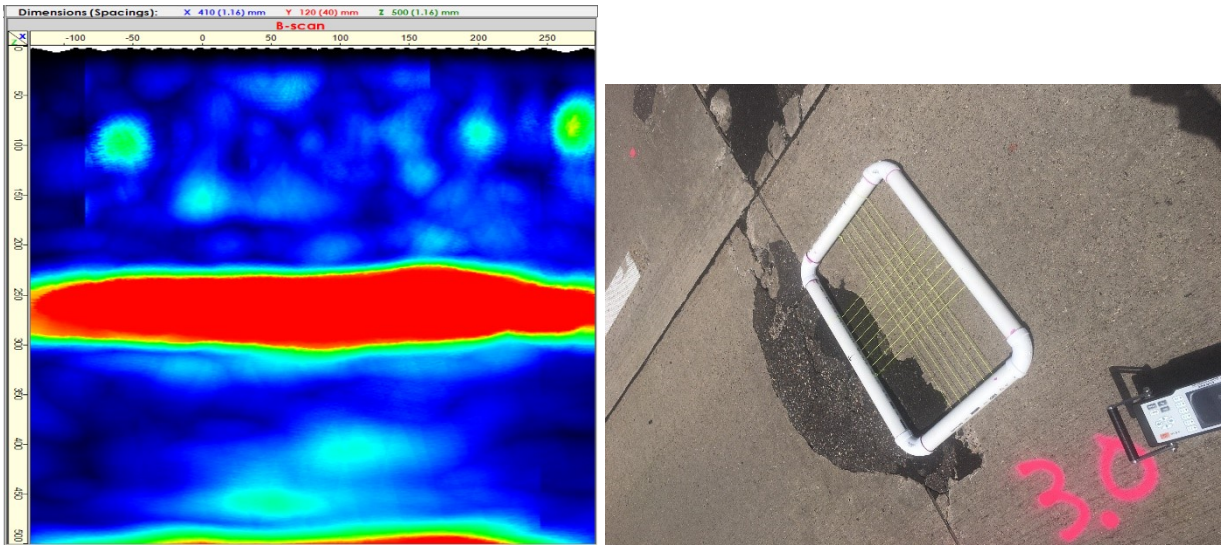


**Figure 9.17 Photo and Contour Plot. MIRA scan showing no delamination cracking signal further away from the joint spall on TH 610 in Hennepin County, MN.**

## 9.1 Key Findings from MIRA Scans

MIRA scans conducted at the Illinois Tollway, Wisconsin, and Minnesota all show significant extents of delamination cracking beneath the pavement surface. These cracks were observed on several joints that did not exhibit any signs of visible distresses at the surface of the concrete. These cracks start at or around the depth of the dowel bars and extend through multiple dowel bars, and in some cases almost the full transverse length of the joint. In some cases, the cracking is so severe that the signals from the cracks overpower the signals from the slab-base interface. MIRA scans showed delamination cracks beneath the concrete surface on both approach side and leave side of the joints.

# Chapter 10: Field Investigations - Coring

Several cores were taken from panels where slab and joint showed distresses and also from the panels where slab and joint had no visible distresses observed at the surface. Figure 10.1 shows the core location and Figure 10.2 shows the approach side of the core and leave side of the same core. Figure 10.3 shows the cross section of the core at the crack. The coring provides evidence that the delamination crack has extended to at least 27 inches from the joint even though no distresses are visible at the surface.

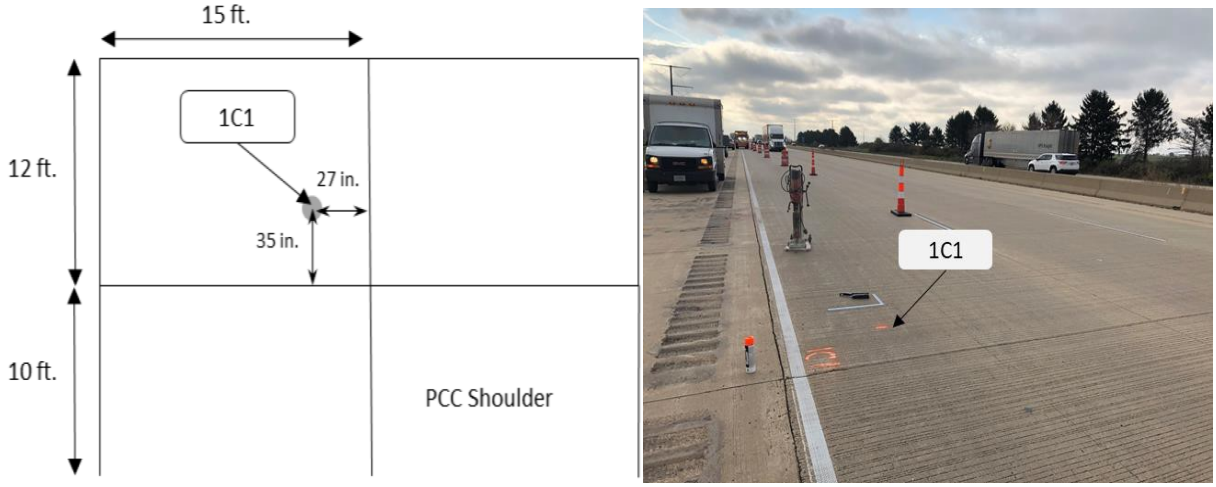


**Figure 10.1 Photo and Illustration. Location of core on I-39 NB in Dane County, Wisconsin, where no visible distresses were observed at the surface.**


**Figure 10.2 Photo. Leave side of 1C1 core (left) and approach side of 1C1 core (right) from I-39 NB in Dane County, Wisconsin.**


**Figure 10.3 Photo. Cross section of 1C1 core from I-39 NB in Dane County, Wisconsin.**

Figure 10.3 shows that the crack propagated through the aggregate, suggesting that at this location, the crack propagated only after the concrete had gained sufficient strength (comparable to that of the aggregate). If the concrete strength was significantly lower than the aggregate when the crack tip approached the aggregate, the crack would have propagated around the aggregate rather than through the aggregate.

A second core was taken near a spot with significant spalling (Figure 10.4). Figure 10.5 shows the approach side of the core and leave side of the same core. The coring provides evidence that the delamination crack has extends the full length of the transverse joint even though only part of the joint has spalled to date. Figure 10.6 shows the cross section of the core at the crack. The figure also shows the concrete cracking through some of the aggregate indicating the crack propagated to this point after the concrete had gained significant strength.

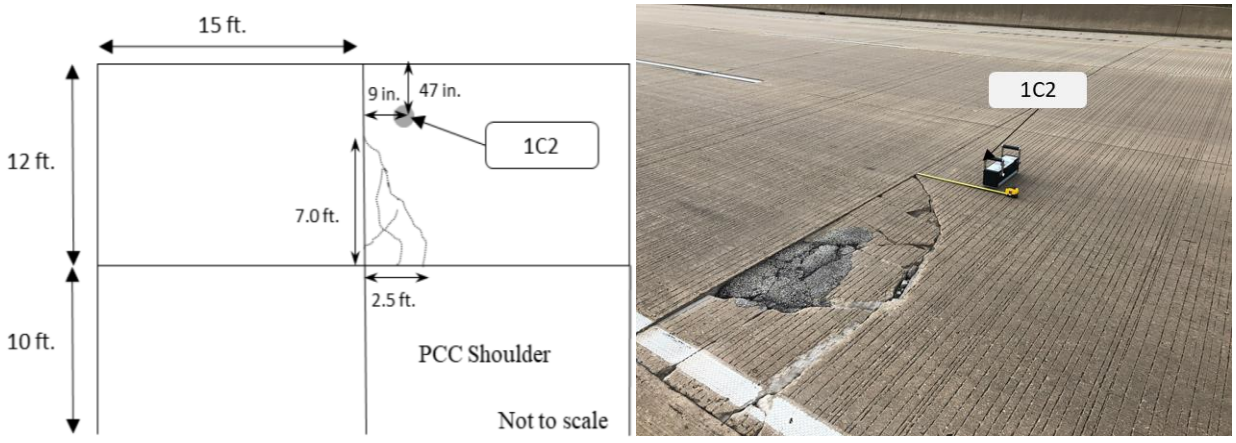


**Figure 10.4 Photo and Illustration. Location of core on I-39 NB in Dane County, Wisconsin, with significantly large spall observed at the surface.**


**Figure 10.5 Photo. Leave side of 1C2 core (left) and approach side of 1C2 core (right) from I-39 NB in Dane County, Wisconsin.**


**Figure 10.6 Photo. Cross section of 1C2 core from I-39 NB in Dane County, Wisconsin.**

Figure 10.7 through Figure 10.9 show coring results from another joint with no visual distresses observed at the surface of the slab. The core taken 39 inches from the transverse joint exhibits delamination cracking suggesting the extent to which the delamination crack extends from the transverse joint. As in the case of core 1C1, Figure 10.9 shows that the crack propagated through the aggregates in the concrete.

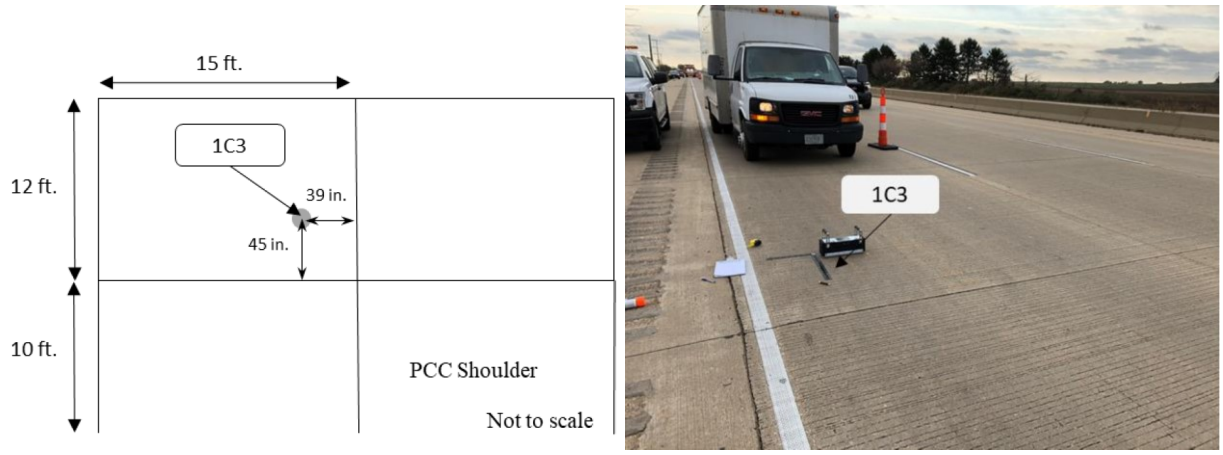


**Figure 10.7 Photo and Illustration. Location of core on I-39 NB in Dane County, Wisconsin, with no distresses observed at the surface.**

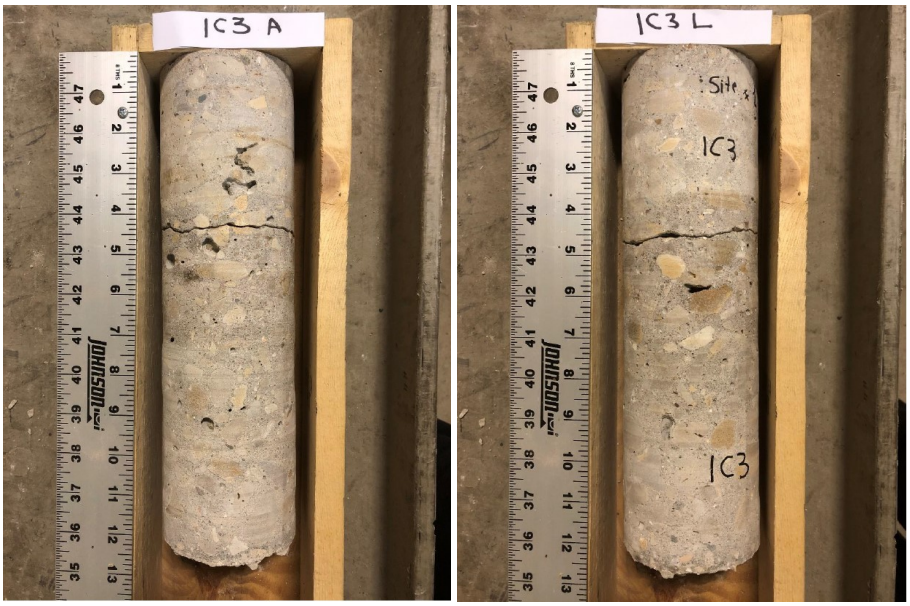


**Figure 10.8 Photo. Approach side of 1C3 core (left) and leave side of 1C3 core (right) from I-39 NB in Dane County, Wisconsin.**

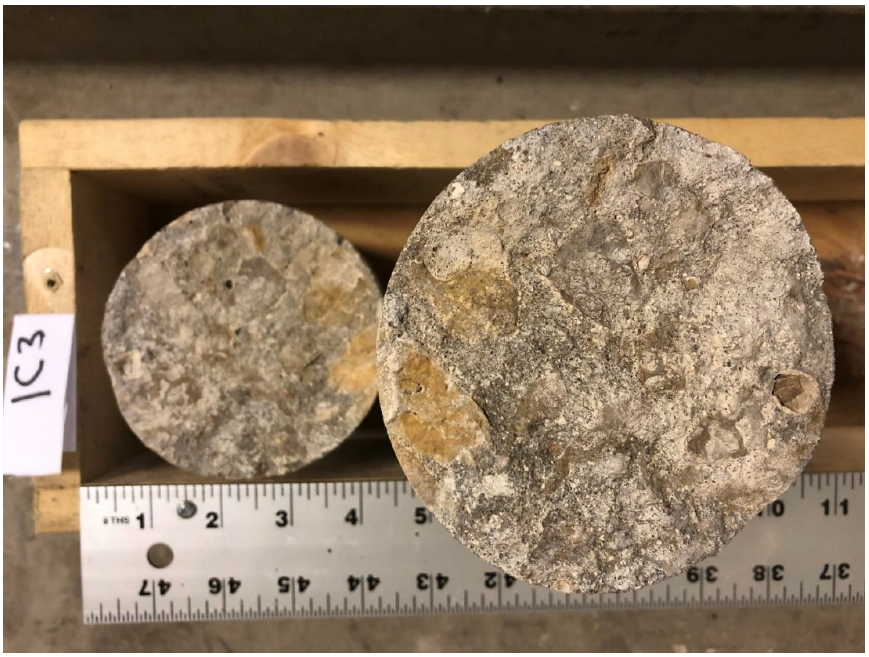


**Figure 10.9 Photo. Cross section of 1C3 core from I-39 NB in Dane County, Wisconsin.**

Two cores were taken from two spots of a slab where slab and joint did not show any signs of distresses (Figure 10.10 through Figure 10.13). In this case, the core taken 10 inches from the transverse joint had delamination cracking whereas the core taken further away from the transverse joint (33 inches) showed no delamination cracking (Figure 10.11). This is an indication that the cracking starts from joints and then propagates further away from the joint. As in the case of the other delamination crack cores, Figure 10.13 shows the 1C5 core had the delamination crack through the aggregate rather than around the aggregate.

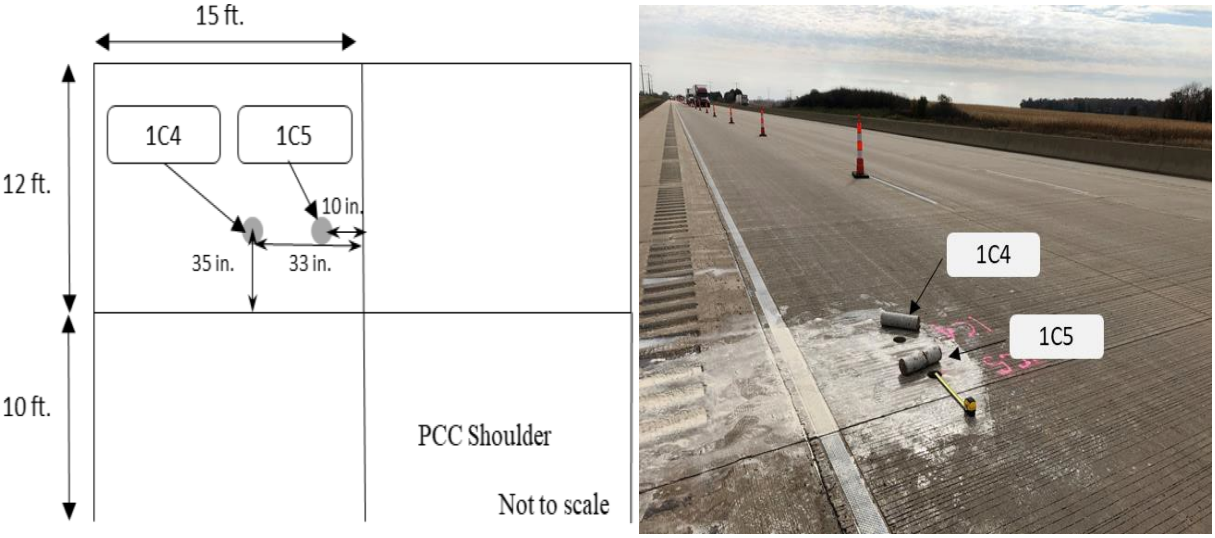


**Figure 10.10 Photo and Illustration. Location of two cores on I-39 NB in Dane County, Wisconsin, with no distresses observed at the surface.**


**Figure 10.11 Photo. Approach side of 1C5 core (top left), leave side of 1C5 core (top right), approach side of 1C4 core (bottom left) and leave side of 1C4 core (bottom right) from I-39 NB in Dane County, Wisconsin.**

**Figure 10.12 Photo. Two cores on I-39 NB in Dane County, Wisconsin, with no distresses observed at the surface. One core away from the joint is intact whereas the core closer to the joint had delamination cracking.**


**Figure 10.13 Photo. Cross section of 1C5 core from I-39 NB in Dane County, Wisconsin.**

Another core was taken from a spot where slab and joint showed spalling that had previously been patched with HMA (Figure 10.14). Horizontal delamination crack was observed on this core taken outside the patch area (Figure 10.15). This suggests that although some of the delamination crack

progressed upwards resulting in spalling of the concrete (which was patched by WisDOT), there is additional delamination cracking within the concrete and could result in further spalling near the existing patched spall, thus compounding the spall. Figure 10.16 shows the delamination crack through the aggregates.

Figure 10.17 through Figure 10.30 show similar coring results from I-39 NB in Columbia County, Wisconsin.

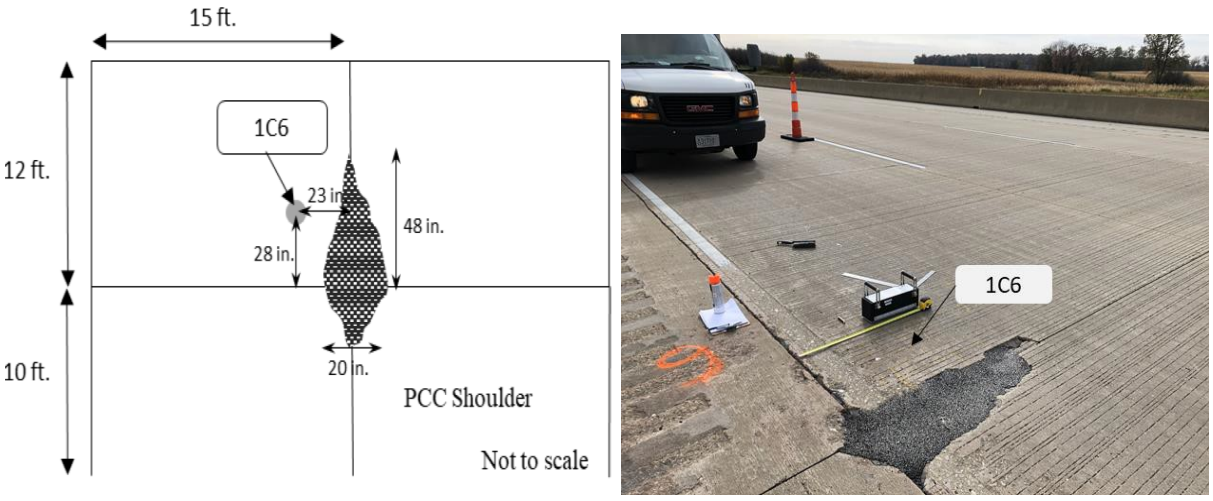


**Figure 10.14 Photo and Illustration. Location of core on I-39 NB in Dane County, Wisconsin, near a patched spall.**


**Figure 10.15 Photo. Approach side of 1C6 core (left) and leave side of 1C6 core (right) from I-39 NB in Dane County, WI.**


**Figure 10.16 Photo. Cross section of 1C6 core from I-39 NB in Dane County, WI.**

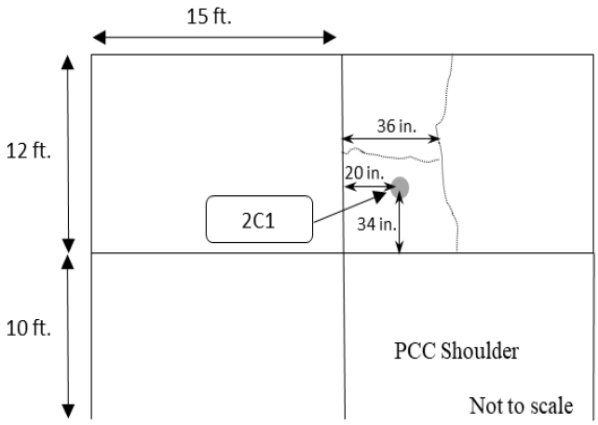



**Figure 10.17 Photo and Illustration. Location of core on I-39 NB in Columbia County, Wisconsin, near a full-length transverse crack and a partial length longitudinal crack.**

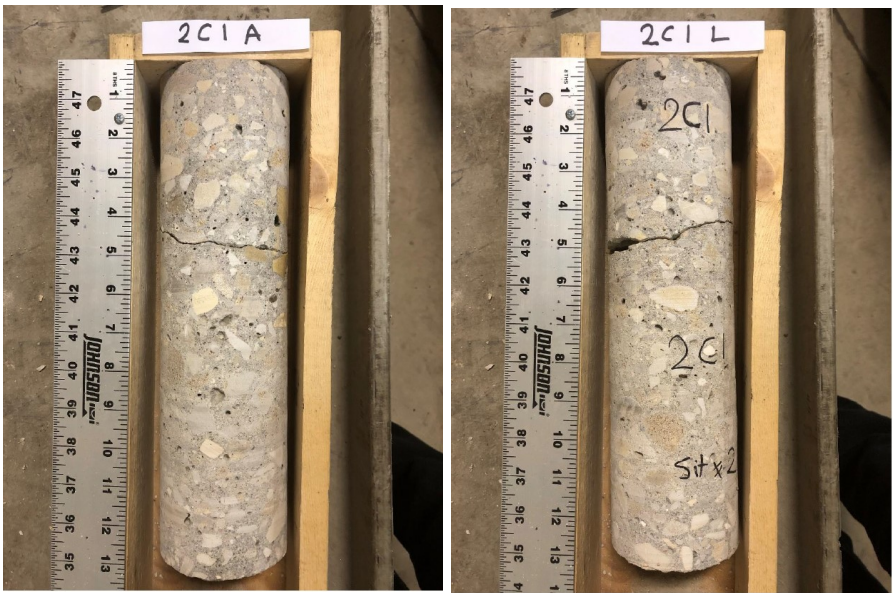


**Figure 10.18 Photo. Approach side of 2C1 core (left) and leave side of 2C1 core (right) from I-39 NB in Columbia County, WI.**


**Figure 10.19 Photo. Cross section of 2C1 core from I-39 NB in Columbia County, WI.**

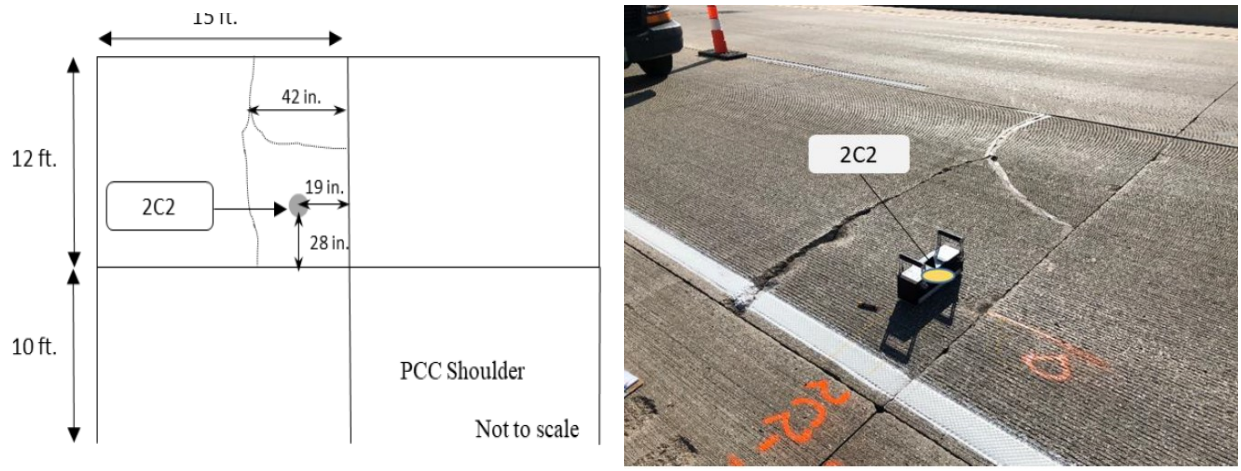


**Figure 10.20 Photo and Illustration. Location of core on I-39 NB in Columbia County, Wisconsin, near a cracked slab exhibiting a transverse crack and a corner break.**

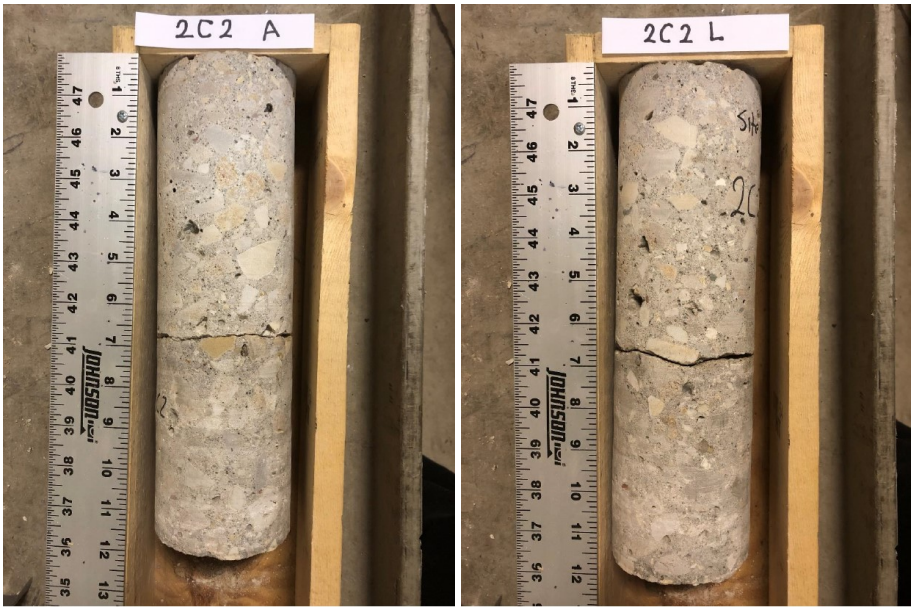


**Figure 10.21 Photo. Approach side of 2C2 core (left) and leave side of 2C2 core (right) from I-39 NB in Columbia County, WI.**


**Figure 10.22 Photo. Cross section of 2C2 core from I-39 NB in Columbia County, WI.**

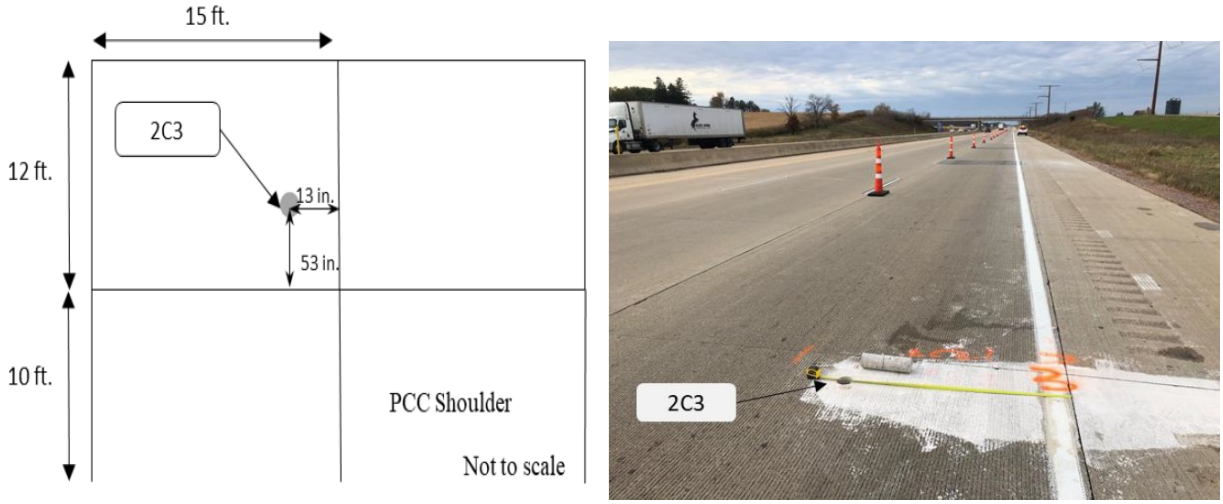


**Figure 10.23 Photo and Illustration. Location of core on I-39 NB in Columbia County, Wisconsin, on concrete with no visible distresses.**

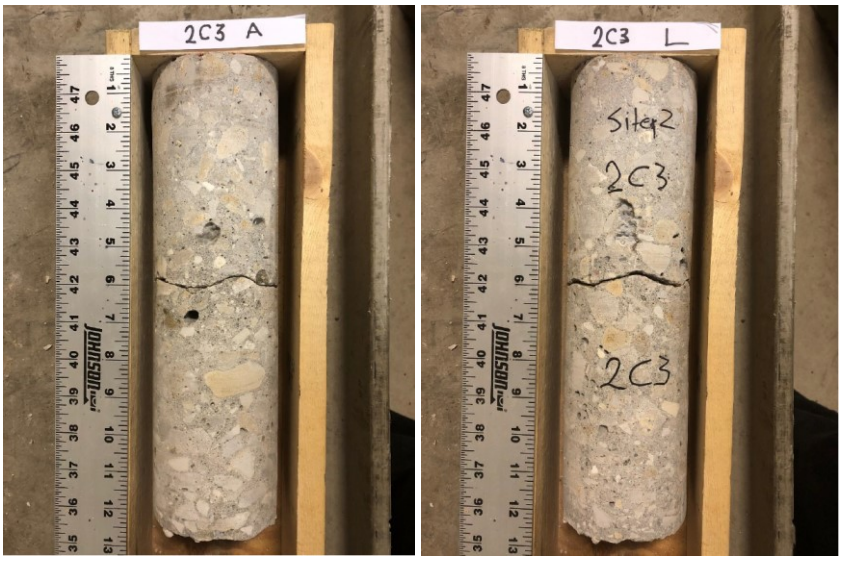


**Figure 10.24 Photo. Approach side of 2C3 core (left) and leave side of 2C3 core (right) from I-39 NB in Columbia County, WI.**


**Figure 10.25 Photo. Cross section of 2C3 core from I-39 NB in Dane County, WI.**

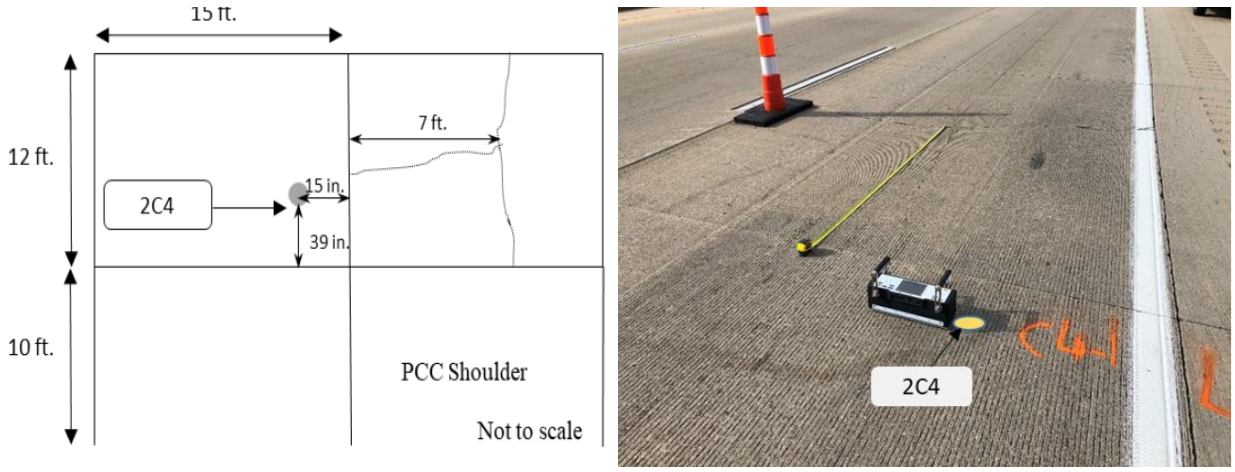


**Figure 10.26 Photo and Illustration. Location of core on I-39 NB in Columbia County, Wisconsin, on a slab with no distresses.**

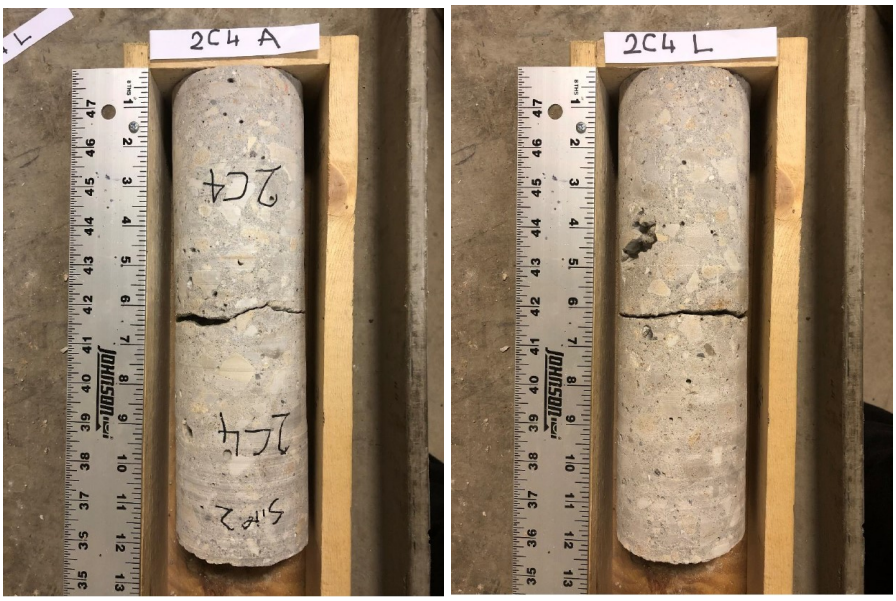


**Figure 10.27 Photo. Approach side of 2C4 core (left) and leave side of 2C4 core (right) from I-39 NB in Columbia County, WI.**


**Figure 10.28 Photo. Cross section of 2C4 core from I-39 NB in Dane County, WI.**

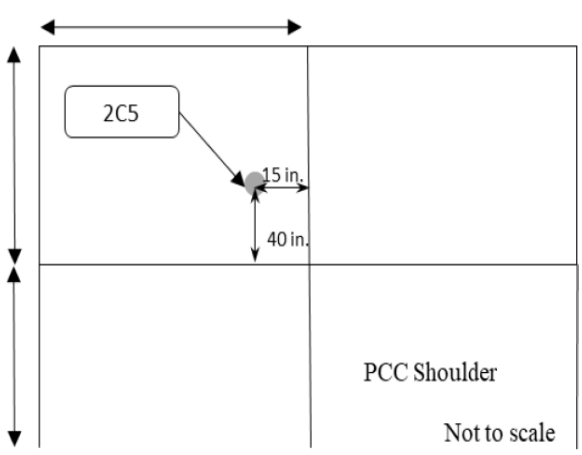



**Figure 10.29 Photo and Illustration. Location of core on I-39 NB in Columbia County, Wisconsin, on a joint with no visible distresses.**


**Figure 10.30 Photo. Approach side of 2C5 core (left) and leave side of 1C6 core (right) from I-39 NB in Columbia County, WI.**

## 10.1 Key Findings from Coring

Coring conducted in Wisconsin suggest the delamination cracks extend for several feet away from the transverse joints in the longitudinal direction. For the sections surveyed, these cracks exist beneath the concrete surface even when there are no visible distresses on the surface. Thus, the coring confirmed the results of the MIRA scans. These cracks clearly start at the depth of the dowel bar and extend horizontally, eventually turning up or down, again confirming the results of the MIRA scans. This is evidenced by the fact that cores taken closer to the joints have the cracks at the mid depth of the core at the level of the dowel bar, whereas cores taken two or more feet away from the joints show the delamination crack at mid depth or higher or lower than mid depth. Cores typically showed cracks progress through the aggregate rather than around the aggregate suggesting the crack tip approached the aggregate when the concrete had gained sufficient strength. In some cases, cores closer to the joint had cracks go around the aggregates (cores 2C2, 2C3 ,and 2C4, Figure 10.22, Figure 10.25, and Figure 10.28), suggesting these cracks near the joints, and consequently near the dowel bars, happened during the early age of the concrete when the concrete was not very strong.

# Chapter 11: Field Investigations - GPR

As part of the multi-step approach to determining the extent and mechanism of deterioration, the joints on I-94 at the Illinois Tollway were scanned using a 3D step-frequency ground penetrating radar (GPR) system. The goal of using the GPR at the locations of joint deterioration were to determine the extent of the non-visible deterioration, the orientation of the dowel bars beneath the joints, whether there is deterioration below the concrete layer, and any insights into the mechanism of deterioration possibly present in the pavement system. The distressed joints are shown using a suffix "A" after their scan numbers, while good joints are shown using a suffix "B". Some scans from both categories are included as part of the analysis.

The GPR system consists of the Geoscope IV from 3D Radar with six-foot-wide antenna (Figure 11.1). The system is GPS enabled with a distance measuring instrument (DMI) to assist in accurate positioning and distance tracking.


**Figure 11.1 Photo. GPR system mounted to a pickup truck.**

The GPR data was collected in three stages. The first stage included higher speed collection runs similar to that performed during a thickness survey. During the thickness survey individual joints can be identified, but no investigation is made to determine if any information about individual joints can be observed from this data. Thickness GPR runs were performed in the westbound and eastbound directions in lanes three and four. The collection spacing for these runs was 12 inches, with an expected depth of penetration of three feet.

The second and third stages of testing were the slow speed, high scan rate collections performed in the eastbound and westbound directions. The high scan rate collection was performed to focus only on the joints that were selected for scanning. Joints were scanned every one inch, to an expected depth of three feet. Each selected joint was scanned twice, once on the right side of the lane, and once on the

left. In cases where the deterioration in a joint was located centrally then the scans were overlapped to ensure full coverage. To capture the entire joint being investigated the slab before the joint, and the slab following the joint, were also collected.

The first analysis completed was a review of the high-speed runs to determine if the deteriorated joints could be identified from the side scan GPR data. The deterioration could be seen from the top-down scanning as shown in Figure 11.2, but this result does not provide any additional insight into the deterioration. The top-down view only mimics a visual survey as can be completed during digital surveys. An example of the side scan GPR signal is presented in Figure 11.3. The side scan shows the individual joints from the long run scanning, but the good and bad joints are indistinguishable. Joints 17A and 18A are present in Figure 11.3, but without prompting on their location through DMI or GPS, the good and bad joints cannot be determined.

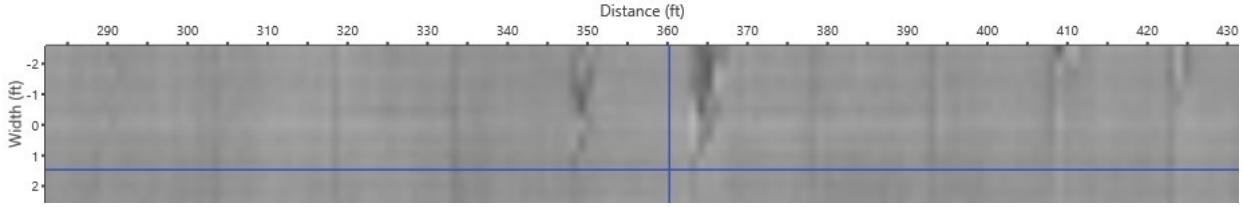


**Figure 11.2 GPR Image. Top-down view of the long run scan at the location of joints 17A and 18A.**

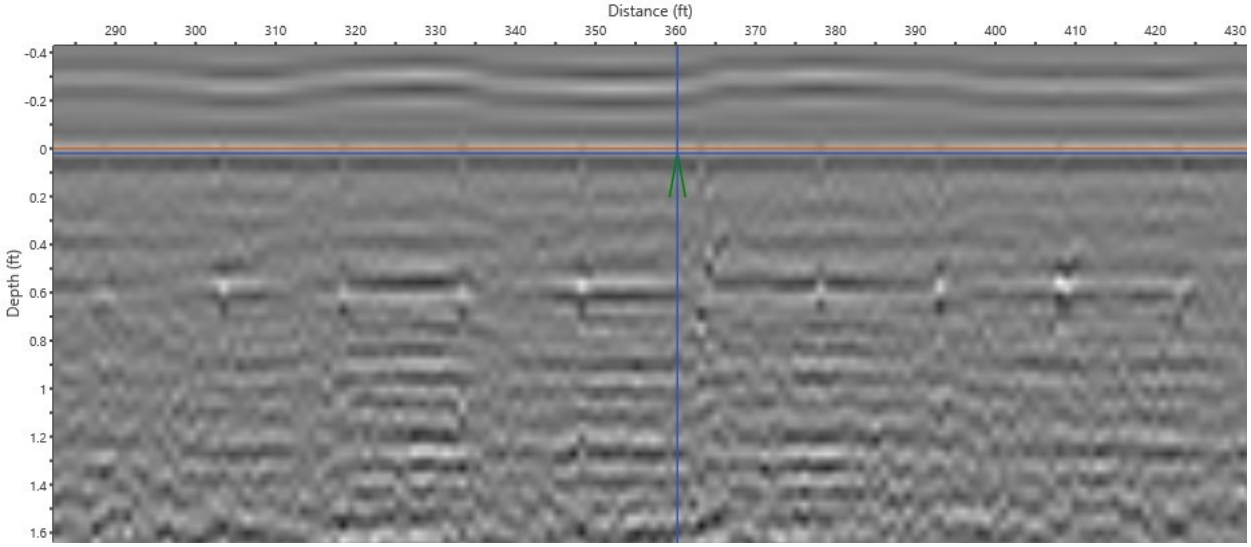


**Figure 11.3 GPR Image. Side scan GPR view of the long run scanning at one foot interval.**

The eastbound direction joints were the first scanned within the mobile traffic control operation. Joints were analyzed individually by looking at the area of deterioration from the three angles provided by the 3D GPR system. The high scan frequency of one inch provided a very unique insight into each joint. The joint conditions in the eastbound direction varied based on the surface condition of the joint. The greater the deterioration at any specific joint, the more significant the impact that could be seen in the

GPR data. For the purposes of describing the results, two deteriorated joints, one good joint, and a full-depth repaired joint, are selected for inclusion in this section.

Figure 11.4 is a top-down image of joints 17A and 18A, with the joints at 19.2 and 34.4 feet respectfully in the image. The other joints in the image are performing as expected and show no deterioration. In the image we can see the extent of the surface deterioration for 17A and 18A, some of the most significant in the eastbound direction. These same joints can be found in Figure 11.5, the side scan view of the 18A scan. The deterioration, highlighted in the squares, shows that the deterioration has progressed to the bottom of the concrete slabs, and into the asphalt support layer. The dashed line indicates the bottom of the concrete, while the dotted and dashed line indicates the bottom of the asphalt layer. These joints would be expected to have little to no load transfer, and potentially significant pumping, as all support has likely been lost. The good joints are barely visible in the image, highlighted with triangles, indicating the layers of concrete and asphalt are still homogeneous, and providing the structural support expected of the pavement section.

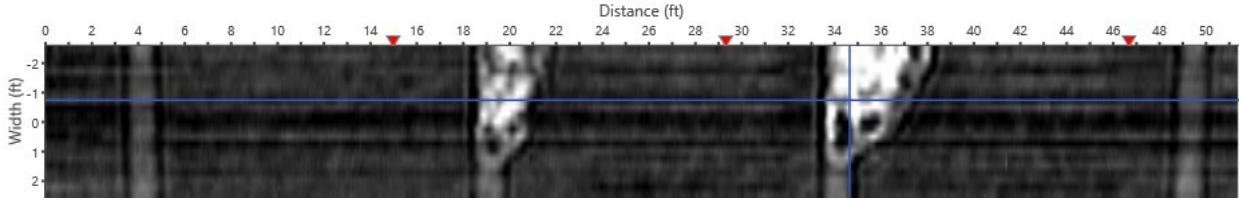


**Figure 11.4 GPR Image. Top down image of GPR scan of joint 18A that includes 17A and two non-deteriorated joints.**

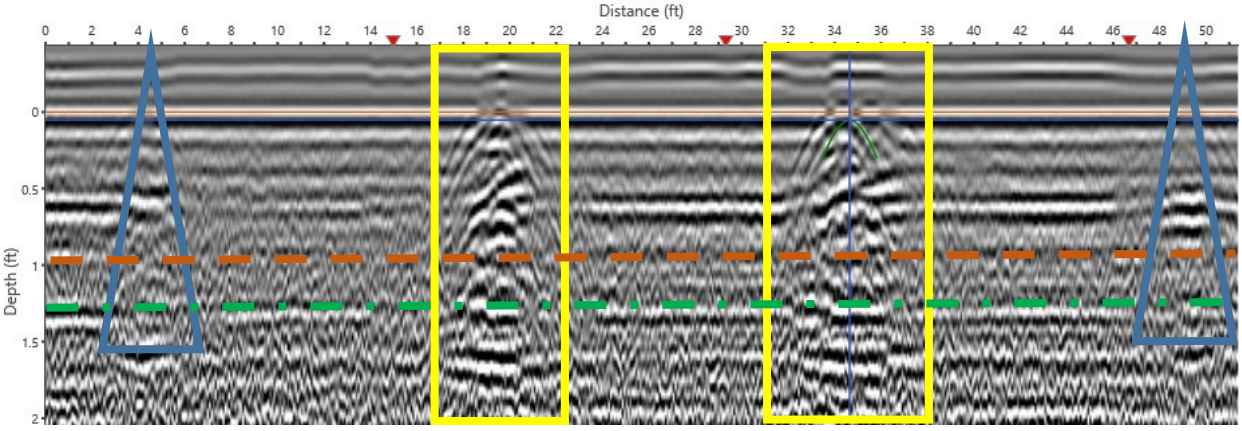


**Figure 11.5 GPR Image. Side scan image of GPR scan of joint 18A that includes 17A and two non-deteriorated joints.**

Another interesting level to explore as part of the joint investigation is the level of the dowel bars. Given the surface deterioration appears to extend to the ends of the dowel bars on the surface of the slab, the GPR investigation included a look at the dowels themselves. Figure 11.6 is the top-down view from the level of the dowels, instead of the top of the pavement presented in Figure 11.4. The individual dowel bars of the good joints, highlighted in ovals, can be observed, with some details observable. However, at

the location of the bad joints, highlighted in the rectangles, the individual dowel bars cannot be distinguished, indicating the deterioration is significant enough to no longer consider them effective. While the two presented joints are the most significant cases of deterioration around the dowel bars for the eastbound direction, all the joints scanned with some level of deterioration show that the deterioration extends at least to the level of the dowels. The majority of low to medium severity deteriorated joints do not show concrete deterioration past the level of the dowels.

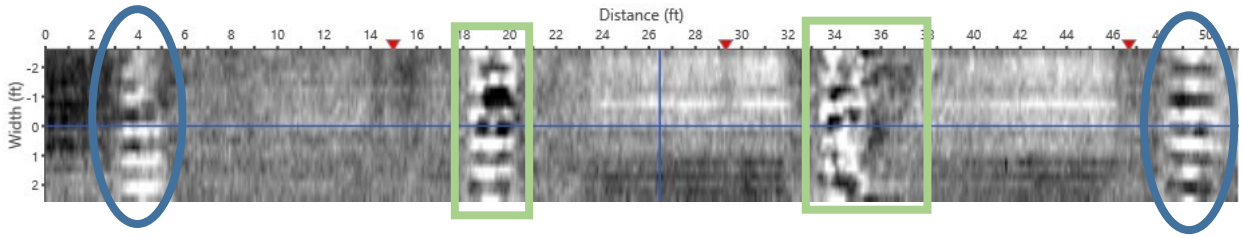


**Figure 11.6 GPR Image. Dowel level view of joint location 18A, including 17A and two good joints.**

The final location type scanned in the eastbound direction was over one of the prior full depth repair locations. The goal was to determine the effectiveness of the repair in returning the joint to an acceptable condition. Figure 11.7 is a top-down view of the location of the scanned repair. The repair is located at the vertical line location and appears to blend seamlessly into the surrounding concrete. This result is to be expected as the GPR relies on changes in material types to provide reflections, and the repair appears to be an integral part of the existing pavement structure. The side scan view of the repair, Figure 11.8, does not show any deterioration remaining at the repair location. These results indicate that the type of repair performed on the joints that have deteriorated previously, should be effective in returning the pavement to a reasonable condition.

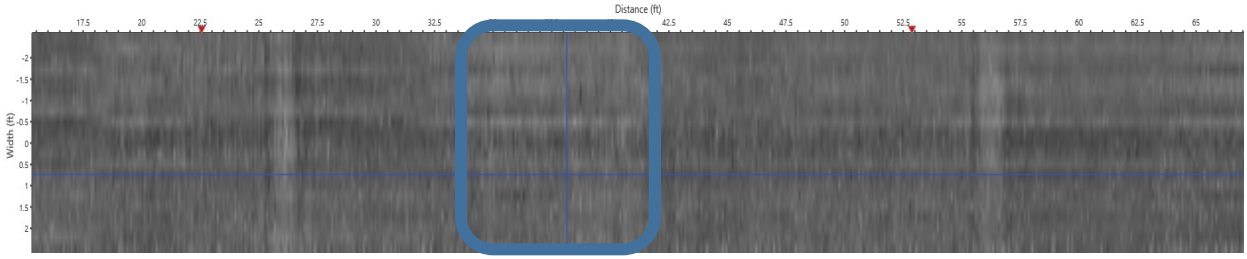


**Figure 11.7 GPR Image. Top-down look at the location of a pavement full-depth repair.**

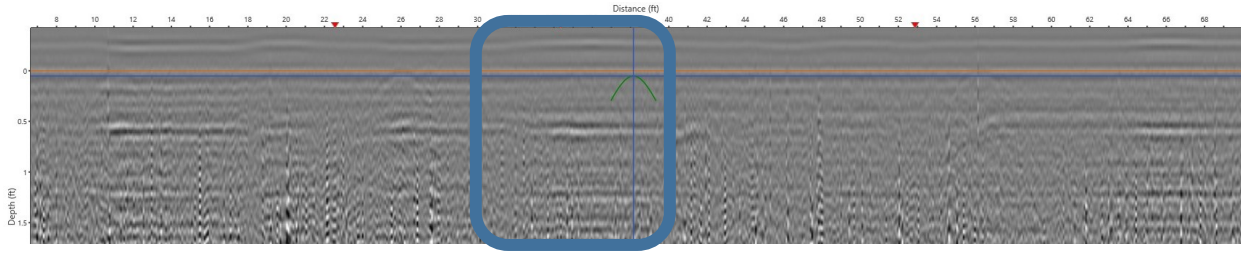


**Figure 11.8 GPR Image. Side view of full-depth repair location in the right wheelpath with repair highlighted by the rectangle.**

Several individual locations were also selected in the westbound direction. Joint 1A was located in Lane 4 and was the first joint scanned in the westbound direction. Joint 1A had noticeable deterioration near the edge of the joint but is greatest in the right wheel path. Figure 11.9 shows the GPR side scan image of joint 1A in the right wheel path. The horizontal slice shows that the distress extended to the level of the dowel bars. Figure 11.10 is a top-down view of the joint at a level three inches below the surface of the pavement that shows how the deterioration progresses beyond the surface of the pavement. Figure 11.11 is the top-down view of the joint at the level of the dowel bar, showing how the deterioration continues into the depth of the slab, but reducing in severity. Figure 11.12 is the top-down view of the joint at a depth of 9.5 inches, just above the bottom of the concrete, where the deterioration is less than the level of the dowel bar. The overall condition of the joint gives indications that the joint spalling is likely initiating from the dowel bar and progresses upwards.

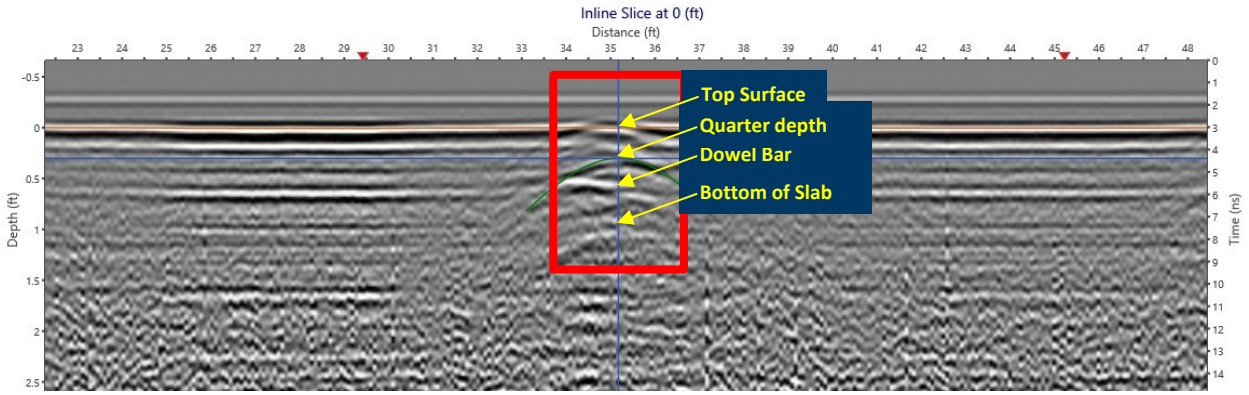


**Figure 11.9 GPR Image. GPR side scan image of joint 1A showing the levels of the deteriorated joint including the dowel bar and the bottom of the slab.**

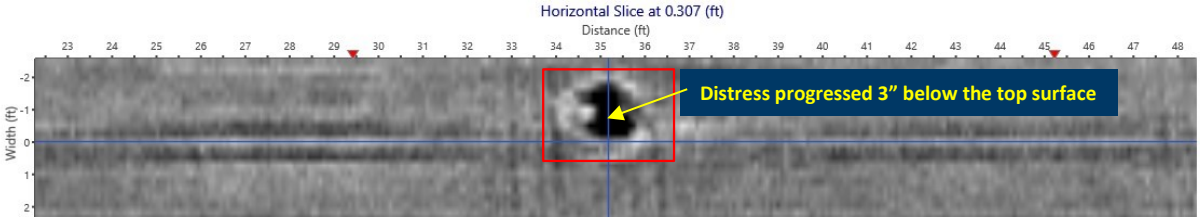


**Figure 11.10 GPR Image. Location of deterioration at joint 1A, 3-inch below the top surface.**

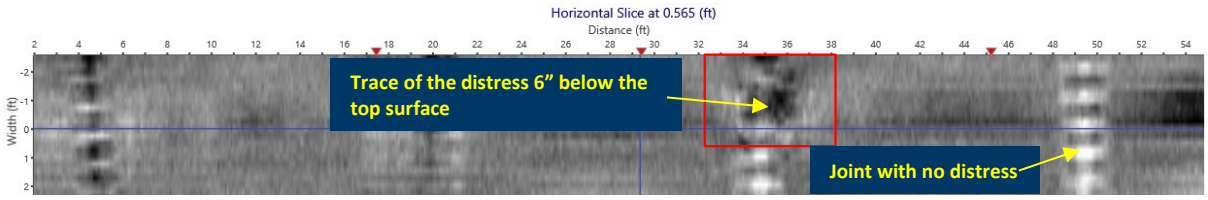


**Figure 11.11 GPR Image. Location of deterioration at joint 1A, 6-inch below the top surface.**

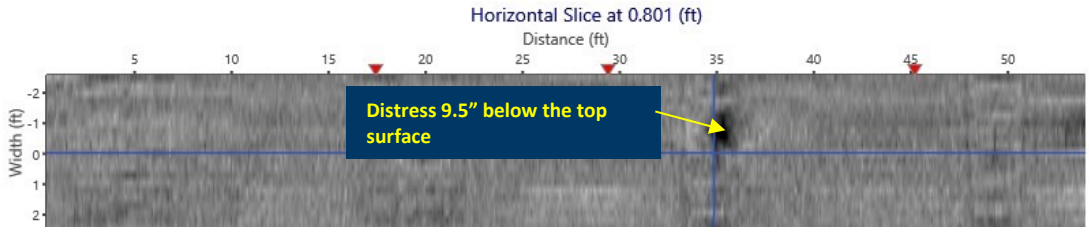


**Figure 11.12 GPR Image. Location of distress at joint 1A-RWP, 9.5-inch below the top surface.**

Joint 3A has not deteriorated to same degree as Joint 1A, or the two joints discussed in the eastbound direction. Figure 11.13 is the side scan view of Joint 3A, where the deterioration appears less than in Joint 1A. Figure 11.14 and Figure 11.15 represent the GPR scan images of Joint 3A at different depths from top surface. Although the distress is obvious in the top surface (Figure 11.14), it is not as obvious at depth 8.6-inch (Figure 11.15).

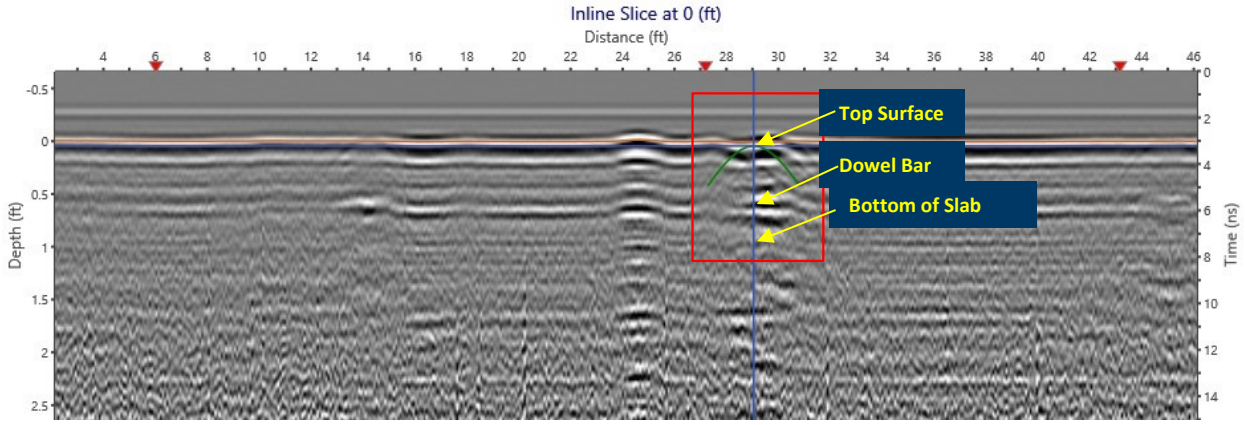


**Figure 11.13 GPR Image. Side scan view of Joint 3A.**

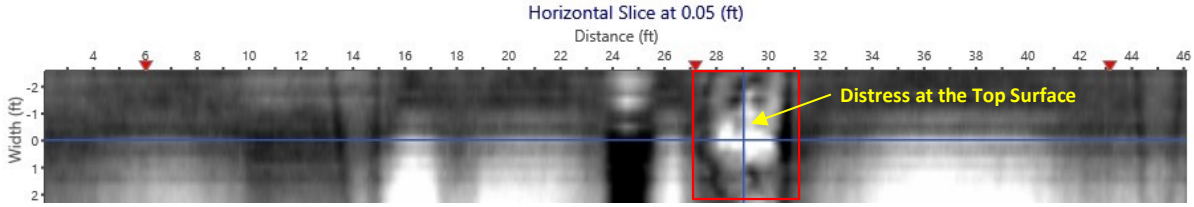


**Figure 11.14 GPR Image. Location of distress at joint 3A, at the top surface.**

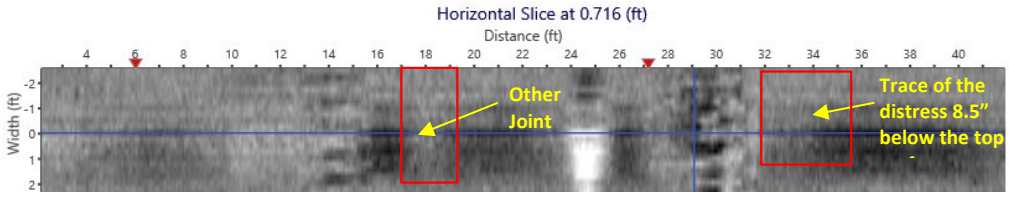


**Figure 11.15 GPR Image. Location of distress at joint 3A, 8.5-inch below the top surface.**

## 11.1 Key Findings from GPR Testing

The goal of using the GPR on the deteriorated joints observed on I-94 at the Illinois Tollway was to determine if the deterioration of the joints was observable in the GPR, and whether these observations would lend insight into the cause of the deterioration of the joints. The section of I-94 was scanned using high speed GPR scanning, and lower speed high intensity GPR scanning. The high-speed scanning was able to determine the location of the concrete joints but was not able to provide any indication of the condition of the joints being scanned. The progression to individual joint scanning provided a deeper understanding of the progression of the joint deterioration. The GPR analysis found that the delamination cracking appears to progress from the dowels to the top of the concrete. As the visible deterioration increases in size and scope at each joint location, using the GPR, the deterioration was observed to progress deeper into the slab.

# Chapter 12: Field Investigations – Pulse Induction

Pulse induction technology scanning was performed on 55 joints at the Illinois Tollway, 25 joints on I-39 NB in Dane County, and 19 joints on I-39 NB in Columbia County to evaluate the impact of dowel bar alignment on the occurrence of delamination cracking (Figure 12.1). Joint scores and alignment information were collected as shown in Figure 12.2 through Figure 12.5. Rotational misalignments of individual dowels within a transverse joint are used to compute the joint score for that joint. A joint score is calculated as 1 plus the sum of the product of the weights empirically assigned to each degree of misalignment and the number of dowels in each misalignment category (Yu and Khazanovich 2005; Yu and Tayabji 2007). Weighting factors for determining the joint score are shown in Table 12.1. In Table 12.1, the range of misalignment represents the total misalignment, which is calculated as the square root of the sum of squares of the horizontal skew and vertical tilt. According to Yu and Khazanovich, transverse joints with joint scores greater than 10 have a higher potential for joint lockup and may require further evaluation and monitoring.

**Table 12.1 Weighting factors used to determine the joint score (Yu and Khazanovich 2005).**

| Range of Misalignment (Inches) | Weighting Factor |
|---|---|
| $0.4 < d < 0.6$ | 0 |
| $0.6 < d < 0.8$ | 2 |
| $0.8 < d < 1.0$ | 4 |
| $1.0 < d < 1.5$ | 5 |
| $d > 1.5$ | 10 |

$d$ = dowel diameter.

Over 90 percent of the dowels had joint score less than 10 and almost all joints had joint score less than 20. Over 95 percent of joints had maximum misalignment less than one inch, concrete cover greater than four inches, and longitudinal translation less than three inches, all well within typical construction tolerances and agency specifications. Images of typical dowel scan images are shown in Figure 12.6.

**Figure 12.1 Photo. Collecting dowel alignment data using pulse induction on I-39 NB in Dane County, Wisconsin.**

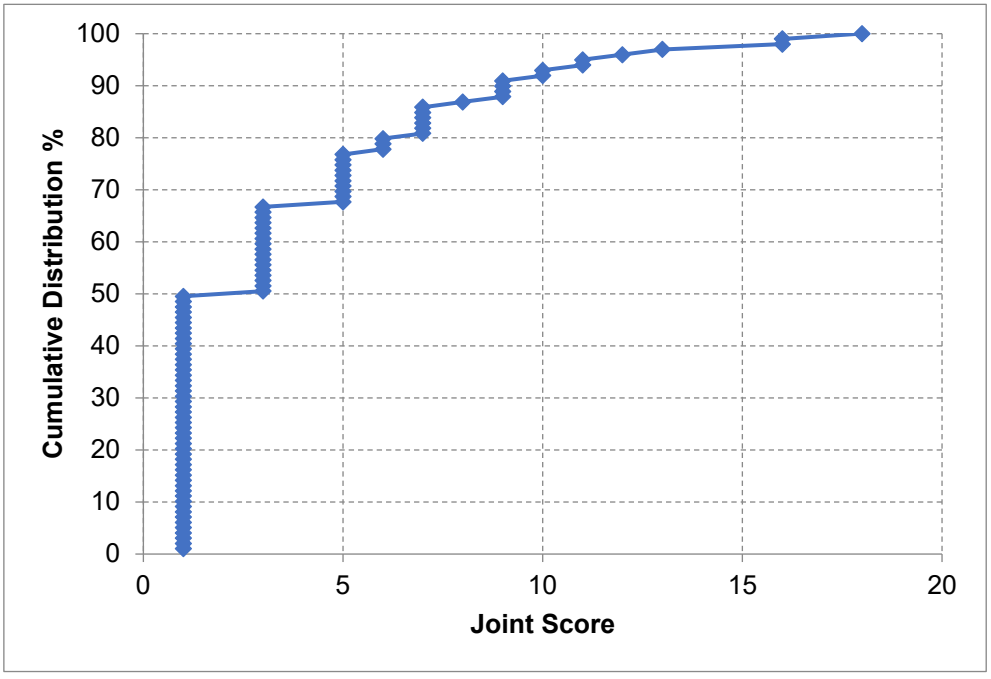


**Figure 12.2 Chart. Joint score distribution of delamination sites.**

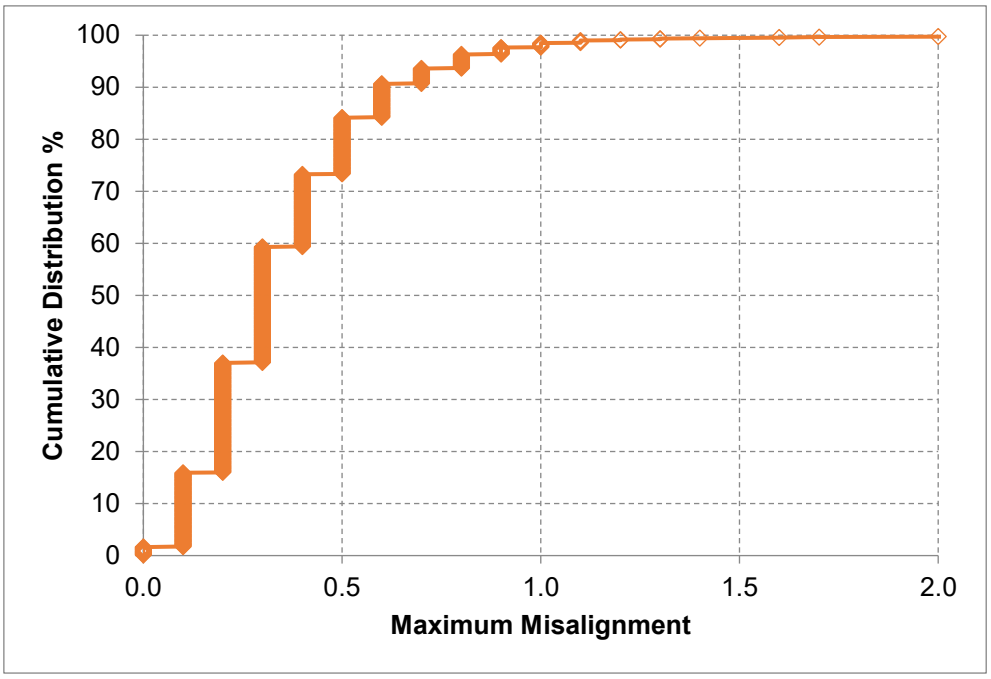


**Figure 12.3 Chart. Maximum misalignment distribution of delamination sites.**

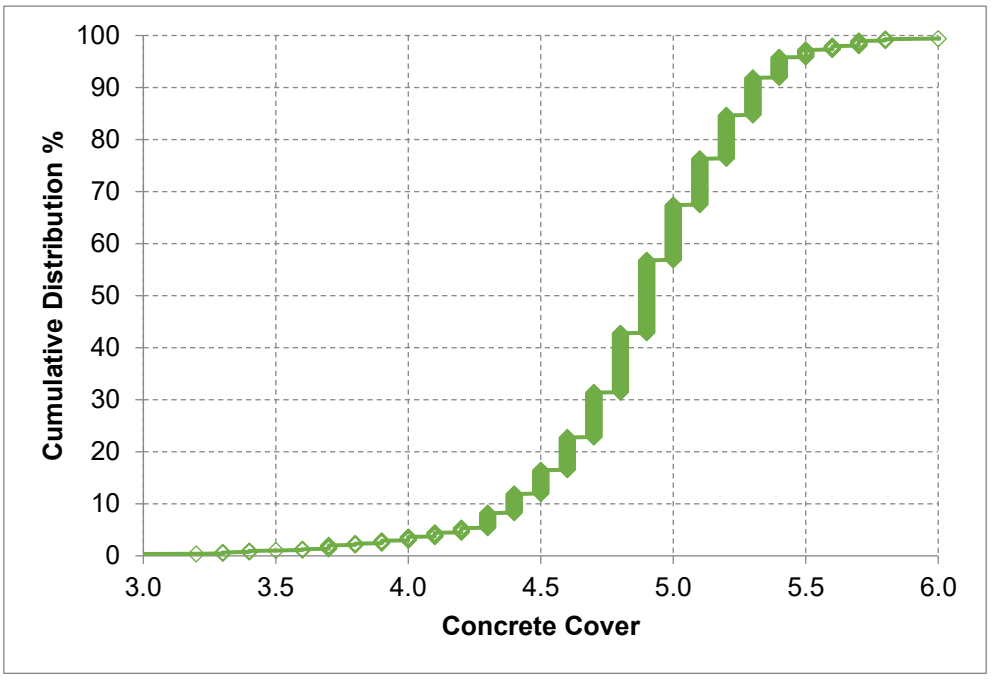


**Figure 12.4 Chart. Cover distribution of delamination sites.**

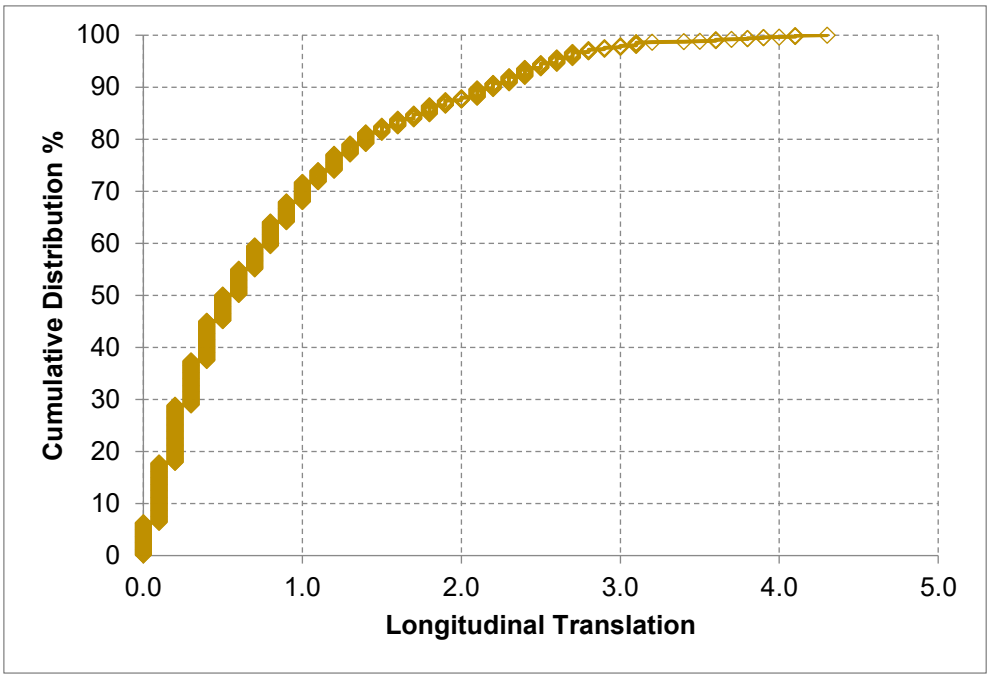


**Figure 12.5 Chart. Longitudinal translation distribution of delamination sites.**

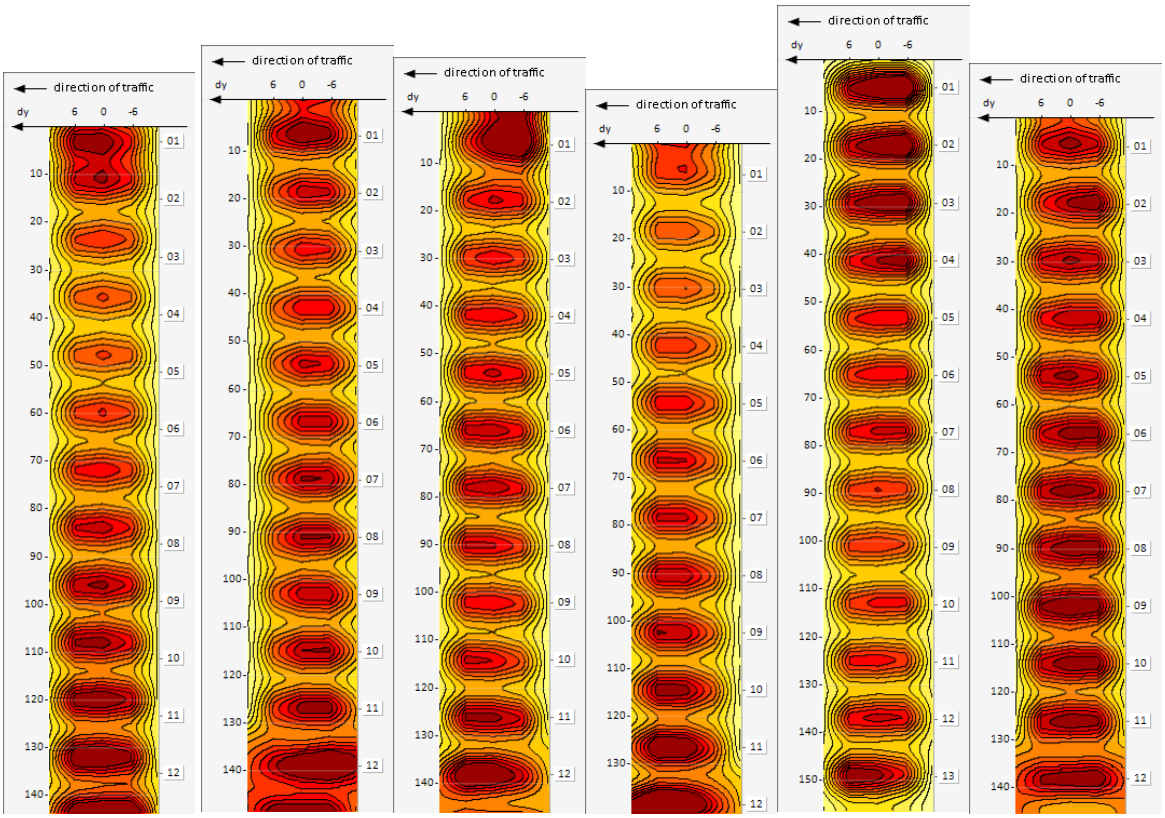


**Figure 12.6 Contour Plots. Pulse induction images of typical scans on delamination sites showing good dowel alignment.**

## 12.1 Key Findings from Dowel Alignment Testing

Based on the pulse induction testing performed for dowel alignment and position, because a vast majority of joints and dowels had very good to excellent alignment, dowel misalignment can be ruled out as a causative factor for the delamination cracking at the sites tested.

# Chapter 13: Field Investigations - Trenching

Figure 13.1 through Figure 13.4 show photos following trenching conducted by the Minnesota Department of Transportation and the Wisconsin Department of Transportation. Figure 13.5 and Figure 13.6shows similar delamination cracking on a city street in central Illinois. These photos show the extent and uniformity of the delamination cracks, again confirming their location as the depth of the dowel bars.

**Figure 13.1 Photo. Stacked slabs of trenched concrete at the disposal/recycle yard from TH 610 in Hennepin County, Minnesota showing horizontal crack at about mid slab depth.**


**Figure 13.2 Photo. Trench showing delamination cracked concrete from TH 610 in Hennepin County, Minnesota.**

**Figure 13.3 Contour Plots. Trench showing delamination cracked concrete from undocumented site in Wisconsin.**

**Figure 13.4 Photo. Trench showing delamination cracked concrete from I-39 NB in Dane County, Wisconsin.**


**Figure 13.5 Photo. Trench showing delamination cracked concrete from a city street in Central Illinois on a relatively new (less than 3 years) concrete pavement.**


**Figure 13.6 Photo. Trench showing concrete split at around mid-depth during trenching from a city street in Central Illinois on a relatively new (less than 3 years) concrete pavement.**

## 13.1 Key Findings from Trenching Operations

The results of the trenching operations conducted by MnDOT and WisDOT are consistent with the results from coring, MIRA scans, and GPR testing. The delamination cracks are at the depth of the dowel bars and extend rather uniformly through significant transverse length of the concrete slab. The uniformity of the crack (i.e., the crack is fairly horizontal and extends through multiple dowel bars) suggests that the delamination action is caused by the combined action of multiple dowel bars (acting in sync) rather than that of one or two dowel bars. At the very least it likely indicates a horizontal zone of weakness for the crack tip to propagate.

# Chapter 14: Summary of Field Investigations

A brief summary from the field investigations is given below:

- Several JPCP projects in Wisconsin and a few in Minnesota and Illinois exhibit large spalls at transverse joints. The occurrence of these spalls is relatively common within a project, observed on approximately one in ten to twenty joints after only ten to fifteen years of pavement service life following construction.
- These spalls are typically one foot or more in length in both the transverse and longitudinal directions. The cracks within the concrete typically start around the depth of the dowel bar near the joint as delamination cracks and migrate upwards towards the surface, eventually breaking up and spalling the concrete. These spalls are related to the presence of steel (dowel bars and tie bars) embedded in the concrete and can be distinguished from typical durability-related spalling by their extent and size, their depth, and lack of any significant amount of hairline cracking associated with or around the spalled concrete.
- The time history images obtained from the Illinois Tollway suggests that the spalls progress rapidly (within 2 years) from small to large and are not limited to approach or leave side of the joint. i.e., the spalls are just as likely to occur on the leave side of the joint as they are on the approach side of the joint.
- MIRA scans conducted at the Illinois Tollway, Wisconsin, and Minnesota all show significant extents of delamination cracking beneath the pavement surface. These cracks were observed on several joints that did not exhibit any signs of visible distresses at the surface of the concrete. These cracks start at or around the depth of the dowel bars and extend through multiple dowel bars, and in some cases almost the full transverse length of the joint. In some cases, the cracking is so severe that the signals from the cracks overpower the signals from the slab-base interface. MIRA scans showed delamination cracks beneath the concrete surface on both approach side and leave side of the joints.
- Coring conducted in Wisconsin suggest the delamination cracks extend for several feet away from the transverse joints in the longitudinal direction. For the sections surveyed, these cracks exist beneath the concrete surface even when there are no visible distresses on the surface. Thus, the coring confirmed the results of the MIRA scans. These cracks clearly start at the depth of the dowel bar and extend horizontally, eventually turning up or down, again confirming the results of the MIRA scans. This is evidenced by the fact that cores taken closer to the joints have the cracks at the mid depth of the core at the level of the dowel bar, whereas cores taken two or more feet away from the joints show the delamination crack at mid depth or higher or lower than mid depth. Cores typically showed cracks progress through the aggregate rather than around the aggregate suggesting the crack tip approached the aggregate when the concrete had gained sufficient strength. In some cases, cores closer to the joint had cracks go around the aggregates suggesting these cracks near the joints, and consequently near the dowel bars, happened during the early age of the concrete when the concrete was not very strong.
- High-speed GPR scanning was able to determine the location of the concrete joints but was not able to provide any indication of the condition of the joints being scanned. The progression to

individual joint scanning provided a deeper understanding of the progression of the joint deterioration. The GPR analysis found that the delamination cracking appears to progress from the dowels to the top of the concrete. As the visible deterioration increases in size and scope at each joint location, using the GPR, the deterioration was observed to progress deeper into the slab.

- Based on the pulse induction testing performed for dowel alignment and position, because a vast majority of joints and dowels had very good to excellent alignment, dowel misalignment can be ruled out as a causative factor for the delamination cracking observed at these sites.
- The results of the trenching operations conducted by MnDOT and WisDOT are consistent with the results from coring, MIRA scans, and GPR testing. The delamination cracks are at the depth of the dowel bars and extend rather uniformly through significant transverse length of the concrete slab. The uniformity of the crack (i.e., the crack is fairly horizontal and extends through multiple dowel bars) suggests that the delamination action is caused by the combined action of multiple dowel bars (acting in sync) rather than that of one or two dowel bars. At the very least it likely indicates a horizontal zone of weakness for the crack tip to propagate.

# Chapter 15: Potential Mechanisms, Factors, and Solutions

The field investigations conducted and summarized above suggests dowel bars (and to a lesser extent tie bars) play a key role in the delamination cracking observed at the surveyed sites. Coring, trenching, GPR, and MIRA scans conducted suggest horizontal stresses exerted by the dowel bar on the hardened concrete are the driving force responsible for or contributing to these cracks. These mechanisms have been discussed by other researchers before including Rasmussen et al. (2007) (Figure 15.1) and Mackiewicz (2015) (Figure 15.2).

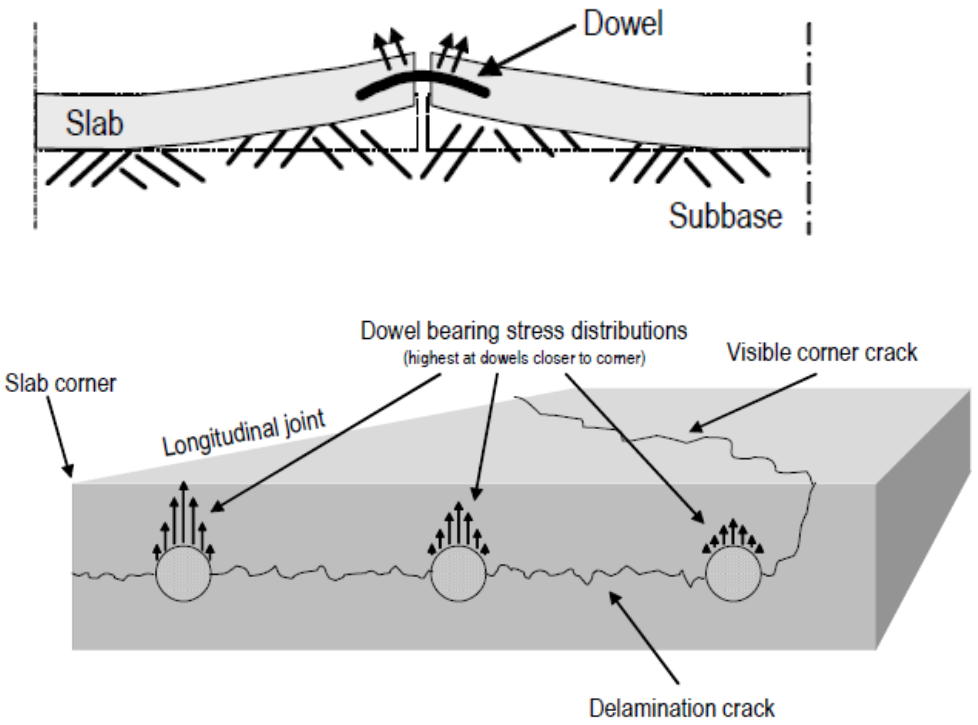


**Figure 15.1 Illustration. Induced dowel bearing stresses due to slab curl and delamination cracking due to dowel bearing stresses (Rasmussen et al. 2007).**

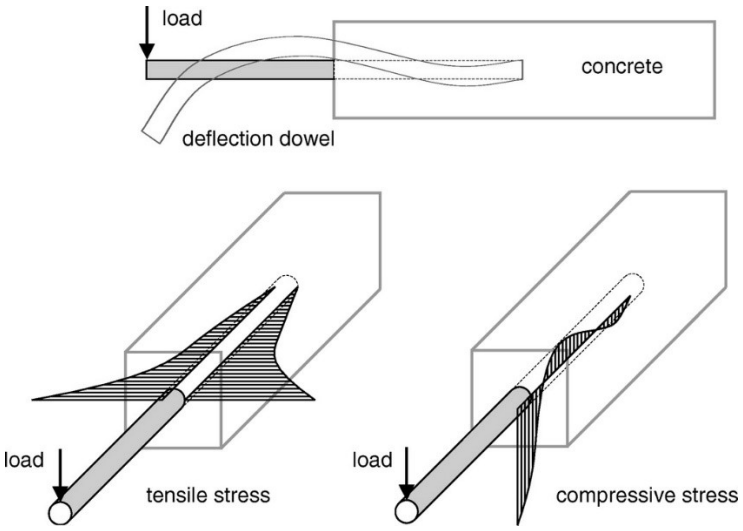


**Figure 15.2 Illustration. Distribution of stresses in a loaded dowel (Mackiewicz 2015).**

Rasmussen et al. based on field evaluation and FE modeling state that "traffic loading can compound this under certain configurations of curl and wheel load. As these stresses continue to increase, they will eventually initiate and propagate cracks in the horizontal direction. Stresses at the dowels decrease with distance from the longitudinal joint. At some point, the stresses that propagate the crack will be smaller than the strength, and under repeated loading cycles, the crack will instead turn upward and appear at the surface of the slab."

Mackiewicz using FE modeling identified "three dangerous zones [around dowel bars] in which microcracks can appear in concrete. When allowable compressive and tensile stresses are exceeded, large cracks and local damages in concrete appear."

It is relevant to note that the phenomenon of microcracking around concrete dowel bars is not new. As early as 1938, Friberg, who conducted laboratory tests on single dowel bars encased in concrete and loaded to failure noted "the initial visible distress of the concrete comes a considerable time before the ultimate load is reached. The initial warning almost always consisted of a small spalling underneath the dowel, first noticeable as a fan-shaped crack from 0.5 inch to 1.5 inch away from the dowel. In the deeper specimens, the first evidence would be a very small, horizontal crack, extending from the dowel toward each side, merging into a fan-shaped failure as the load increased." (Figure 15.3).

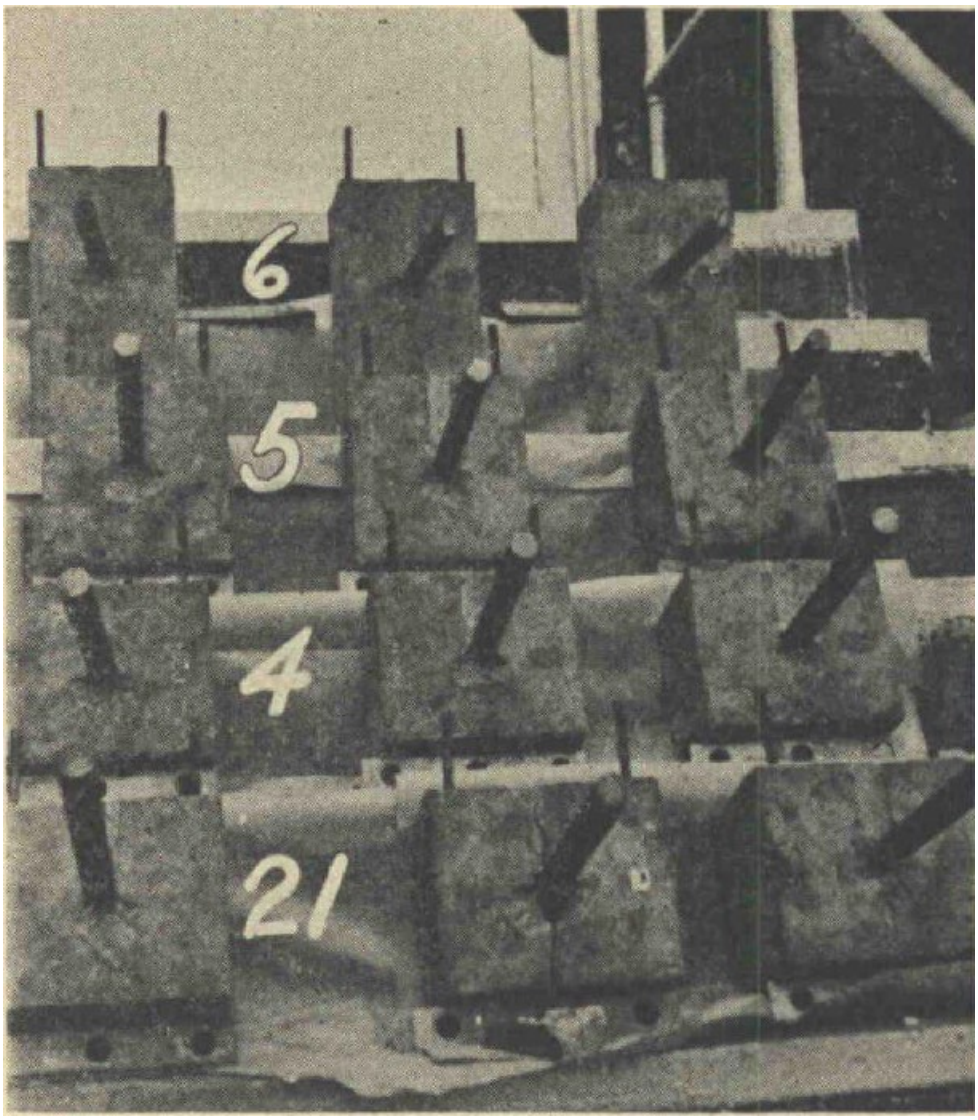


**Figure 15.3 Photo. Specimens from laboratory testing of dowel bars showing typical failures around dowel bars (Friberg 1938).**

The available information suggests a potential mechanism for the delamination cracking observed at the field sites. In the early ages of the concrete hydration and setting, concrete tensile strengths are low. During this time, concrete is increasingly vulnerable to high stress concentrations around dowel bars. External loads induced at this time (due to environmental factors such as temperature curling and moisture warping and traffic factors such as early truck loading) are restrained by the slab weight and dowels. This restraint results in a concentration of stresses around dowel bars and if these local stresses exceed local strengths, microcracks develop around the dowel bars. If the concrete has not fully hydrated, it is possible that these microcracks heal and close with further hydration. Over time, the concrete gains sufficient strength to where the local stresses around dowel bars are lower than the local strengths. However, the microcracks that have already developed during the early ages, and have not healed, continue to deteriorate over several years due to the impact of daily truck traffic and

curling/warping of the slabs. Eventually, these microcracks coalesce to form cracks that propagate horizontally, then turn upward and appear at the surface of the slab.

Potential factors that impact this microcrack formation include:

- Concrete properties (strength gain characteristics, elastic modulus),
- Early age (during and immediately following concrete placement) ambient temperature fluctuations (difference between daytime and nighttime ambient temperatures which are typically impacted by construction time of year and are highest during early spring and late fall),
- Curing,
- Dowel bar properties (size [diameter and length], stiffness, and friction between dowel bars and concrete), and
- Slab-base friction.

Potential solutions to control and reduce formation of these microcracks include:

- Review cold weather concreting practices to reduce the likelihood of concrete placed during times of substantial temperature changes (between daytime and nighttime temperatures).
- Reduce stresses around dowel bars by using less stiff dowel bars and reducing friction by specifying (ensuring) properly lubricated dowel bars.
- Employ proper curing techniques to maintain satisfactory temperature and moisture conditions during early ages of concrete setting and strength gain.
- Specify strong durable concrete. Higher strength, if can be achieved with durable concrete, acts as a counterweight to high stresses. Higher strength concrete can withstand higher stresses build up within the concrete resulting in increased strains within the concrete before it fails/cracks locally, which happens when the stresses exceed the strength. However, there is a limit to how much strength can be increased. As such, higher concrete strengths could be specified if and only if it meets all the specified durability requirements in a cost-effective manner.
- Use a stabilized base course. Stabilized base courses have higher friction between the base and the concrete. This could reduce thermal movements and stresses in the concrete around the dowel bars.
- Use concrete with lower CTE. Lower CTE results in less thermal movement of the concrete. Using coarse aggregates with a lower CTE may sometimes not be a practical option if the costs to transport lower CTE aggregates are exceedingly high.

# Chapter 16: Proposed Analytical Modeling and Laboratory Testing

## 16.1 Purpose

The field investigations suggest dowel bars (and to a lesser extent tie bars) play a key role in the delamination cracking observed at the surveyed sites. Coring, trenching, GPR, and MIRA scans conducted suggest horizontal stresses exerted by the dowel bar on the hardened concrete are the driving force responsible for or contributing to these cracks. However, even with the notional knowledge of the above mechanism, the extent of the impacts of various potential parameters driving this mechanism is not fully understood. For example:

- To what extent do concrete properties (strength gain characteristics [both early age and long term], elastic modulus) impact initiation, propagation, and deterioration of delamination cracks?
- What level of stresses under different ambient conditions can be expected during the early ages in the concrete around and between dowel bars and how do these stresses compare with the concrete tensile and flexural strengths?
- Are environmental stresses sufficient to cause early age cracking (and subsequent propagation over the life of the pavement) around and between dowel bars, or does early age traffic loading also contribute and play a role to a measurable extent?
- What criteria should be established to ensure that localized stresses that develop in the concrete around and between dowel bars during early ages is low (below the concrete tensile or flexural strength at that age)?
- How do dowel bar properties (size [diameter and length], stiffness, and friction between dowel bars and concrete) impact initiation, propagation, and deterioration of delamination cracks in the concrete matrix around and between dowel bars?
- What is the impact of temperature and moisture gradients and the associated curling and warping on stresses in the concrete around and between dowel bars?
- Are there other factors such as curing and slab-base friction that can be amended (by design, by material selection, or by specification) to control stresses within the concrete around and between the dowel bars?

To address these questions and help develop solutions to mitigate delamination cracking caused by dowel bar and/or tie bar stresses a combination of analytical modeling and laboratory testing is proposed.

## 16.2 Analytical Modeling

Due to the large number of potential parameters that are responsible for damage with likely interaction between several of these parameters, the first order of evaluation is proposed to be analytical modeling rather than a detailed laboratory investigation. For the analytical modeling, first-principles analysis tools

using FE analysis are proposed to evaluate the thermomechanical stresses that cause cracking. The overall approach is to use nonlinear FE analysis to perform several deterministic analyses of this large parameter space. A powerful approach is to use computational experimental designs to perform efficient parameter variations and conduct sensitivity studies to identify the main effects driving the damage in the concrete around and between dowel bars. This approach is useful in evaluating the potential interactions between the many parameters that drive damage.

Based on the FE analysis results, a subset of analyses is proposed to be validated by performing laboratory experiments that provide the best potential for improvements to the models. Using conclusions drawn from literature review and field investigations in the previous tasks, the following are key material and design property parameters to evaluate using the FE analysis:

- Concrete elastic modulus
- Concrete slab thickness
- Dowel elastic modulus
- Dowel diameter
- Dowel spacing (optional)
- Dowel-concrete friction
- Concrete slab-base friction
- Concrete unit weight
- Concrete coefficient of thermal expansion
- Concrete drying shrinkage (may be combined with concrete coefficient of thermal expansion for purposes of analysis).

For various combinations of these listed material and design property parameters, a combination of load and environmental stresses due to (1) temperature and moisture differentials (through the depth of the concrete slab), (2) horizontal movements due to temperature and moisture changes, and (3) traffic loads need to be subjected to the concrete slab-dowel system.

In addition to this large set of parameters, uncertainties exist in various model input parameters and in the concrete pavement environment. It is important to understand and quantify the effect of these uncertainties on the predicted outcome to develop bounds on the potential variability of the predicted results. A fractional factorial experimental design is proposed to perform critical modeling parameter screenings that drive the concrete cracking and to bound the variability in the amount of concrete damage. Fractional factorial designs are two-level designs that are executed at high and low values for each variable. These designs require fewer than the usual $2^k+1$ runs needed for a one at a time plus one center point design. Using fractional factorial experimental design will allow to (1) optimize the number of simulations required to study the various combinations of parameters and (2) identify the parameters driving the concrete cracking.

### 16.2.1 Finite Element Analysis Modeling Tool

The FE analysis modeling tool selected will need to explicitly model concrete damage well. An example of one such tool that can be used to perform the proposed analyses is LS-DYNA. Other capable software tools include ABAQUS and ANSYS. For Phase 2 of this research, we propose the use of LS-DYNA.

LS-DYNA is a nonlinear explicit FE analysis code for the dynamic analysis of structures and has widespread acceptance in the engineering community. LS-DYNA is based on the public domain DYNA3D FE code developed at the Lawrence Livermore National Laboratory. LS-DYNA is also well-suited for a transient analysis of the stresses developed in doweled concrete due to heat of hydration, thermal expansion, wheel loading, etc. LS-DYNA is not limited to any particular type of simulation. In a given simulation, any of LS-DYNA's many features can be combined to model a wide variety of physical events. LS-DYNA's analysis capabilities include:

- Full 2D & 3D capabilities
- Quasi-static simulations
- Normal modes
- Linear statics
- Thermal analysis
- Failure analysis
- Crack propagation
- Multi-physics coupling
- Structural-thermal coupling
- Adaptive remeshing

LS-DYNA provides more than 130 metallic and non-metallic material models. LS-DYNA's library of material models include:

- Metals
- Concrete & soils
- User-defined materials

Some of the element types available in LS-DYNA include:

- Discrete elements (springs and dampers)
- Solids (4 and 10-node tetrahedrons, 6-node pentahedrons, and 8-node hexahedrons) (with over 20 solid element formulations)

LS-DYNA's contact algorithms include:

- Single surface contact
- Eroding contact
- Resultant force contact
- Rigid body to rigid body contact
- Heat transfer across the contact surface
- User-defined contact options

Several friction models are available in LS-DYNA:

- Static and dynamic Coulomb friction
- User-defined friction models.

### 16.2.2 Fractional Factorial Design

Full factorial analytical modeling can require many combinations of runs. For example, for the ten material and design properties listed earlier, a full factorial requires $2^{10} + 1 = 1{,}025$ runs at each loading condition, assuming each factor is analyzed at two levels (high and low). Even if these parameters are reduced to eight, a full factorial requires $2^8 + 1 = 257$ runs at each loading condition, assuming each factor is analyzed at two levels. The solution to this problem is to use only a fraction of the runs specified by the full factorial design. In general, a fraction such as 1/2, 1/4, 1/8, 1/16, etc. of the runs called for by the full factorial is used. Properly chosen fractional factorial designs for 2-level experiments have the desirable properties of being both balanced and orthogonal. Centerpoint runs interspersed among the experimental setting runs are added following the initial set of runs to provide a measure of process stability and inherent variability and to check for curvature.

For the analyses to be performed under this study, we suggest a $2^{(10-5)} = 32$ fractional factorial design corresponding to 10 factors and 2 levels to identify key factors influencing stresses. The resolution of this fractional factorial design corresponds to no main effects confounded with two factor interaction, but main effects are confounded with 3-factor interactions and higher. The fractional factorial is shown in Table 16.1 where X1 through X10 are the 10 material and design property parameters and -1 and +1 correspond to the high and low values of these parameters.

If the number of parameters under study are reduced to eight, we suggest a $2^{(8-3)} = 32$ fractional factorial design corresponding to 8 factors and 2 levels to identify key factors influencing stresses. The fractional factorial is shown in Table 16.2 where X1 through X8 are the 8 material and design property parameters and -1 and +1 correspond to the high and low values of these parameters. The resolution of this fractional factorial design corresponds to no main effects confounded with two and three factor interactions. The fractional factorial FE analysis is followed by targeted centerpoint analyses or other FE analysis targeted at specific parameter values based on the results. For example, elastic modulus should be evaluated at early age (~ 1,000,000 psi) and long-term values (3,000,000 to 6,000,000 psi).

**Table 16.1 32 run fractional factorial design for 10 parameters with two levels.**

| X1 | X2 | X3 | X4 | X5 | X6 | X7 | X8 | X9 | X10 |
|---|---|---|---|---|---|---|---|---|---|
| -1 | -1 | -1 | -1 | -1 | 1 | 1 | 1 | 1 | 1 |
| 1 | -1 | -1 | -1 | -1 | -1 | -1 | -1 | -1 | 1 |
| -1 | 1 | -1 | -1 | -1 | -1 | -1 | -1 | 1 | -1 |
| 1 | 1 | -1 | -1 | -1 | 1 | 1 | 1 | -1 | -1 |
| -1 | -1 | 1 | -1 | -1 | -1 | -1 | 1 | -1 | -1 |
| 1 | -1 | 1 | -1 | -1 | 1 | 1 | -1 | 1 | -1 |
| -1 | 1 | 1 | -1 | -1 | 1 | 1 | -1 | -1 | 1 |
| 1 | 1 | 1 | -1 | -1 | -1 | -1 | 1 | 1 | 1 |
| -1 | -1 | -1 | 1 | -1 | -1 | 1 | -1 | -1 | -1 |
| 1 | -1 | -1 | 1 | -1 | 1 | -1 | 1 | 1 | -1 |
| -1 | 1 | -1 | 1 | -1 | 1 | -1 | 1 | -1 | 1 |
| 1 | 1 | -1 | 1 | -1 | -1 | 1 | -1 | 1 | 1 |
| -1 | -1 | 1 | 1 | -1 | 1 | -1 | -1 | 1 | 1 |
| 1 | -1 | 1 | 1 | -1 | -1 | 1 | 1 | -1 | 1 |
| -1 | 1 | 1 | 1 | -1 | -1 | 1 | 1 | 1 | -1 |
| 1 | 1 | 1 | 1 | -1 | 1 | -1 | -1 | -1 | -1 |
| -1 | -1 | -1 | -1 | 1 | 1 | -1 | -1 | -1 | -1 |
| 1 | -1 | -1 | -1 | 1 | -1 | 1 | 1 | 1 | -1 |
| -1 | 1 | -1 | -1 | 1 | -1 | 1 | 1 | -1 | 1 |
| 1 | 1 | -1 | -1 | 1 | 1 | -1 | -1 | 1 | 1 |
| -1 | -1 | 1 | -1 | 1 | -1 | 1 | -1 | 1 | 1 |
| 1 | -1 | 1 | -1 | 1 | 1 | -1 | 1 | -1 | 1 |
| -1 | 1 | 1 | -1 | 1 | 1 | -1 | 1 | 1 | -1 |
| 1 | 1 | 1 | -1 | 1 | -1 | 1 | -1 | -1 | -1 |
| -1 | -1 | -1 | 1 | 1 | -1 | -1 | 1 | 1 | 1 |
| 1 | -1 | -1 | 1 | 1 | 1 | 1 | -1 | -1 | 1 |
| -1 | 1 | -1 | 1 | 1 | 1 | 1 | -1 | 1 | -1 |
| 1 | 1 | -1 | 1 | 1 | -1 | -1 | 1 | -1 | -1 |
| -1 | -1 | 1 | 1 | 1 | 1 | 1 | 1 | -1 | -1 |
| 1 | -1 | 1 | 1 | 1 | -1 | -1 | -1 | 1 | -1 |
| -1 | 1 | 1 | 1 | 1 | -1 | -1 | -1 | -1 | 1 |
| 1 | 1 | 1 | 1 | 1 | 1 | 1 | 1 | 1 | 1 |

**Table 16.2 32 run fractional factorial design for 8 parameters with two levels.**

| X1 | X2 | X3 | X4 | X5 | X6 | X7 | X8 |
|---|---|---|---|---|---|---|---|
| -1 | -1 | -1 | -1 | -1 | -1 | -1 | 1 |
| 1 | -1 | -1 | -1 | -1 | 1 | 1 | 1 |
| -1 | 1 | -1 | -1 | -1 | 1 | 1 | -1 |
| 1 | 1 | -1 | -1 | -1 | -1 | -1 | -1 |
| -1 | -1 | 1 | -1 | -1 | 1 | -1 | -1 |
| 1 | -1 | 1 | -1 | -1 | -1 | 1 | -1 |
| -1 | 1 | 1 | -1 | -1 | -1 | 1 | 1 |
| 1 | 1 | 1 | -1 | -1 | 1 | -1 | 1 |
| -1 | -1 | -1 | 1 | -1 | -1 | 1 | -1 |
| 1 | -1 | -1 | 1 | -1 | 1 | -1 | -1 |
| -1 | 1 | -1 | 1 | -1 | 1 | -1 | 1 |
| 1 | 1 | -1 | 1 | -1 | -1 | 1 | 1 |
| -1 | -1 | 1 | 1 | -1 | 1 | 1 | 1 |
| 1 | -1 | 1 | 1 | -1 | -1 | -1 | 1 |
| -1 | 1 | 1 | 1 | -1 | -1 | -1 | -1 |
| 1 | 1 | 1 | 1 | -1 | 1 | 1 | -1 |
| -1 | -1 | -1 | -1 | 1 | -1 | -1 | -1 |
| 1 | -1 | -1 | -1 | 1 | 1 | 1 | -1 |
| -1 | 1 | -1 | -1 | 1 | 1 | 1 | 1 |
| 1 | 1 | -1 | -1 | 1 | -1 | -1 | 1 |
| -1 | -1 | 1 | -1 | 1 | 1 | -1 | 1 |
| 1 | -1 | 1 | -1 | 1 | -1 | 1 | 1 |
| -1 | 1 | 1 | -1 | 1 | -1 | 1 | -1 |
| 1 | 1 | 1 | -1 | 1 | 1 | -1 | -1 |
| -1 | -1 | -1 | 1 | 1 | -1 | 1 | 1 |
| 1 | -1 | -1 | 1 | 1 | 1 | -1 | 1 |
| -1 | 1 | -1 | 1 | 1 | 1 | -1 | -1 |
| 1 | 1 | -1 | 1 | 1 | -1 | 1 | -1 |
| -1 | -1 | 1 | 1 | 1 | 1 | 1 | -1 |
| 1 | -1 | 1 | 1 | 1 | -1 | -1 | -1 |
| -1 | 1 | 1 | 1 | 1 | -1 | -1 | 1 |
| 1 | 1 | 1 | 1 | 1 | 1 | 1 | 1 |

### 16.2.3 Finite Element Modeling

The FE analysis is to be performed on a multi-layered pavement structure consisting of two concrete slabs connected using a doweled transverse joint and supported by a base and subgrade. While the delamination cracking originates and extends in the concrete immediately around and between dowel bars, modeling full slabs with multiple dowel bars and a transverse joint as shown in Figure 16.1 allows for more realistic simulations of the pavement system, and reduces or eliminates potential boundary conditions influences.

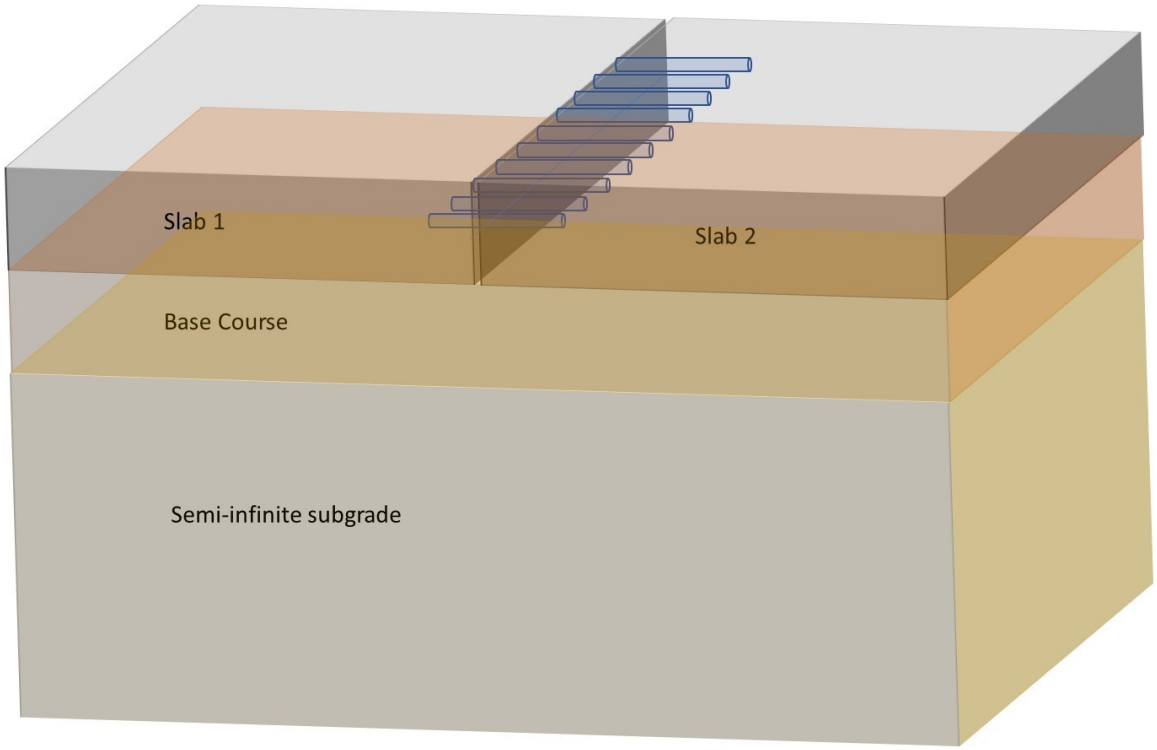


**Figure 16.1 Illustration. Structure for FE analysis modeling.**

To accurately model stresses around and between the dowel bars, the FE analysis meshing, elements, and degrees of freedom per element should be developed with the highest mesh resolution at critical stress zone around dowel bars and mid depth of the slab in between dowel bars (Figure 16.2 and Figure 16.3).

A sliding interface between dowel bars and concrete should be used and evaluated at both low and high friction values. The concrete base interface should be modeled to account for separation and loss of support due to temperature curling and moisture warping of the concrete slab. For purposes of FE analysis, boundary conditions should match those of typical pavement structures. Semi-infinite layers should be used for the bottom and sides of the subgrade to ensure FE analysis captures the pavement system without reflection of stress waves from subgrade. The concrete material model used should allow for progressive deterioration due to stresses while linear elastic material model can be used for the dowel bars, base, and subgrade.

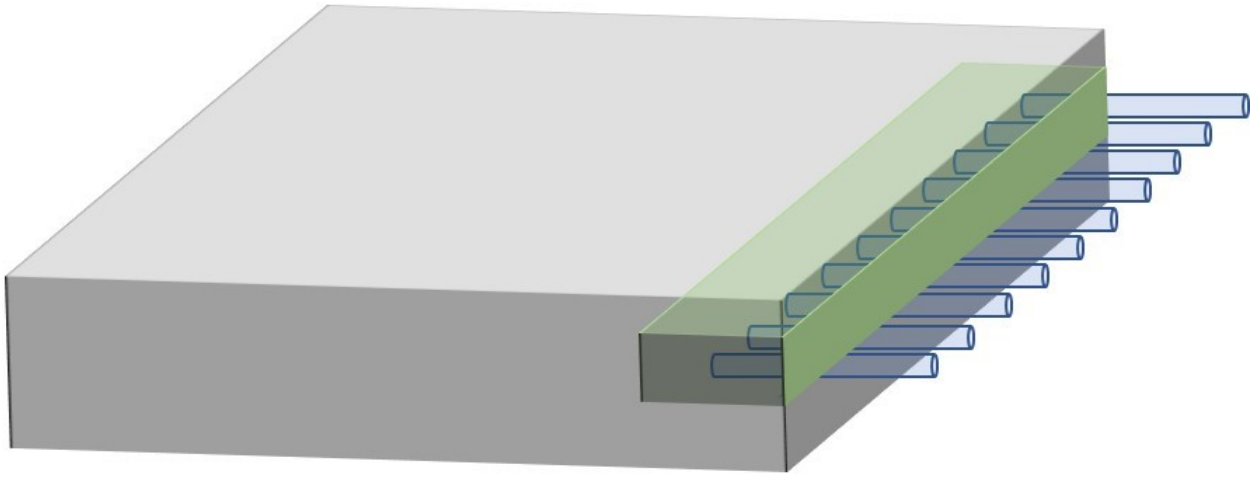

**Figure 16.2 Illustration. High resolution zone for FE analysis modeling.**

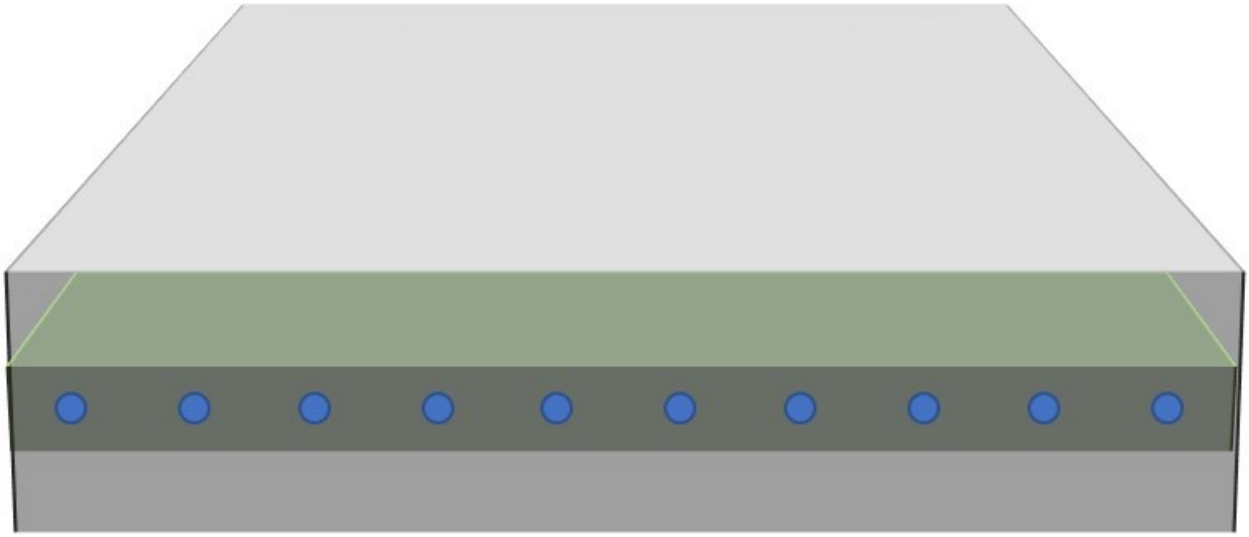

**Figure 16.3 Illustration. High resolution zone for FE analysis modeling.**

The structural thermal FE analysis should include linear temperature difference through the concrete slab resulting in curling of the slab and concrete weight and dowel bar restraint stresses. Note that a true nonlinear temperature gradient through the concrete slab might result in too many simulations and can be approximated by effective linear temperature difference through the slab thickness. The analyses should be performed at multiple linear temperature differences ranging from flat slab condition (0 °F) to high (-40 to +40 °F). The loading condition should also include addition of traffic load (e.g., by adding a single axle load on one or both sides of the joint) as shown in Figure 16.4. Varying the levels of traffic load should be considered.

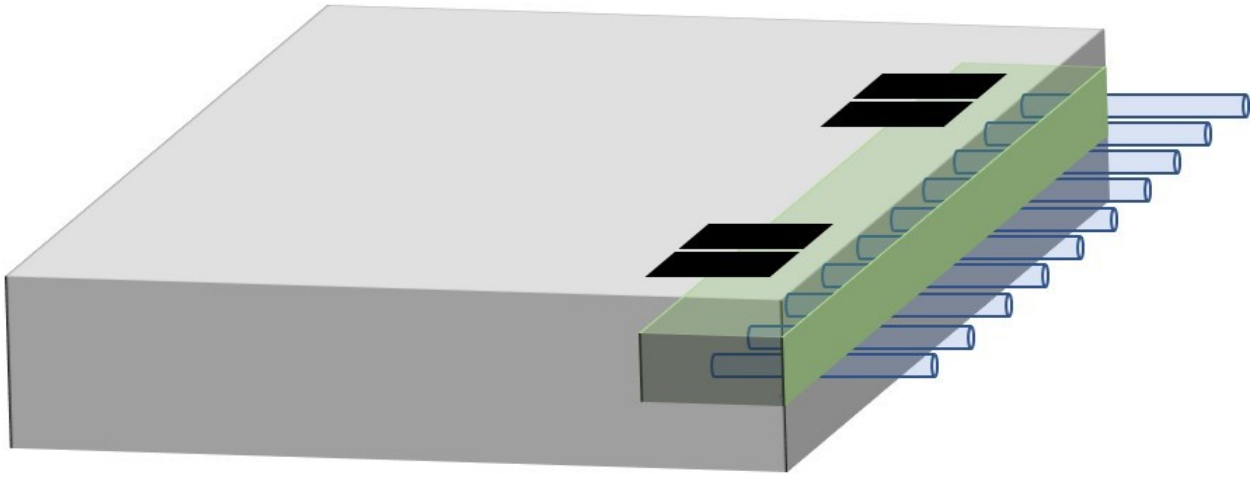

**Figure 16.4 Illustration. Wheel load location for FE analysis modeling.**

### 16.2.4 Finite Element Analysis Parameter Inputs

The input parameter values for the FE analysis should be chosen carefully to cover the full range of practical input values prior to performing the analyses. A starting point for these inputs is shown in Table 16.3. Typical values should be chosen for all other inputs that are needed for the analysis such as Poisson's ratio, base modulus, tire pressure, thermal conductivity, heat capacity, etc.

**Table 16.3 Potential input parameter values for FE analysis.**

| Parameter | Low Value | High Value |
|---|---|---|
| Concrete Elastic Modulus (early age) | 500,000 psi | 1,000,000 psi |
| Concrete Elastic Modulus | 3,000,000 psi | 6,000,000 psi |
| Concrete Slab Thickness | 6 inches | 14 inches |
| Dowel elastic modulus | 5,000,000 psi | 30,000,000 psi |
| Dowel diameter | 1 inch | 1.75 inch |
| Dowel spacing | 6 inches | 18 inches |
| Dowel-concrete friction coefficient | 0.05 | 0.95 |
| Concrete slab-base friction coefficient | 0.05 | 0.95 |
| Concrete unit weight | 120 pcf | 160 pcf |
| Concrete coefficient of thermal expansion | 3 × 10-6in/in/°F | 8 × 10-6in/in/°F |
| Concrete drying shrinkage (percent of total) | 0.02% | 0.1% |
| Concrete compressive strength | - | Function of elastic modulus (300 psi, 2,700 psi, 11,000 psi) |
| Temperature difference (top to bottom of slab) | - | Ranging from -40 °F to +40 °F |
| Axle load | - | Ranging from 0 to 30,000 lbs |

## 16.3 Laboratory Testing

The results of the FE analysis fractional factorial study along with the center point runs are analyzed to compare principal stresses around the dowel bars under various loading conditions and identify key parameters and the extent of their influence on dowel bar cracking. Select cases from the FE analysis study are chosen for laboratory experiments. The results from the field investigation and preliminary FE analysis are used to establish the laboratory experimental setup and the testing matrix. The goal of the laboratory experiment is to validate the FE analysis models and to confirm the potential cracking in the concrete that could occur.

An economical way to conduct these tests is to develop a test article consisting of a two to three dowel bars in two concrete slabs (Figure 16.5). Then, it could be supported to best approximate the substrate and void beneath the slab. Results from the FE analysis study should be used to guide the experimental design. The loads derived from the FE analysis study on the dowel bars would then be applied with a load frame to the test article. A FE model of this test setup would then be used for comparison and validation with the FE analysis study. The FE analysis model should be compared with strain gauges installed immediately around and between the dowel bars.

The test setup consists of a loading frame where concrete specimens are mounted and tested. The supporting system should be a rigid frame, such as a structural steel frame, so as to not influence the test results. The load application and data collection from the strain gauges should be controlled using a data acquisition system to reduce errors. For the purposes of validation of the FE analysis models, the application of a static load is likely sufficient. While this option might validate the FE analysis models, crack propagation studies would require repetitive loadings. The loading frame setup should be able to apply tire loads of varying magnitude up to a typical half axle truck load.

In addition to strain gauges installed around dowel bars, vertical displacements of the slabs can be measured at multiple locations using installed linear voltage displacement transducers (LVDTs). To install strain gauges around dowel bars, the construction of the test specimens will need to be done in two stages with half the concrete specimen with partially embedded dowel bars cast in the first stage, followed by installation of the strain gauges on the face of the hardened concrete around the dowel bars. The second half of the specimen should be cast following the installation of the strain gauges. The strain gauges should be protected during the casting of the second half of the specimen. Figure 16.6 shows potential strain gauge locations.

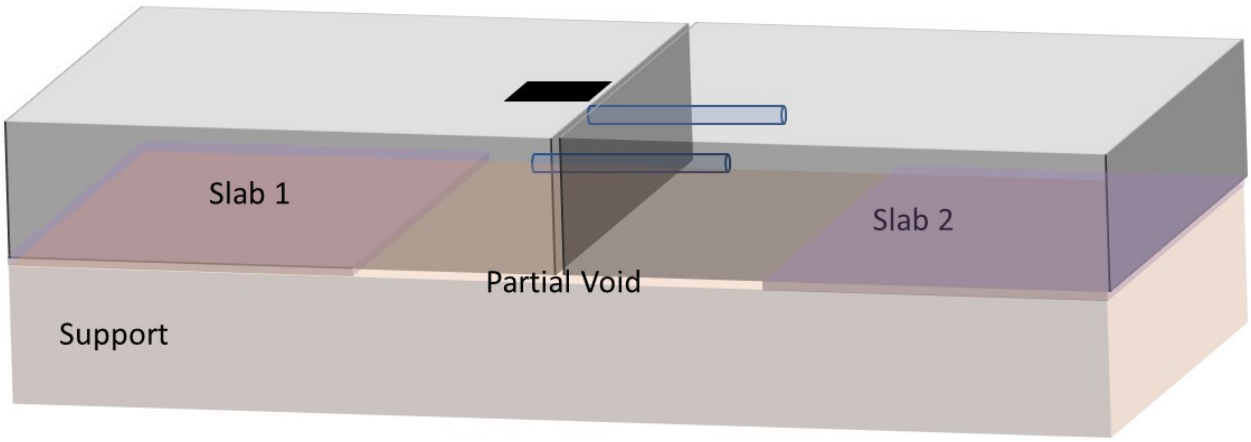


**Figure 16.5 Illustration. Two-dowel full setup for laboratory testing.**

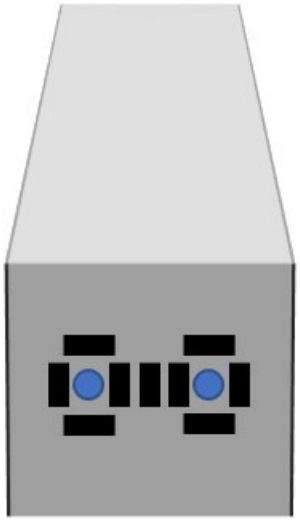

**Figure 16.6 Illustration. Strain gauge locations.**

Alternatively, the test setup could consist of a partial slab setup, with load applied directly onto the dowel bars as shown in Figure 16.7.

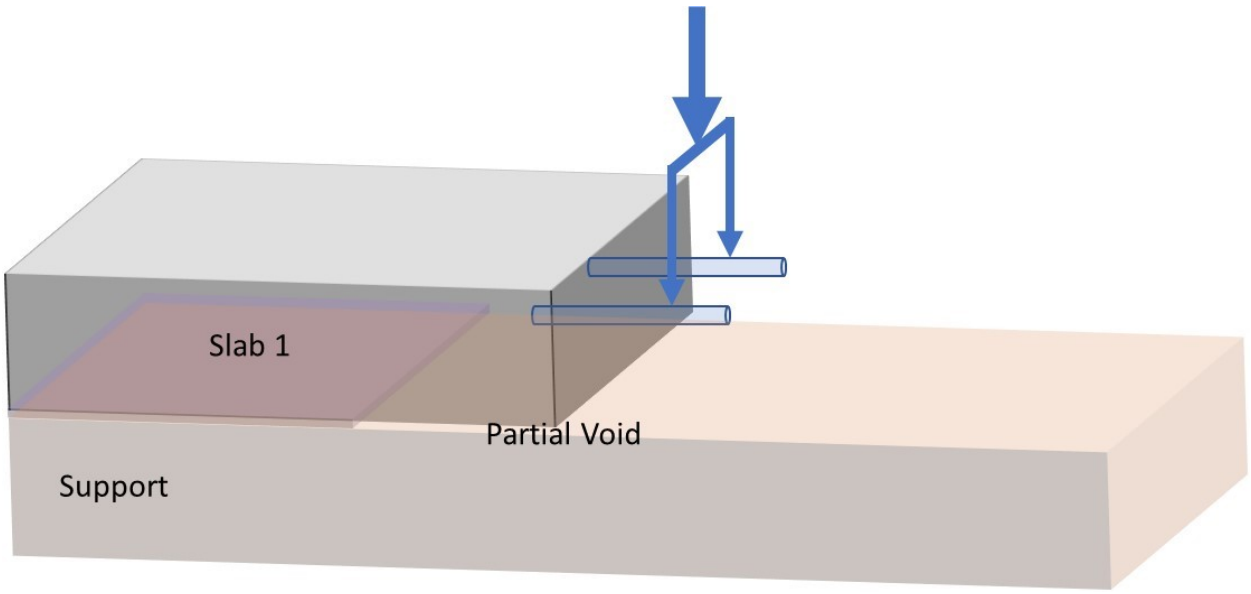


**Figure 16.7 Illustration. Two-dowel partial setup for laboratory testing.**

## 16.4 Update Finite Element Model

The laboratory testing is used to refine the results of the FE analysis. The laboratory setup should be modeled using the FE analysis and the modeled stresses compared with those measured in the laboratory. The FE analysis model should be adjusted based on the laboratory results as appropriate prior to using the model for evaluation of dowel cracking under a variety of conditions.

# Chapter 17: Conclusions

This Phase 1 study was undertaken to evaluate cracking related to dowel bars and tie bars in concrete pavement. A literature study was performed to review work performed by other researchers. Several studies that discussed the issue of dowel bar/tie bar cracking were summarized in this report. While several researchers have contributed significantly to the state of the knowledge, the findings of the literature review indicated that a thorough understanding of the factors and mechanisms responsible for dowel bar/tie bar cracking was still deficient. The literature review was followed by a field evaluation that consisted of six sites in Wisconsin, Illinois, and Minnesota. Field evaluation testing included MIRA, pulse induction scans, GPR, coring, and visual inspection.

The results of the literature review and field studies suggest that concrete slabs within a concrete pavement structure are constantly undergoing movement due to the action of environmental (temperature and moisture) and traffic loading. Generally, this movement is not significantly damaging to the concrete and does not measurably impact the long-term performance of the concrete pavement. However, at some locations, such as around tie bars and dowel bars, the free movement of concrete is restrained by the stiffness of the bars. This restraint results in tensile stresses within the concrete around the dowel bars. If these stresses are well below the concrete tensile strength, the concrete around the dowel bars stays intact and relatively undamaged. During early ages, concrete tensile strength is low enough so that these stresses, under certain conditions, can result in microscopic damage to the concrete around the dowel bars. Over time, due to regular environmental and traffic loading, the damaged concrete causes microcracks to coalesce into larger cracks that propagate through the concrete resulting in delamination cracking.

Even with the notional knowledge of the above mechanism, the extent of the impacts of various potential parameters driving this mechanism is not fully understood. To gain a more comprehensive understanding, a combination of detailed FE analysis with a laboratory experiment is proposed. The FE analysis proposed includes an evaluation of key parameters and their influence on dowel bar cracking. The FE analysis would be validated through laboratory experimentation and analysis. The results of the laboratory testing would then be used to refine the FE models and quantify the impact of various parameters that influence dowel bar cracking. Once the impact of various parameters is quantified, the potential factors and solutions can be updated to take into account the model predictions.

# References


ACI-224R-01 (2001). *Control of Cracking in Concrete Structures*. Farmington Hills, MI: American Concrete Institute.

Antommattei, O. R. (2018). *Dealing with Plastic Settlement Cracking: Case Studies and Lessons Learned*. Salt Lake City, UT: American Concrete Institute.

Ayers, M., Cackler, T., Fick, G., Harrington, D., Schwartz, D., Smith, K., … & Van Dam, T. (2018). *Guide for Concrete Pavement Distress Assessments and Solutions: Identification, Causes, Prevention, and Repair*. Ames, IA: National Concrete Pavement Technology Center at Iowa State University.

Balakumaran, S. S., Weyers, R. E. & Brown, M. C., 2018. *Linear Cracking in Bridge Decks.* Virginia Transportation Research Center.

Brettmann, R., Darwin, D., & O'Reilly, M. (2015). *Developing a Test Procedure to Evaluate Settlement Cracking Performance*. Lawrence, KS: University of Kansas Center for Research, Inc.

Combrinck, R., & Boshoff, W.P. (2014). Fundamentals of Plastic Settlement Cracking In Concrete. *Construction Materials and Structures: Proceedings of the First International Conference on Construction Materials and Structures*, p. 354.

Concrete Construction Associate of Australia (CCAA). 2005. *Plastic Settlement Cracking, Guide to Concrete Construction (T41/HB64)*. Mascot, Australia: Cement and Concrete Association of Australia and Standards Australia.

Dakhil, F. H., Cady, P. D., & Carrier, R. E. (1975). Cracking of Fresh Concrete as Related to Reinforcement. *ACI Materials Journal*, *72*(8), 421-428.

Darter, M., & Rufino, D. (2007). *Forensic Study of Premature Cracking of Tarija-Potosi Highway in Bolivia.* Champaign, IL: Applied Research Associate, Inc.

Harrington, D., Ayers, M., Cackler, T., Fick, G., Schwartz, D., Smith, K., … & Van Dam, T. (2018). *Guide for Concrete Pavement Distress Assessments and Solutions: Identification, Causes, Prevention, and Repair*. Washington, DC: Federal Highway Administration.

Kumar, B., & Mathur, R. (2009). *Early Cracking of Concrete Pavement – Cause and Repairs*. New Delhi: Central Road Research Institute. https://www.nbmcw.com/tech-articles/roads-and-pavements/4988-early-cracking-of-concrete-pavement-causes-and-repairs.html

Khajehdehi, R. (2018). *Controlling Cracks in Bridge Decks*. Doctoral dissertation. Lawrence, KS: University of Kansas.

Kosmatka, S. H., & Panarese, W. C. (2011). *Design and Control of Concrete Mixtures* (No. EB001. 13T, 15th edition). Skokie, IL: Portend Cement Association.

Kyle N., L. (2001). Subsidence Cracking of Concrete Over Steel Reinforcement Bar in Bridge Decks (M.S. Thesis), Virginia Polytechnic Institute and State University, Blacksburg, VA.

Li, L., Tan, Y., Gong, X., & Li, Y. (2012). Characterization of Contact Stresses Between Dowels and Surrounding Concrete in Jointed Concrete Pavement. In *Proceedings of the 10th International Conference on Concrete Pavements*, Québec, Canada, pp. 8-12.

Lim, S. W., & Tayabji, S. D. (2005). Analytical Technique to Mitigate Early Age Longitudinal Cracking in Jointed Concrete Pavements. Paper presented at the 8th International Conference on Concrete Pavements, Colorado Springs, CO, Aug. 14–18.

Luoke, L., Yiqiu, T., Xiangbing, G., & Yunliang, L. (2012). *Characterization of Contact Stresses Between Dowels and Surrounding Concrete in Jointed Concrete Pavement*. In *International Journal of Civil and Environmental Engineering*, 16-24.

Mackiewicz, P. (2015). Finite-Element Analysis of Stress Concentration around Dowel Bars in Jointed Plain Concrete Pavement. *Journal of Transportation Engineering*, *141*(6), p. 06015001.

Mallela, J., Gotlif, A., Darter, M. I., Ardani, A., & Littleton, P. (2009). *A Mechanistic-Empirical Tie Bar Design Approach for Concrete Pavements*. Submitted to the American Concrete Pavement Association, Skokie, IL.

Mehta, P., K., & Monteiro, P. (2006). *Concrete Microstructure, Properties, and Materials* (Third edition). New York: McGraw-Hill Publishing.

Nadelman, E., Krauss, P., & Nelson, T. (2017). *Investigation of Bridge Decks*. Helena, MT: Montana Department of Transportation.

Nassiri, S. (2011). Establishing Permanent Curl/Warp Temperature Gradient in Jointed Plain Concrete Pavements (PhD dissertation), University of Pittsburgh, PA.

Qi, C., Weiss, J. & Olek, J. (2005). Assessing the Settlement of Fresh Concrete Using a Non-Contact Laser Profiling Approach. *International Conference on Construction Materials Research*, *20*, 129-136.

Rasmussen, R. O., Agosto, A., & Cramer, S. (2007). *Analysis of Concrete Pavement Joints to Predict the Onset of Distress (*SPR# 0092-05-05). Madison, WI: Wisconsin Highway Research Program.

Saadeghvaziri, M. A., & Hadidi, R. (2002). *Cause and Control of Transverse Cracking in Concrete Bridge Decks* (Report No. FHWA-NJ-2002-019). Washington, DC: Federal Highway Administration U.S. Department of Transportation.

Safiuddin, M., Kaish, A. M., Woon, C. O., & Raman, S. N. (2018). Early Age Cracking in Concrete: Causes, Consequences, Remedial Measures, and Recommendations. *Applied Sciences*, *8*(10), 1730.

Senn, K. (2018). *Performance Experience and Lessons Learned from the SPS 2 Test Sections of the Long-Term Pavement Performance Program (LTPP).* Washington, DC: Moving Advancement into Practice, Federal Highway Administration National Consortium.

Seo, Y., & Kim, S. M. (2013). Longitudinal Cracking at Transverse Joints Caused by Dowel Bars in Jointed Concrete Pavements. *KSCE Journal of Civil Engineering*, *17*(2),395-402.

Soroka, I., & Ravina, D. (1998). Hot Weather Concreting with Admixtures. *Cement and Concrete Composites*, *20*(2-3), 129-136.

Transportation Research Board (TRB). (2006). *Control of Cracking in Concrete* (Number E-C107 Transportation Research Circular). Washington, DC: TRB.

Tyson, S. S., Tayabji, S. D., & Yu, H. T. (2008). Assessment and Mitigation of Early Age Cracking in Concrete Pavements Due to Restrained Movement. In *Pavement Cracking: Mechanisms, Modeling, Detection, Testing and Case Histories*, *Proceedings of the 6th RILEM International Conference on Cracking in Pavements,* Chicago, IL, pp. 145-153.

Voigt, G. F. (2002). Early Cracking of Concrete Pavement - Causes and Repairs. Paper presented at the 2002 Federal Aviation Administration Airport Technology Transfer Conference, Atlantic City, New Jersey, May 5–8.

Yu, H. T., & Khazanovich, L. (2005). *Use of Magnetic Tomography Technology to Evaluate Dowel Placement* (Report No. FHWA-IF-06-006). Washington, DC: Federal Highway Administration.

Yu, H. T., & Tayabji, S. D. (2007). *Best Practices for Dowel Placement Tolerances* (Report No. FHWA-HIF-07-021). Washington, DC: Federal Highway Administration.

Zuzulova, A., Grosek, J., & Janku, M. (2020). Experimental Laboratory Testing on Behavior of Dowels in Concrete Pavements. *ACI Materials Journal*, *13*(10), 2343.